Specifics of Forced-Convection Heat Transfer to Supercritical Water Flowing Upward in Annular and Bundle Flow Geometries

by

Khalil Sidawi

A Thesis Submitted in Partial Fulfillment of the Requirements
for the Degree of

Master of Applied Science
in
Nuclear Engineering

The Faculty of Energy Systems and Nuclear Science

University of Ontario Institute of Technology

August 2016

Abstract

Bundle-flow geometries, even simple ones such as: single-rod (annulus), 3- and 4-rod bundles, are more representative of conditions within a nuclear reactor core than bare tubes. Since annulus- and bundle-flow geometries impede coolant flow, heat transfer to the coolant would occur differently than in bare tubes. However, there have been relatively few publications detailing specifics of forced-convection heat transfer to SuperCritical Water (SCW) flowing upward inside annular- and bundle-flow geometries compared to those in bare tubes. This is due to the more complex experimental setups and the abundance of bare tube experimental data.

This work compares experimental Heat Transfer Coefficients (HTCs) and wall temperatures in annular- and bundle-flow geometries to those predicted using bare tube HTC correlations. The viability of these correlations as a conservative preliminary approach is also assessed. Differences in onset of Deteriorated Heat Transfer (DHT) regime in bare tubes, annular- and bundle-flow geometries are explored.

The objectives of this work are as follows:

1. Propose and verify a universal method to accurately predict wall temperatures and HTCs using HTC correlation(s) for various annular- and bundle-flow geometries cooled with upward flow of SCW.
2. Investigate onset of DHT and Improved Heat Transfer (IHT) regimes in various annular- and bundle-flow geometries cooled with SCW as compared to bare tubes.

A set of several HTC correlations are identified from literature for comparison with various annulus and bundle data. These comparisons are modelled using a code developed using Matlab, in which properties of SCW are obtained from NIST REFPROP software [1]. The accuracy of wall temperature predictions (based on Root Mean Square (RMS) error) of each HTC correlation is then discussed.

It was determined that while it was possible to use some HTC correlations to obtain a conservative estimate of HTCs and wall temperatures in annular- and bundle-flow geometries, some correlations could not be used above the heat flux at which DHT appears in bare tubes.

This phenomenon is due to the fact that the DHT regime was reached in annular- and bundle-flow geometries at higher heat fluxes than in bare tubes. Results show experimental HTCs and wall temperatures to be in good agreement with the Dittus-Boelter (1930) [2] correlation (outside the pseudocritical region) and the Jackson (2002) [3] correlation. Wall temperature RMS errors were below 5% (within experimental uncertainties) for all trials except regions of DHT. The Dittus-Boelter (1930) [2] correlation was not sensitive to regions of DHT, as it is solely dependent on bulk-fluid conditions.

Acknowledgements

This work falls under the International Atomic Energy Agency (IAEA) Research Agreement #18417 (Coordinated Research Project (CRP) #I31025) "Understanding and Prediction of Thermal-Hydraulics Phenomena Relevant to Supercritical Water-Cooled Reactors (SCWRs)" (2014-2017).

Writing this thesis would not have been possible without the support and encouragement I received every step of the way. This is by no means a comprehensive list, but I would like to acknowledge a select few.

I am deeply grateful to my supervisor, Professor Igor Pioro, for his constant support and guidance in my research. I would not have been able to finish this work without his direction and insight.

I am especially thankful to Ph.D. students Amjad Farah and Jeffrey Samuel; I truly valued their advice and enjoyed their friendship, on and off the court. I would like to thank my colleagues Juan Carlos Jouvin, Jason Runge, and Dr. Eugene Saltanov for their valuable insights and discussions. Their thoughts were very valuable to my research and to the writing of this thesis.

Finally, to my parents: Issam Sidawi and Aida El Baf, and to my sisters: Aliaa Sidawi and Mariam Sidawi who helped me edit this work and supported me through the difficult times. Thank you for everything…

Table of Contents

Table of Figures

Table of Tables

Nomenclature

A	area, m^2
c_p	specific heat, $\frac{J}{kg \cdot K}$
$\overline{c_p}$	integrated specific heat within the range of $(T_w - T_b)$, $\frac{J}{kg \cdot K}$; $\left(\frac{h_w - h_b}{T_w - T_b}\right)$
D_{hy}	hydraulic-equivalent diameter, m; $\left(\frac{4 \cdot A_{fl}}{p_{wet}}\right)$
dx	step axial length change, m
G	mass flux, $\frac{kg}{m^2 s}$; $\left(\frac{\dot{m}}{A_{fl}}\right)$
g	acceleration due to gravity, $\frac{m}{s^2}$
HTC	heat transfer coefficient, $\frac{W}{m^2 K}$
h	specific enthalpy, $\frac{J}{kg}$
i	axial step position
k	thermal conductivity, $\frac{W}{m \cdot K}$
L	length, m
$\dot{m}$	mass flow rate, $\frac{kg}{s}$
P	pressure, Pa
p	perimeter, m
Q	power, W
q	heat flux, $\frac{W}{m^2}$
q_v	heat generated per unit volume, $\frac{W}{m^3}$
R	electrical resistance, Ω
T	temperature, °C
x	axial position, m

Greek Letters

Δ	difference

η	fin efficiency
η_{th}	thermal efficiency
μ	dynamic viscosity, $\mathrm{Pa} \cdot \mathrm{s}$
v	kinematic viscosity, $\frac{\mathrm{m}^2}{\mathrm{s}}$
ξ	friction factor; $((1.82 \cdot \log_{10} \mathbf{Re}_b - 1.64)^{-2})$
ρ	density, $\frac{\mathrm{kg}}{\mathrm{m}^3}$
$\bar{\rho}$	integrated density, $\frac{\mathrm{kg}}{\mathrm{m}^3}; \left(\frac{1}{T_w - T_b} \int_{T_b}^{T_w} \rho \, dT\right)$
ρ_{el}	electrical resistivity, $\Omega \cdot \mathrm{m}$

Dimensionless Numbers

$\mathbf{E}$	Eckert number; $\left(\frac{T_{pc} - T_b}{T_w - T_b}\right)$
$\overline{\mathbf{Gr}_b}$	Grashof number based on $\bar{\rho}$; $\left(\frac{g(\rho_b - \bar{\rho}) D_{hy}^3}{\rho_b^2}\right)$
$\mathbf{Nu}$	Nusselt number; $\left(\frac{HTC \cdot D_{hy}}{k}\right)$
$\mathbf{Pr}$	Prandtl number; $\left(\frac{\mu \cdot c_p}{k}\right)$
$\overline{\mathbf{Pr}}$	Prandtl number based on $\bar{c_p}$; $\left(\frac{\mu \cdot \bar{c_p}}{k}\right)$
$\mathbf{Re}$	Reynolds number; $\left(\frac{G \cdot D_{hy}}{\mu_b}\right)$
St	Stanton number; $\left(\frac{\mathbf{Nu}}{\mathbf{Re} \cdot \mathbf{Pr}}\right)$
$\mathbf{X}$	Modified Boiling number; $\left(\frac{h_b - h_{pc}}{q/G}\right)$

Subscripts

ave	average
b	bulk-fluid
C	cold temperature
calc	calculated
cr	critical point

el	electrical
exp	experimental
fl	flow
H	hot temperature
h	heated
hy	hydraulic
i	inner
in	inlet
is	inner sheath
o	outer
os	outer sheath
out	outlet
pc	pseudocritical
rib	rib
sat	saturation
sur	surface
t	total
v	volumetric
w	wall
wet	wetted

Acronyms

AC	Alternating Current
ACR	Advanced CANDU Reactor
AGR	Advanced Gas-cooled Reactor
BWR	Boiling Water Reactor
CANDU	CANada Deuterium Uranium nuclear reactor
CHF	Critical Heat Flux
DHT	Deteriorated Heat Transfer
Gen	Generation

GFR	Gas-cooled Fast Reactor
GIF	Generation-IV International Forum
HTC	Heat Transfer Coefficient
ID	Inner Diameter
IHT	Improved Heat Transfer
IPPE	Institute of Physics and Power Engineering (Obninsk, Russian Federation)
KPI	Kiev Polytechnic Institute
LFR	Lead-cooled Fast Reactor
LWR	Light Water Reactor
MSR	Molten Salt Reactor
NIST	National Institute of Standards and Technology (United States of America)
NPP	Nuclear Power Plant
OD	Outer Diameter
PHWR	Pressurized Heavy Water Reactor
Ph.D.	Doctor of Philosophy
PWR	Pressurized Water Cooled Reactor
RBMK	Reactor of Large Capacity Channel type (in Russian abbreviations)
RMS	Root Mean Square
RSC	Russian Scientific Centre “Kurchatov Institute” (Moscow, Russian Federation)
SCW	SuperCritical Water
SCWR	SuperCritical Water-cooled Reactor
SFR	Sodium-cooled Fast Reactor
SS	Stainless Steel
VHTR	Very High Temperature Reactor

Chapter 1. Introduction

The use of supercritical fluids in different processes is not new and, in fact, not even a human invention; nature has been processing minerals in aqueous solutions near or above the critical point of water for billions of years [4, 5]. Unlike subcritical pressure cases, there is no phase change at pressures beyond the critical point. This makes supercritical fluids attractive in situations where there is concern regarding onset of Critical Heat Flux (CHF) or dryout phenomena. However, heat transfer to supercritical fluids is highly affected by the significant variations in thermophysical properties that occur near the critical and pseudocritical points. Therefore, the ability to predict heat transfer to supercritical fluids despite these variations is necessary before any large-scale applications.

As such, analysis of heat transfer at supercritical pressure started as early as the 1930s [6]. Schmidt et al. (1946) [7] have found that fluids near the critical point have high free convection Heat Transfer Coefficients (HTCs) making them attractive as intermediate working fluids in single-phase thermosyphons. Power applications were explored in the 1950s with several experimental supercritical "steam" generator units built for use in research institutions [4].[1] Although there was interest in the application of Supercritical Water (SCW) to cool nuclear reactors in the 1950s and 1960s, it was not feasible due to an absence of appropriate materials. Nonetheless, research on the heat transfer properties of supercritical fluids in bare tubes, especially water, continued [8, 9, 10].

There was renewed interest, 30 years later, in the application of supercritical fluids in nuclear reactors to achieve a safer and more economical design [11]. This research bore fruition in January 2000 with the creation of the Generation-IV International Forum (GIF), which recognized the SuperCritical Water-cooled Reactor (SCWR) concept as one of six promising designs to be used as a basis for Generation-IV (Gen-IV) nuclear reactor research [12]. The SCWR design aims to increase the thermal efficiency by operating the primary-side coolant (SCW) at supercritical conditions: a coolant pressure of approximately 25 MPa, an inlet temperature between 300 − 350°C and an outlet temperature between 550 − 625°C [12].

[1] Proper supercritical phase terminology is discussed in Section 2.5.

However, since the pseudocritical point of water ($T_{pc@25MPa}$ = 384.9°C) lies within the SCWR's proposed operating parameters, significant changes to the thermophysical properties of water (and thus, the heat transfer regime) would occur along the heated length [4, 1]. This variation can also lead to a deterioration in heat transfer, which could result in a loss of bundle integrity. As such, knowledge of degree of the heat transfer from the fuel bundle to the coolant is of paramount importance for safe reactor operation.

Heat transfer from bundles is especially dependant on the geometry and presence of various appendages in the channel; many of the correlations developed for certain bundle geometries are very inaccurate when applied to others. There have been relatively few publications detailing HTC correlations for heat transfer in SCW flowing inside bundle flow geometry [13, 14, 15]; in fact, the vast majority of supercritical research has been dedicated to studying heat transfer in bare tubes [4, 8, 16, 17]. Thus, heat transfer characteristics of SCW-cooled bundles are still largely unknown. However, rather than developing a new correlation for each unique bundle design, analysis of experiments in simple bundle-flow geometries gives a conservative estimate of heat transfer in a sub-channel within a complex bundle.

Since the final SCWR channel design has yet to be decided, an HTC correlation is needed in the interim that can provide an accurate conservative estimate of heat transfer for proposed bundle designs (within ~5% RMS error of wall temperature). This work compares experimental wall temperatures of annular- and bundle-flow geometries to those predicted using bare tube HTC correlations. The viability of these correlations as a conservative preliminary approach is also assessed. Differences in the onset of Deteriorated Heat Transfer (DHT) regime in bare tubes, annulus-, and bundle-flow geometries are explored. The main objective of this work is to investigate specifics of heat transfer to SCW flowing upward in annular- and (3 & 4-rod) bundle-flow geometries compared to those in bare tubes.

The following paragraphs outline the method, by chapter, used to achieve the objectives of this work.

Chapter 2 outlines background information on Gen-IV reactors and illustrates the variation of thermophysical properties of water in the supercritical region. Additionally, several published empirical HTC correlations are presented and assessed. DHT is discussed and difficulties

arising in the prediction of heat transfer in this regime are explained.

Chapter 3 gives a description of all the test facilities and test sections where the experimental data were collected. A systematic outline of the methodology used to create each one-dimensional model is presented. The synergy between Matlab and NIST REFPROP [1] software is explained, and the solutions to heat transfer equations unique to each geometry are presented. Results and discussions of the experiments introduced in Chapter 3 are presented in Chapter 4 & Chapter 5.

Chapter 4 analyzes heat transfer in single-rod and 3-rod bundle experiments which have been performed in an SCW loop at the National Technical University of Ukraine "Kiev Polytechnic Institute" in 2009. Bulk-fluid and wall temperatures, and HTC profiles for the modelled experiments are illustrated. The temperature profile of a UO_2 fuel pellet assuming heat is generated by it rather than by electrical resistance in a single-rod channel is also presented.

Chapter 5 analyses heat transfer in 2×2 rod bundles which have been performed in an SWAMUP test facility at Shanghai Jiao Tong University in 2015. Bulk-fluid and wall temperatures, and HTC profiles for the modelled experiments are illustrated.

Finally, concluding remarks are given based on the analyses conducted, and recommendations are provided for future research.

Chapter 2. Literature Review

2.1. Current Status of Electricity Generation in the World

As the world's energy demand increases, there is a dire need for carbon emission-free energy sources [18]. Although renewable energy sources such as solar and wind are desirable due to their low environmental impact, they are not reliable for industrial power generation due to their relatively high electrical energy generation costs and intermittent nature [19].[2] Additionally, given their high dependence on weather conditions, they cannot solely offset base-load power [20].[3] On the other hand, while large hydroelectric power plants generate cheap electrical energy, they cause large environmental impacts and displace the native population [21].

Non-renewable energy sources, such as fossil fuels, provide the majority of the world's energy due to their high economic output, as shown in Figure 2-1.

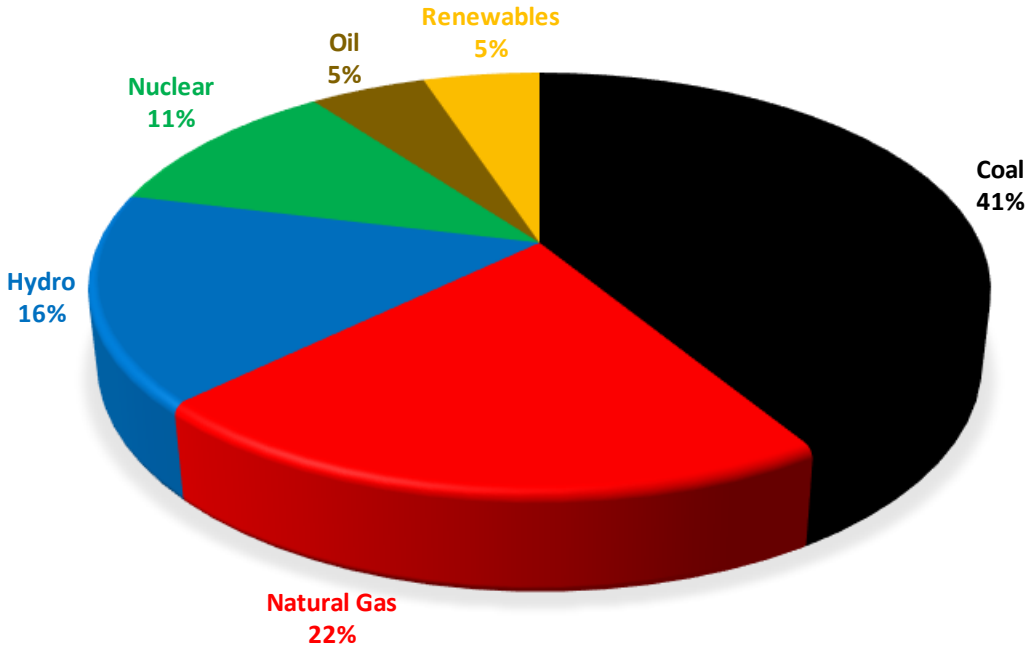

Figure 2-1. World electricity generation by source as of 2013 [20].

[2] Solar energy is further constrained by the length of time the Sun is up. The world nuclear organization estimates solar's levelised cost of electricity to be $119/MWh [20].
[3] Base-load power is the amount of continuous electrical demand 24/7/365 [19].

Fossil fuel (thermal) power plants operate using a Rankine thermodynamic cycle, in which heat generated by burning fossil fuels is converted into electrical energy [22]. The thermal efficiency of the Rankine cycle is ultimately limited by the temperature of the steam at the inlet of a turbine [22]. While the thermal efficiency of thermal power plants has greatly improved over the last 20 years, the fact that they produce harmful greenhouse gases makes them unattractive in today's environmentally conscious culture [18].

The most widely used type of fossil fuel, coal, produces large amounts of greenhouse gases, slag, and ash [19]. Recent efforts were aimed at reducing dependence on coal;[4] however, its low price, abundance and ability for "fast-response" during periods of peak demand make it an attractive option.[5] Alternatively, natural gas is less harmful to the environment than coal. It has fewer impurities, is less chemically complex and its combustion generally results in less pollution. However, there are major concerns over its transport (especially in tankers), its emission of Carbon Dioxide gas (CO_2) when burned (a greenhouse gas), and its distribution in pipelines.

Nuclear fission is an alternative means of generating the heat required in a thermal power plant and has vastly lower fuel costs and net carbon emissions [19].[6] While nuclear power is not suited to offset variable power demands, its reliability has been proven to provide large-scale continuous electricity to supply base-load power demands [19].[7]

2.2. Current Generation Nuclear Power Plants

The Rankine cycle is the fundamental thermodynamic cycle of most thermal power plants in operation, including Nuclear Power Plants (NPPs). The thermal efficiency of a Rankine cycle is directly dependent on the temperature of steam at the turbine inlet. However, the temperature of steam at the turbine inlet in current water-cooled NPP designs is limited by the temperature of coolant at the outlet of the reactor, which is in turn limited by the saturation

[4] Electrical production in Ontario, Canada is coal free as of 2014 [59].
[5] The world nuclear organization estimates coal's levelised cost of electricity to be $104/MWh [20].
[6] The world nuclear organization estimates nuclear energy's levelised cost of electricity to be $90.5/MWh [20].
[7] It is important to note that nuclear reactors do in fact release a small amount of CO_2 over its life cycle (indirectly) [20].

temperature at the operating pressure.[8]

Reactor outlet temperatures of current generation NPPs are below 330°C, which limits their overall efficiency [19].[9] The overall efficiency of NPPs is reduced further due to inefficiencies and losses throughout the primary cycle and auxiliary systems (pumps, turbines. etc.). The thermal efficiencies as well as some operational parameters of operational NPPs can be seen in Table 2-1.

Table 2-1. Some thermal efficiencies of current generation NPPs [19].

Nuclear Power Plant	Actual Thermal Efficiency
Pressurized Water Reactor (PWR) – Generation III+ NPPs • Reactor coolant: light water • $P_{out} \approx 16$ MPa → $T_{sat@16MPa} = 347°C$; $T_{out} \approx 327°C$	36% – 38%
PWR – Current Generation NPPs • Reactor coolant: light water • $P_{out} \approx 16$ MPa → $T_{sat@16MPa} = 347°C$; $T_{out} \approx 325°C$	32% – 36%
Boiling Water Reactor (BWR) – Current Generation NPPs • Reactor coolant: light water • $P_{in} \approx 7.2$ MPa → $T_{in} = T_{sat@7.2MPa} = 288°C$	~ 34%
RBMK (boiling, pressure-channel) – Generation III NPPs • Reactor coolant: light water • $P_{in} \approx 6.6$ MPa → $T_{in} = T_{sat@6.6MPa} = 282°C$	~ 32%
Pressurized Heavy Water Reactor (PHWR) NPPs • Reactor coolant: heavy water • $P_{out} \approx 10$ MPa → $T_{sat@10MPa} = 311°C$; $T_{out} \approx 310°C$	~ 32%

The dependence of the reactor outlet temperature on the saturation temperature indicates that fundamental design changes are necessary for a significant increase in thermal efficiency.

[8] The saturation temperature for a corresponding saturation pressure at which a liquid boils into its vapour phase.
[9] Conceptually, the Carnot Cycle gives the maximum possible thermal efficiency of a cycle operating between two temperatures: T_C and T_H. The Carnot efficiency for this outlet temperature assuming a heat sink at 20°C is: $\eta_{th} = 1 - \frac{T_C}{T_H} = 1 - \frac{20+273.15}{330+273.15} = 48.6\%$.

2.3. Generation-IV Reactor Concepts

The evolution of nuclear technology is briefly outlined in Figure 2-2.

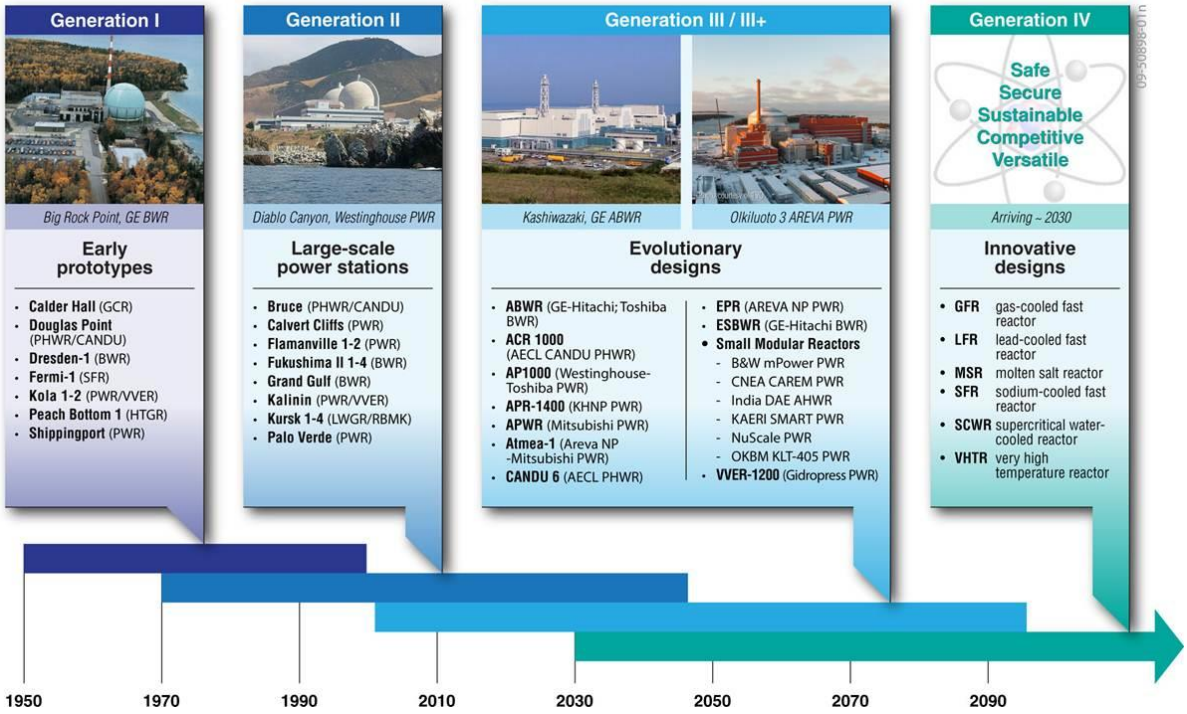

Figure 2-2. Evolution of Nuclear Technology (courtesy of GIF) [12].

The GIF was created in January 2000 as an international co-operative endeavor between countries and corporations alike to assess the performance capabilities and feasibility of Gen-IV NPPs [23]. The agreement addresses four major areas of improvements that all Gen-IV NPPs need to address [23].

1. Sustainability: ensure that nuclear waste is minimized and destroy long-lived isotopes from spent fuel of current generation reactors [23].
2. Economics: establish a life-cycle cost advantage over other energy sources [23].
3. Safety & Reliability: reduce the risk and scale of reactor core damage and eliminate the need for offsite emergency response [23].
4. Proliferation Resistance & Physical Protection: increase physical barriers to prevent acts of terrorism, and reduce the risk of theft of weapon-grade nuclear materials [23].

In order to move purposefully forward, GIF members selected six concept reactors to become the basis for Gen-IV research [23]. Key features of each proposed Gen-IV concept are

presented in Table 2-2.

Table 2-2. Proposed operational parameters of Gen-IV Reactors [12].

System	Neutron Spectrum	Coolant	Outlet Temperature, °C	Fuel Cycle	Electric Power, MW_{el}
GFR	Fast	Helium	850	Closed	1200
LFR	Fast	Lead	480 – 570	Closed	20 – 180 300 – 1200 600 – 1000
MSR	Thermal/Fast	Fluoride Salts	700 – 800	Closed	1000
SFR	Fast	Sodium	500 – 550	Closed	50 – 150 300 – 1500 600 – 1500
SCWR	Thermal/Fast	Water	510 – 625	Open/ Closed	300 – 700 1000 – 1500
VHTR	Thermal	Helium	900 – 1000	Open	250 – 300

A short summary of each Gen-IV concept is given below.

1. Gas-cooled Fast Reactor (GFR) designs are characterized by a fast neutron reactor core cooled with helium gas to achieve high outlet temperatures [23]. The use of dense nuclear fuels such as uranium carbide or nitride allows for the possibility of plutonium breeding, and minor actinide burning [23].[10]
2. Lead-cooled Fast Reactor (LFR) designs are characterized by a fast neutron reactor core cooled with either lead or a lead/bismuth eutectic [23]. It can be operated as a breeder, a burner of actinides from spent fuels, or a burner/breeder using thorium matrices [23].[11]
3. Molten Salt Reactor (MSR) designs are characterized by liquid nuclear fuel [23]. MSR designs allow breeding at any neutron spectrum: fast spectrum for a uranium-plutonium fuel cycle or thermal spectrum for a thorium fuel cycle [23].
4. Sodium-cooled Fast Reactor (SFR) designs are characterized by a liquid sodium coolant. A closed fuel cycle allows for fuel breeding or burning of actinides [23].

[10] Actinide burning involves the destruction of minor actinides (such as: neptunium, americium, and curium) to reduce the length of time that spent fuel remains highly radioactive [64].
[11] A type of reactor that generates more fissile material than it consumes.

5. Supercritical Water-cooled Reactor (SCWR) designs are characterized by a high temperature and pressure water coolant. This reactor type is further discussed in Section 2.4.
6. Very-High Temperature Reactor (VHTR) designs are characterized by a thermal neutron spectrum reactor core, a graphite moderator, and helium coolant. The high temperature outlet conditions allow for other applications such as the production of hydrogen by thermo-chemical processes [23].

2.4. Supercritical Water-cooled Reactors

The absence of a liquid-vapour transition makes supercritical fluids an attractive coolant as it eliminates concerns of reaching dryout conditions or exceeding the CHF that may occur in current water-cooled NPPs.[12] Current SCWR research focuses on increasing the thermal efficiency of water-cooled NPPs much like what was done to supercritical pressure coal-fired power plants.[13]

Major advantages of the SCWR concept include higher thermal efficiency, design and operation experience gained from hundreds of water-cooled reactors, and 50 years of experience in supercritical pressure fossil fuel power plants [12]. Consequently, many of the corresponding equipment, layouts and plant designs have already been worked through and tested in the field. A few of the drawbacks of SCWR concepts are: unreliability of in-core materials at supercritical pressures (namely the need of advanced steels for cladding), high heat fluxes, high neutron fluxes, aggressive reactor coolant (SCW), transient heat transfer models for describing the depressurization from supercritical to subcritical conditions, and unknown heat transfer characteristics of SCW-cooled bundles [12]. Furthermore, no experimental, transport, or any other kind of prototype SCWR design has been tested.

In contrast to other Gen- IV nuclear systems, the SCWR is being developed incrementally from current water-cooled reactors [12]. An illustration of a Canadian SCWR pressure-

[12] Dryout conditions occur when there is total depletion of liquid in the channel due to evaporation [67]. CHF is achieved when the heat flux is sufficiently high such that only the liquid near the heated surface evaporates [67].
[13] For a comparison with previous generation reactors, the Carnot efficiency for an SCWR, assuming a heat sink at 20°C: $\eta_{th} = 1 - \frac{T_C}{T_H} = 1 - \frac{20+273.15}{625+273.15} = 67.3\%$. That is a 16% increase over the Gen III NPPs.

channel concept is shown in Figure 2-3.

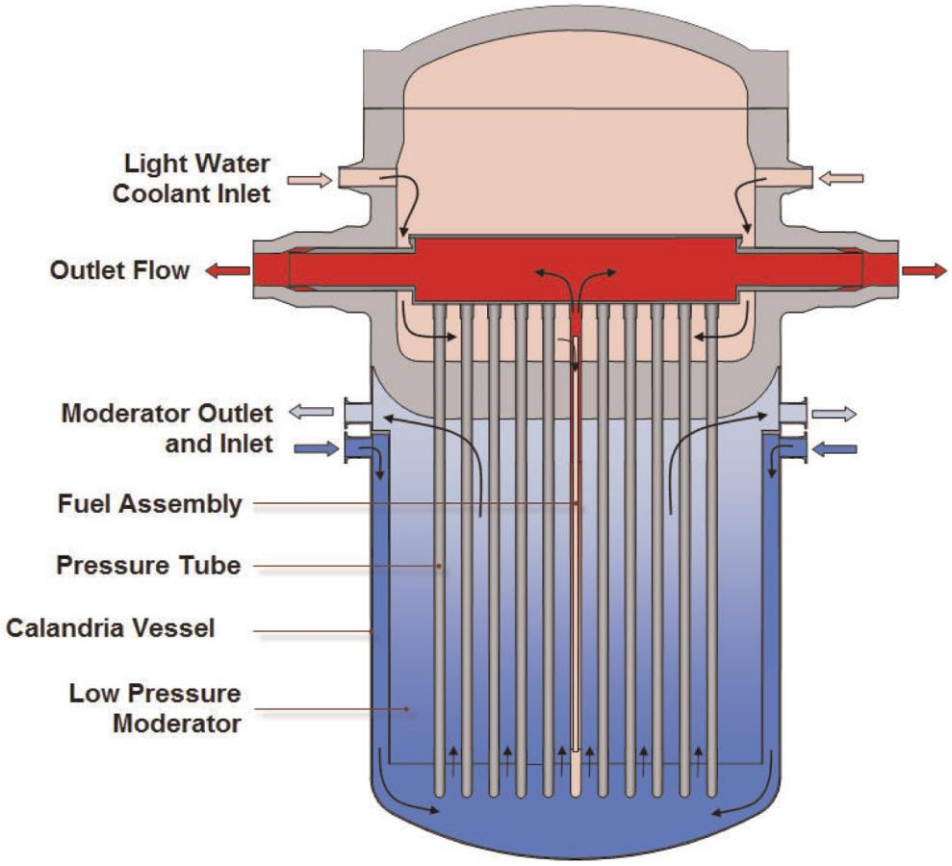

Figure 2-3. Schematic of a conceptual Canadian SCWR core (courtesy of GIF) [24].

Unlike the horizontal core of current Canadian Pressurized Heavy Water Reactor (PHWR) (CANDU), the Canadian SCWR concept features a vertical core with SCW flowing upward inside pressure-channels.[14] SCW is supplied directly to the high-pressure turbine while feedwater from the steam cycle is supplied back to the core [12].

While there are still several challenges associated with SCWR concepts, this thesis will focus on unknown heat transfer characteristics of SCW-cooled bundles.

Phenomena specific to heat transfer to supercritical fluids are discussed in Section 2.5.

[14] It should be noted that heat transfer differs between horizontal and vertical flow; indeed, due to buoyancy forces, the flow direction (upward versus downward) also plays a major effect [4]. Furthermore, the final bundle design for SCWRs is not yet finalized.

2.5. Definition of Relevant Supercritical Terminology

A summary of relevant terminology is presented to assist the reader in understanding supercritical phase terms [4]. These definitions are referenced in Figure 2-4 & Figure 2-5.

Compressed fluid is a fluid at a pressure above the critical pressure but at a temperature below the critical temperature.

Critical point (also called a critical state) is a point at which the distinction between the liquid and vapour phases disappears, i.e., both phases have the same temperature, pressure and volume or density. The critical point is characterized by the phase-state parameters: T_{cr}, P_{cr}, and ρ_{cr}, which have unique values for each pure substance.[15]

Deteriorated Heat Transfer (DHT) is characterized with lower values of the HTC compared to those for Normal Heat Transfer (NHT); and hence, has higher values of wall temperature within some part of a test section or within the entire test section.

Improved Heat Transfer (IHT) is characterized with higher values of the HTC compared to those for NHT; and hence, lower values of wall temperature within some part of a test section or within the entire test section. In our opinion, the IHT regime includes peaks or "humps" in the HTC near the critical or pseudocritical points.

Near-critical point is a narrow region around the critical point, where all thermophysical properties of a pure fluid exhibit rapid variations.

Normal heat transfer (NHT) can be characterized, in general, with HTCs similar to those of subcritical forced-convection heat transfer far from the critical or pseudocritical regions calculated using the conventional single-phase Dittus-Boelter (1930) [2] correlation: $\mathbf{Nu} = 0.023\ \mathbf{Re}^{0.8}\ \mathbf{Pr}^{0.4}$.

Pseudo-film boiling is a physical phenomenon similar to subcritical-pressure nucleate boiling, which may appear at supercritical pressures. Due to heating of a supercritical fluid with a bulk-fluid temperature below the pseudocritical temperature (high-density fluid, i.e., "liquid-

[15] The critical pressure of water is: P_{cr} = 22.064 MPa, and the critical temperature of water is: T_{cr} = 373.95°C.

like"), some layers near the heating surface may attain temperatures above the pseudocritical temperature (low-density fluid, i.e., "gas-like"). This low-density "gas-like" fluid leaves the heating surface in a form of variable density (bubble) volumes. During pseudo-film boiling, the HTC usually increases (IHT regime).

Pseudocritical line is a line consisting of all pseudocritical points at supercritical pressures.

Pseudocritical point (characterized by P_{pc} and T_{pc}) is a point at a pressure above the critical pressure ($P_{pc} > P_{cr}$), and at a temperature greater than the critical pressure ($T_{pc} > T_{cr}$), corresponding to the maximum value of specific heat at this particular pressure.

Supercritical fluid is a fluid at pressures and temperatures that are higher than the critical pressure and critical temperature. However, in the present work, the term supercritical fluid includes both terms – a supercritical fluid and compressed fluid.

Supercritical "steam" is actually SCW, because at supercritical pressures, the fluid is considered a single-phase substance. However, this term is widely (and incorrectly) used in the literature in relation to supercritical "steam" generators and turbines.

Superheated steam is steam at pressures below the critical pressure, but at temperatures above the critical temperature.

2.6. The Supercritical Region

The supercritical region encompasses fluids whose temperature and pressure exceed the critical point, as shown for water in Figure 2-4 & Figure 2-5. Other phases of water are also shown relative to the supercritical phase.

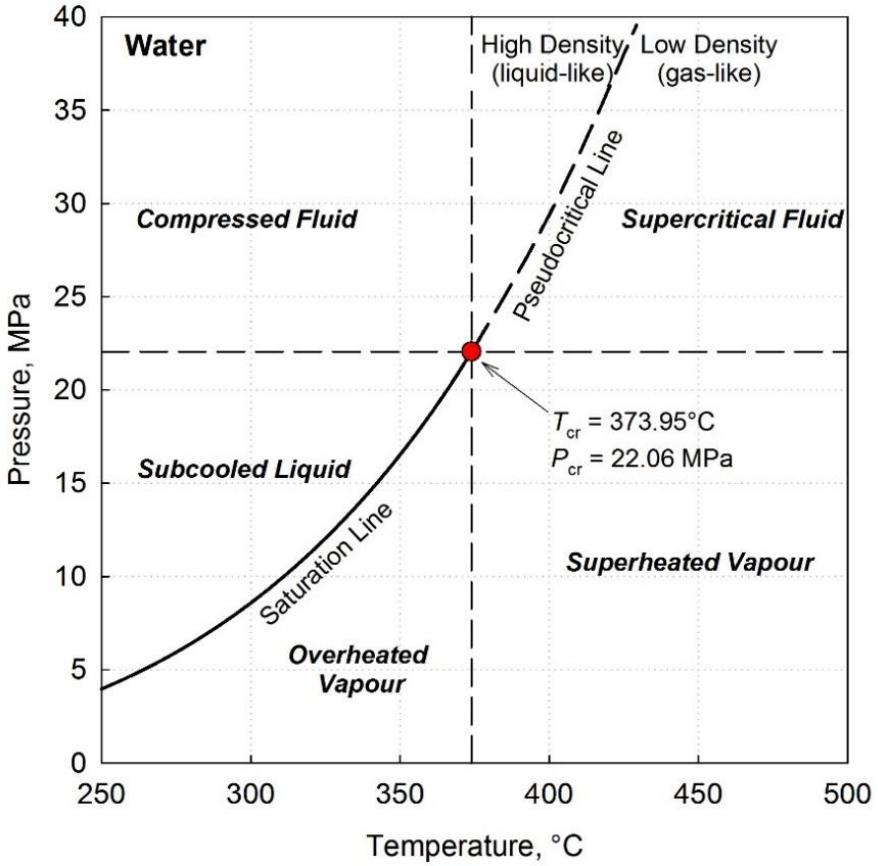

Figure 2-4. Pressure versus Temperature of water.

The supercritical region is separated by the pseudocritical line, which follows the trend of the saturation line, as shown in Figure 2-4. However, the saturation line divides the vapour and liquid phases: two distinct phases, whereas the pseudocritical line separates the supercritical region, a single phase. X-ray diffraction experiments show that SCW at temperatures below the pseudocritical temperature has a higher density (liquid-like), whereas SCW at temperatures above the pseudocritical temperature has a lower density (gas-like) [25].

In some tables, thermophysical properties of subcooled liquids are listed for compressed fluids as well, as most thermophysical properties are highly dependent on temperature rather than pressure [26]. Figure 2-5 illustrates another diagram of the supercritical region based on temperature and specific entropy.

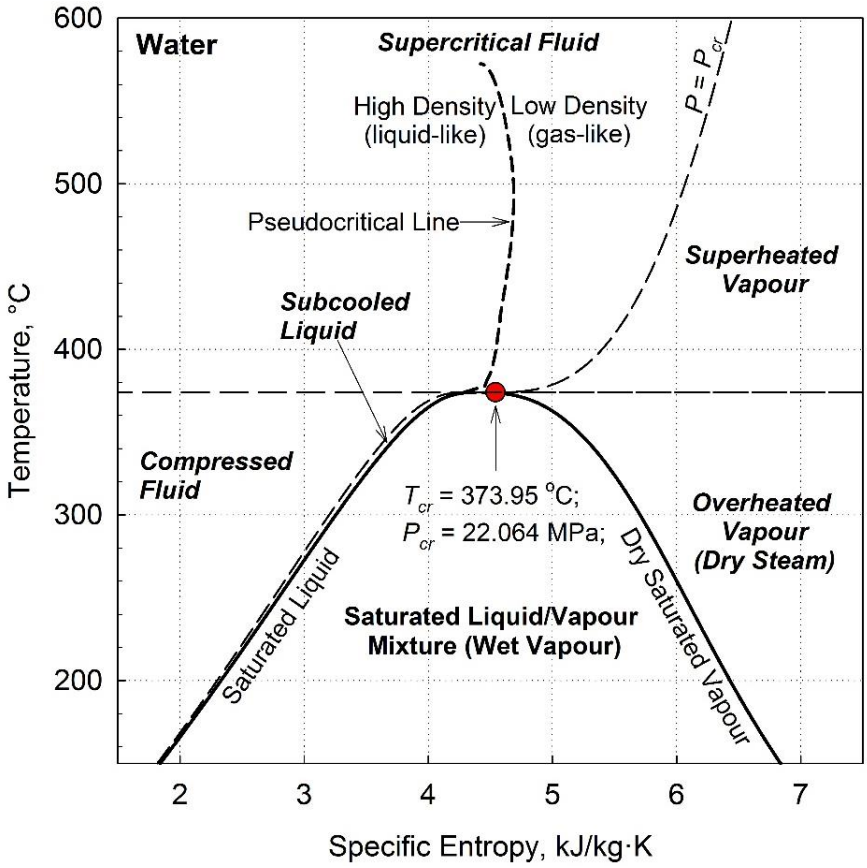

Figure 2-5. Temperature versus specific entropy of water.

It is interesting to note the relative area occupied by subcooled liquids between Figure 2-5 and Figure 2-4. The subcooled phase exists only for a small range of specific entropy, as the phase is 'sandwiched' between the saturated liquid line and the critical pressure line.

2.7. Thermophysical Properties of Supercritical Water

There is significant variation in most thermophysical properties of water in the supercritical region, as shown for a pressure of 25 MPa in Figure 2-6.

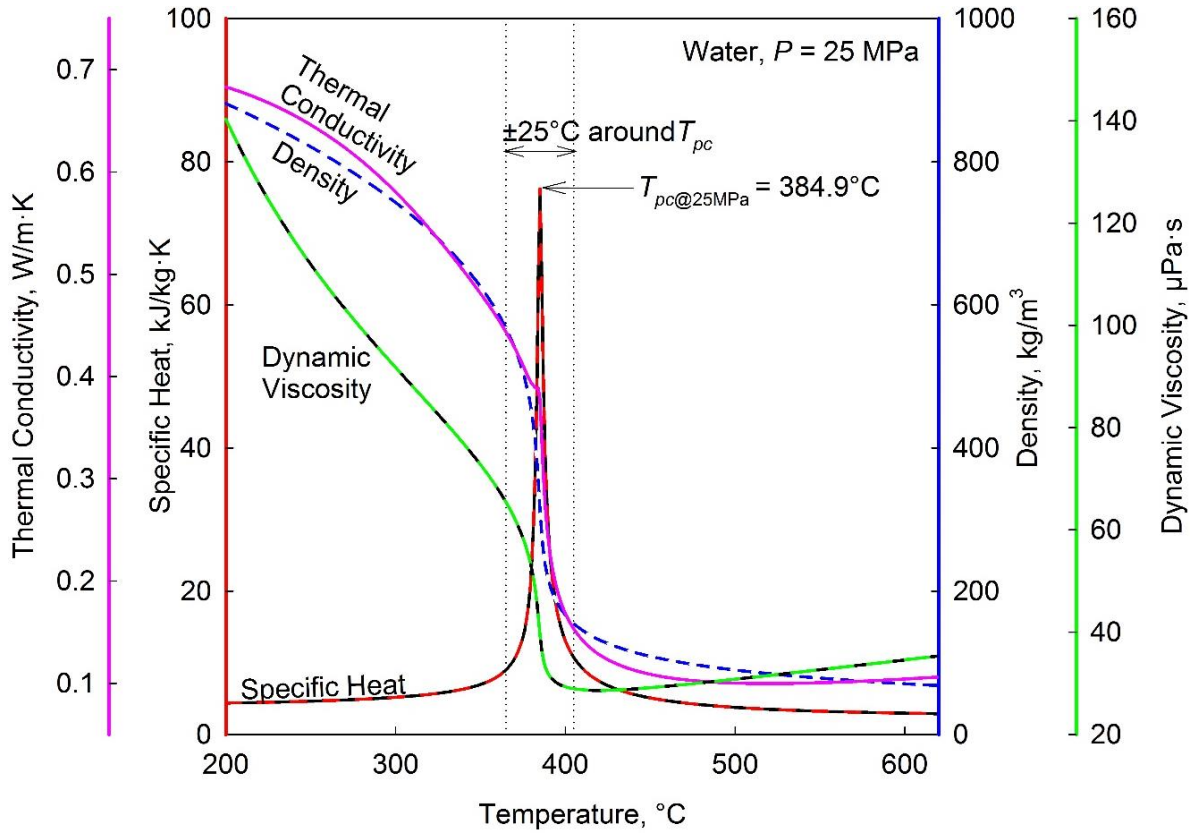

Figure 2-6. Thermal Conductivity, Specific Heat, Density and Dynamic Viscosity of Water at 25 MPa between 200°C and 600°C.

The vertical dotted lines surrounding the peak in specific heat highlight a ±25°C temperature range where the largest variation in thermophysical properties occur. Unfortunately, drastic changes occur to SCW's thermophysical properties as it nears and crosses the pseudocritical point.[16] The dynamic viscosity, specific heat, and thermal conductivity all have non-uniform variations across the supercritical region, whereas only density changes uniformly, as shown in Figure 2-6.

For a heated channel where the bulk-fluid temperature is less than, but sufficiently close to the pseudocritical temperature, conditions at the wall will be significantly different from those of the bulk-fluid. Ackerman (1970) [9] suggested that a phenomenon similar to subcritical voiding, termed pseudo-film boiling might occur near the walls due to the large variation in density.

[16] $T_{pc@25MPa}$ = 384.9°C, which is located within the proposed operating range of SCWRs [4, 1].

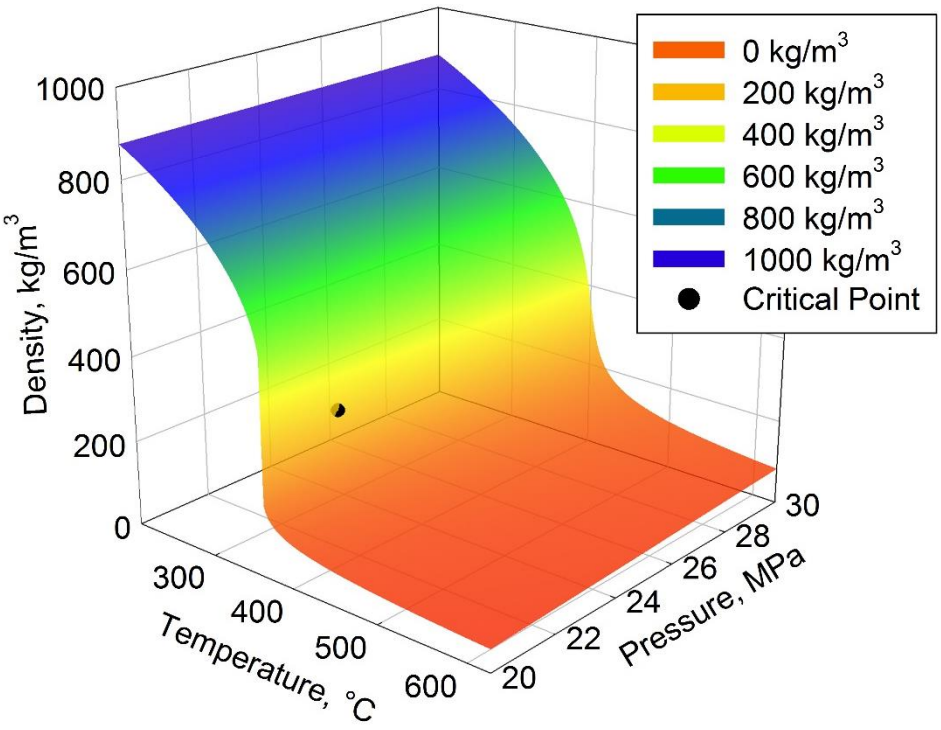

Figure 2-7. Density of Water between 20 – 30 MPa and 200 – 550°C.

As shown in Figure 2-7, the density curve at each pressure is uniformly decreasing between 200°C to 550°C; there is a point of inflection at each pseudocritical point.

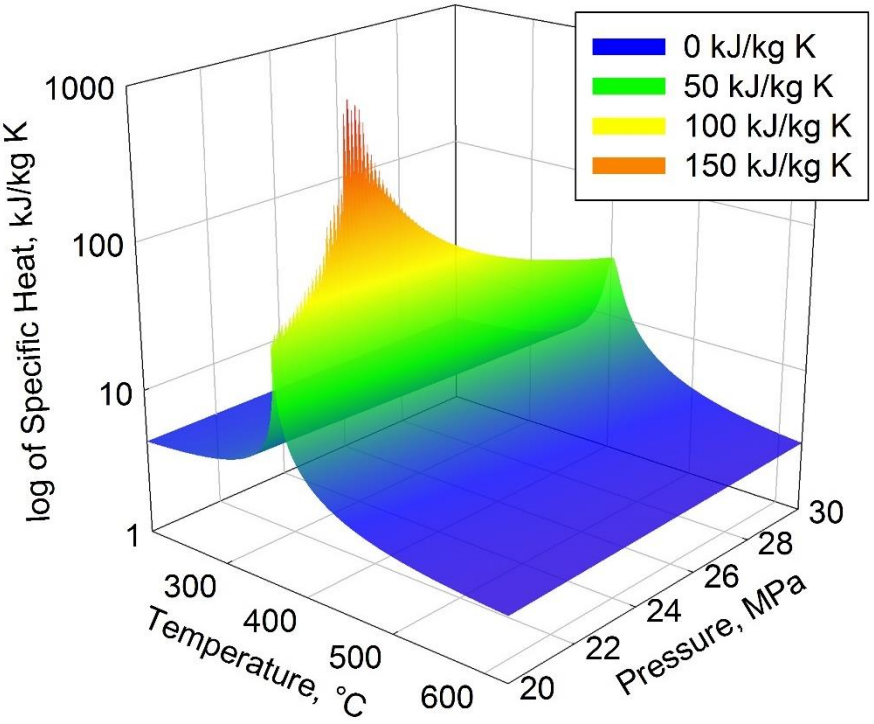

Figure 2-8. Specific Heat of Water between 20 – 30 MPa and 200 – 550°C.

Unlike density, the plot of specific heat is non-uniform at all pressures, and peaks at the pseudocritical line, as shown in Figure 2-8.[17]

2.8. Heat Transfer Regimes

Fewster and Jackson (2004) [27] outlined three modes of heat transfer in the supercritical region: NHT, IHT, and DHT.[18] The following figure illustrates these modes of heat transfer for SCW flowing upward in a bare tube obtained using data from Kirillov et al. (2003) [28].

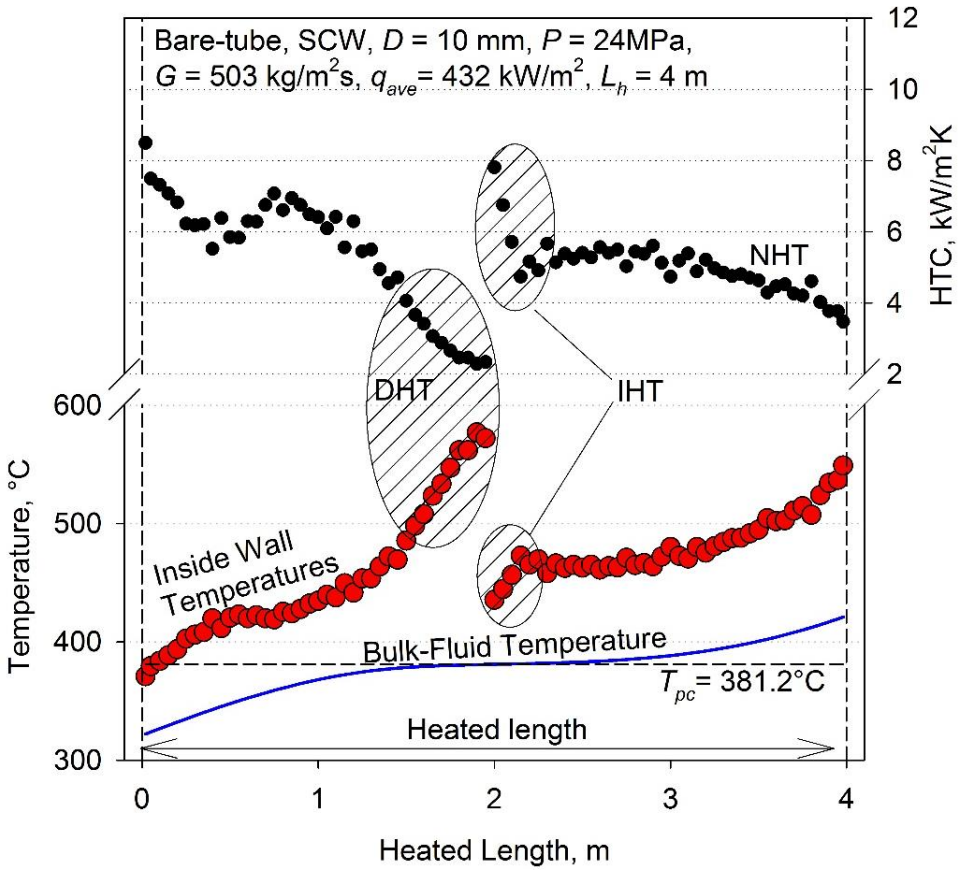

Figure 2-9. Temperature and HTC profiles along heated length of vertical bare tube; data obtained using data from Kirillov et al. (2003) [28].

DHT is a phenomenon characterized with lower values of HTC and higher values of wall temperature compared to NHT, as shown in Figure 2-9. This is of concern, as rapid increases

[17] It is curious that such a discontinuity in specific heat occurs at the pseudocritical temperature, as this phenomenon is indicative of phase change. Since the density changes uniformly, this type of phase change occurs continuously across the transition temperature [69].

[18] Large increases in wall temperature due to DHT can lead to loss of rod integrity or meltdown. It should be noted that bundle integrity can be compromised by a failure in either the sheath or the fuel.

in temperature could lead to possible fuel failures. Vikhrev et al. (1967) [29] found that, in general, there are two types of DHT: one that appeared in the entrance region, while the other within a certain temperature range. DHT in the entrance region can be avoided by adding an unheated length before the test section, which allows the development of turbulent flow (improving heat transfer).[19]

Many researchers have tried to mathematically predict onset of DHT. Styrikovich et al. (1967) [30] and Swenson et al. (1965) [31] observed a relationship between onset of DHT and an increase in wall temperature beyond the pseudocritical temperature for $q/G \gtrsim 0.4$ kJ/kg. On the other hand, Shiralkar and Griffith (1970) [32] found that onset of DHT occurred when $T_b < T_{pc} < T_w$ at high heat fluxes. Interestingly, Pis'mennyy et al. (2006) [33] found that cooling vertical bare tubes with SCW at $T > T_{pc}$ given $q/G \leq 0.70$ kJ/kg and $G \leq 2200$ kg/m^{2}s occurred at NHT regime with stable temperature profiles along the heated length.

In terms of enhancement, Yamagata et al. (1972) [34] found that heat transfer is enhanced as the bulk-fluid enthalpy increased through the pseudocritical point. This enhancement was diminished as the heat flux increased, and at some heat flux, disappeared completely. Shitsman (1963) [35] showed that as heat flux increases at low mass fluxes (430 kg/m^{2}s) there is a migration from an IHT regime to a DHT regime. However, unlike the CHF, a two-phase flow phenomenon, heat transfer at supercritical conditions recovers after deterioration.

Although there is no definitive way to identify DHT other than by visual inspection, some authors have developed simplified correlations that can provide a very rough estimate of the minimum heat flux at which DHT occurs. For example, Mokry et al. (2011) [36] proposed a simple empirical correlation for calculating the minimum heat flux at which DHT occurs.

$$q_{DHT} = -58.97 + 0.745 \cdot G \tag{2.1}$$

Where G is in kg/m^{2}s and q_{DHT} is in kW/m^2.

Silin et al. (1993) [37] reported that the most important difference between water behaviour inside bare tubes versus behaviour inside bundles was that there was no onset of DHT regime

[19] This type of DHT is why some HTC correlations account for an entrance effect in the form of: $\left(1 + C\frac{D_{hy}}{x}\right)$.

in multi-rod bundles at the same test parameter range for which heat transfer deterioration occurred in bare tubes.[20] This claim was based on a large database for water flowing in large bundles at supercritical pressures at the Russian Scientific Centre (RSC) "Kurchatov Institute" (Moscow, Russian Federation). It is important to verify this statement using experimental data in annuli and bundles cooled with SCW as no experimental data was provided in support of this statement.

Richards et al. (2013) [15] studied 20 cases of 7-rod bundles cooled with upward flow of supercritical Freon R-12 collected at the Institute of Physics and Power Engineering (IPPE, Obninsk, Russian Federation). They observed DHT in 15 of 20 cases proving that it can occur in bundles cooled with supercritical fluids [15]. Figure 2-10 shows a 7-rod bundle cooled with upward flow of supercritical R-12 illustrating the three heat-transfer regimes in one heated length. A drop in wall temperatures is indicative of IHT, which is observed near the channel inlet (~0.1m), as shown in Figure 2-10. NHT is observed in the middle of the channel, while rapid increases in wall temperature, which are indicative of DHT, are observed near the channel outlet (~0.85m), as shown in Figure 2-10.

[20] It should be noted that this phenomenon is most likely observed inside more complex bundles (greater than 7-rods).

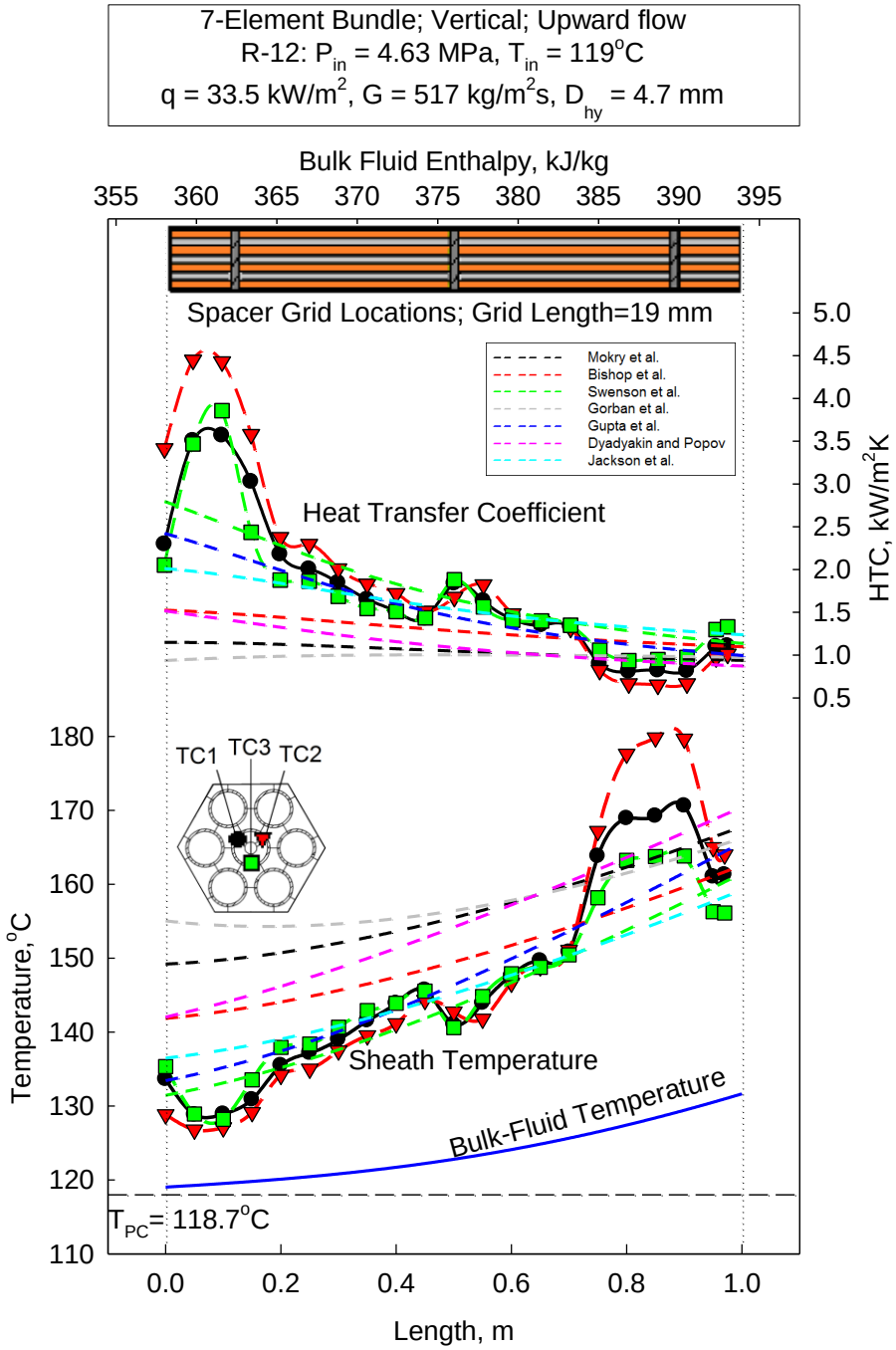

Figure 2-10. Bulk-fluid temperature, sheath temperature and HTC profiles along heated length of 7-rod bundle cooled with R-12 (Courtesy of I.L. Pioro [15]).

However, it should be noted that supercritical R-12 has significantly different thermophysical properties and (possibly) heat transfer behaviour than SCW. Therefore, experimental data in SCW-cooled bundles is required as most nuclear reactors are not designed based on modelling fluids such as R-12.

2.9. Types of Convection

The type of convection (forced, natural, or mixed) in channels is dependent on the ratio of the Grashof number to the Reynolds number [38].[21] Onset of DHT is most likely due to buoyancy forces dominating heat transfer at the boundary layer near the heated wall [4]. Ackerman (1970) [9] referred to this phenomenon as pseudo-film boiling. For upward flow of SCW, Jackson et al. (1988) [38] recommended that the effect of the buoyancy force, represented by a Grashof number based on the integrated density could be considered negligible if:[22]

$$\frac{\overline{\mathbf{Gr}}_b}{\mathbf{Re}_b^{2.7}} < 2.4 \cdot 10^{-5} \tag{2.2}$$

Even at values significantly lower than $2.4 \cdot 10^{-5}$, peaks in this ratio along the heated length seem to correlate to regions of DHT.

2.10. Characterization of SCW flow in Tubes

Some non-dimensional numbers can be used to characterize heat transfer properties of a fluid in a cross section of a tube.

2.10.1. Eckert Number

At high heat fluxes for a given cross-section, especially for a fluid near the pseudocritical region, wall and bulk-fluid properties can diverge. The Eckert number is a ratio that can be used to give a value to the degree of that divergence.

$$\mathbf{E} = \frac{T_{pc} - T_b}{T_w - T_b} \tag{2.3}$$

Where $T_w \neq T_b$.

1. At $\mathbf{E} > 1$, the supercritical fluid is assumed to be liquid-like over the cross section [39].

---

[21] The Grashof number represents the ratio of the buoyancy to viscous forces acting on a fluid, $\mathbf{Gr} = \frac{g\beta(T_s - T_\infty)D^3}{\nu^2}$ [51]. The Reynolds number represents the ratio of inertial to viscous forces, $\mathbf{Re} = \frac{G \cdot D}{\mu}$ [51].

[22] The equation of the Grashof number based on integrated density is: $\overline{\mathbf{Gr}}_b = \frac{g(\rho_b - \bar{\rho})D_{hy}^3}{\rho_b^2}$, where the integrated density equation is: $\bar{\rho} = \frac{1}{T_w - T_b}\int_{T_b}^{T_w} \rho \, dT$.

Specific heat is monotonic within the cross section [10].[23]

2. At $\mathbf{E} < 0$, the supercritical fluid is assumed to be gas-like over the cross section [39]. Specific heat is monotonic across the cross section [10].
3. For $0 \leq \mathbf{E} \leq 1$, the fluid is assumed to be gas-like near the heated wall and liquid-like farther from the heated wall [39]. Here, there is a peak in specific heat within the cross section [10].

One drawback of the Eckert number is that the outer wall temperature is needed, which is usually determined from HTC correlations (unless it is experimentally measured).

2.10.2. Modified Boiling Number

Saltanov (2015) [40] developed a unique method to correlate heat transfer data without the need to distinguish the mode of heat transfer. This eliminates the need to visually (i.e. subjectively) determine regions of DHT. By using a non-dimensional number similar to the Boiling number[24] and the Stanton number[25], the new dimensionless number, **X**, relates the enthalpy required to reach the pseudocritical point, and the heat flux to mass flux ratio.

$$\mathbf{X} = \frac{h_b - h_{pc}}{q/G} \tag{2.4}$$

The numerator in Equation (2.4) represents the specific enthalpy required for a fluid at the current state to reach the pseudocritical state. The denominator represents the specific rate of heat addition to the fluid. Therefore, a large negative number may indicate either a fluid at a temperature significantly below the pseudocritical temperature under average heat load conditions, or a fluid at a temperature very close to the pseudocritical temperature under extremely low heat load conditions [40].

---

[23] A function is called monotonic if and only if it is either entirely increasing or entirely decreasing.

[24] The Boiling number represents a ratio of the actual heat flux to the maximum heat flux achievable by complete evaporation of the liquid, $\mathbf{Bo} = \frac{q}{\dot{m} \cdot h_{fg}}$.

[25] The Stanton number is a measure of the ratio of heat transferred to a fluid to the thermal capacity of the fluid, $\mathbf{St} = \frac{HTC}{G \cdot c_p} = \frac{\mathbf{Nu}}{\mathbf{Re} \cdot \mathbf{Pr}}$.

2.11. Empirical One-Dimensional HTC correlations

Although solving the conservation equations (of mass, momentum, and energy) is an accurate method for determining flow dynamics and heat transfer inside channels in a nuclear reactor core, it is not feasible for everyday operational use due to the large calculation time, complexity of models, and computer memory required. However, since it is necessary to obtain an accurate estimate of heat transfer inside channels for safe reactor operation, a faster and simpler approach is needed.

One such method involves the use of empirically derived HTC correlations (based on experimental trials) to approximate the degree of enhancement of heat transfer due to forced-convection. However, heat transfer in bundles flow geometry is especially dependant on the geometry and various appendages found in the channel; many correlations developed for certain bundle geometries are very inaccurate when applied to others [4].[26] Given that the final channel design of an SCWR has not been finalized as of yet, an HTC correlation is needed in the interim that can provide an accurate conservative estimate of heat transfer. This eliminates the need to develop a new correlation for each unique bundle design, which can become quite expensive, and ultimately irrelevant to the final SCWR design.

Although only a few correlations have been developed for SCW bundle flow geometries, many have been developed for bare tubes. However, their accuracy at determining HTC values can vary significantly depending on flow conditions. Furthermore, variations in the thermophysical properties of SCW can either enhance or impede heat transfer.

In general, HTC correlations relate the degree of enhancement of convective heat transfer in an expression of several non-dimensional numbers.[27]

$$\mathbf{Nu} = f(\mathbf{Re}, \mathbf{Pr}) \tag{2.5}$$

[26] Experiments using bundle flow geometry at supercritical pressures are expensive and require sophisticated equipment and measuring techniques. Furthermore, many of these studies are actually proprietary and not published in the open literature [12].
[27] HTC correlations are given based on the Nusselt number.

Equation (2.5) can be expanded to the following form:[28]

$$\frac{HTC \cdot D}{k} = f_1\left(\frac{G \cdot D}{\mu}\right) \cdot f_2\left(\frac{\mu \cdot c_p}{k}\right) \tag{2.6}$$

The hydraulic diameter is used to relate non-circular channels (such as channels containing bundles) to an equivalent circular value to allow pressure drop and fluid flow calculations.[29] The hydraulic diameter is used in this work [41].[30]

$$D_{hy} = \frac{4 \cdot A_{fl}}{p_{wet}} \tag{2.7}$$

Some HTC correlations specify that thermophysical properties in Equation (2.6) should be obtained at wall conditions while others specify bulk-fluid conditions. It is important to note that this merely depends on the method the author used to correlate the experimental data; there is no set standard. HTC correlations simply try to fit trends of experimental data using non-dimensional numbers and a ratio of some thermophysical properties at wall versus bulk-fluid conditions. The accuracy of their prediction is highly dependent on whether conditions match the experimental parameters from which they were developed.

The most commonly used HTC correlation to predict forced-convection heat transfer at subcritical conditions is the Dittus-Boelter (1930) [2] correlation.[31]

$$\mathbf{Nu_b} = 0.023 \cdot \mathbf{Re}_b^{0.8} \cdot \mathbf{Pr}_b^{n} \tag{2.8}$$

Where, n = 0.4 for heating and 0.3 for cooling. It is valid for single-phase heat transfer in channels for the following parameters: $0.6 \lesssim \mathbf{Pr} \lesssim 160$, $\mathbf{Re}_D \gtrsim 1 \cdot 10^4$, and $L/D_{hy} \gtrsim 10$ [4].

---

[28] The Nusselt number is a measure of the convective heat transfer occurring at the interphase, $\mathbf{Nu} = \frac{HTC}{k} D$ [51]. The Prandtl number is a measure of the relative effectiveness of momentum and heat transport by diffusion in the velocity and thermal boundary layer, respectively, $\mathbf{Pr} = \frac{\mu \cdot c_p}{k}$ [51].

[29] The wetted perimeter includes the portion of perimeter that creates drag to the coolant.

[30] The hydraulic diameter for bare tubes is simply: $D_{hy} = \frac{4 \cdot A_{fl}}{p_{wet}} = \frac{4\left((\pi D^2)/4\right)}{\pi D} = D$.

[31] It is quite curious that while Equation (2.8) is infamously referred to as Dittus-Boelter (1930) [2] correlation, Winterton (1998) [65] showed that the correlation does not in fact appear in the paper from which it is quoted. He recommended referring to the correlation as the Dittus-Boelter (1930) [2] as introduced by McAdams (1942) [66]. However, for the purposes of this thesis, this correlation will be referred to as the Dittus-Boelter (1930) [2] correlation with n = 0.4 assumed by default.

Although the Dittus-Boelter (1930) [2] correlation was developed for subcritical conditions, it can be used to reference enhancement or deterioration of heat transfer at supercritical conditions.[32] The appeal of this correlation lies in its simplicity (it does not require an assumption of wall temperature), especially when compared to more complex correlations that will be discussed in the following sections.

Improvements of these HTC correlations have been ongoing since their inception. One interesting idea, most likely proposed by Petukhov et al. (1961) [42], is to use an integral average of the Prandtl number, $\overline{\mathbf{Pr}}$, (instead of a Prandtl number assessed at the bulk-fluid or wall temperature) across a cross section to better capture properties at the wall versus the bulk-fluid.[33]

$$\overline{\mathbf{Pr}} = \frac{\mu \overline{c_p}}{k} \tag{2.9}$$

Using the integral average Prandtl number requires the calculation of the integrated specific heat.

$$\overline{c_p} = \frac{1}{T_w - T_b} \int_{T_b}^{T_w} c_p \, dT \approx \frac{h_w - h_b}{T_w - T_b} \tag{2.10}$$

Approximately equal to (≈) is used in Equation (2.10) instead of an equal sign (=) as the peak in specific heat (shown in Figure 2-6) might not be accurately captured if it occurred between wall and bulk-fluid conditions.

2.11.1. Conventional SCW HTC correlations

Early SCW HTC correlations closely followed the Dittus-Boelter (1930) [2] correlation approach, however, they were developed based on regions that did not have much change in the thermophysical properties. It was only later, when more complexity was added, that better prediction of heat transfer was reported [4]. The following section outlines efforts made to improve accuracy of HTC correlations and briefly describes the application of each improvement.

---

[32] It is used to provide a conservative estimate of heat transfer.

[33] It should be noted that: $\overline{\mathbf{Pr}}_b = \frac{\mu_b \overline{c_p}}{k_b}$ while $\overline{\mathbf{Pr}}_w = \frac{\mu_w \overline{c_p}}{k_w}$

Bishop et al. (1964) [8] conducted experiments using SCW flowing upward inside tubes and annuli; the correlation developed using their data had a fit of ±15%.

$$\mathbf{Nu}_b = 0.0069 \cdot \mathbf{Re}_b^{0.9} \cdot \overline{\mathbf{Pr}}_b^{0.66} \left(\frac{\rho_w}{\rho_b}\right)^{0.43} \left(1 + 2.4\frac{D_{hy}}{x}\right) \tag{2.11}$$

This correlation is based on experimental data within the following parameters: P = 22.8 – 27.6 MPa, T_b = 282 – 527°C, G = 651 – 3662 kg/m^{2}s, q = 0.31 – 3.46 MW/m^2 [8]. The range of the data set is quite encompassing, specifically as it applies to SCWR, as this covers the majority of proposed operating conditions. However, this correlation was developed in 1964; updated values of thermophysical properties of water have since been published. Therefore, this skews the accuracy of this correlation as it was developed using older, less accurate values. It should be noted that the entrance region term (the last term in Equation (2.11)) is highly dependent on the geometry of the test section.

Unlike the Dittus-Boelter (1930) [2] correlation which only takes into account bulk-fluid properties, the Bishop et al. (1964) [8] correlation uses a ratio of wall to bulk-fluid densities. This makes the correlation more difficult to use, as a wall temperature must be initially assumed (and a loop must be established to solve for the convergence criteria). For experiments with high heat flux, the variation in wall and bulk-fluid thermophysical properties (as modelled by the density ratio) is significant due to the abrupt changes around the pseudocritical point.

While using the same basic correlation structure as the Bishop et al. (1964) [8] correlation, Swenson et al. (1965) [31] proposed the following correlation based on wall conditions.

$$\mathbf{Nu}_w = 0.00459 \cdot \mathbf{Re}_w^{0.923} \cdot \overline{\mathbf{Pr}}_w^{0.613} \left(\frac{\rho_w}{\rho_b}\right)^{0.231} \tag{2.12}$$

This correlation is based on experiments with SCW flowing upward inside bare tubes within the following parameters: P = 22.8 – 41.4 MPa, T_b = 75 – 576°C, T_w = 93 – 649°C, G = 542 – 2150 kg/m^{2}s [31]. Swenson et al. (1965) [31] found that due to the abrupt changes in the thermophysical properties of SCW around the pseudocritical point, conventional correlations based on bulk-fluid temperature did not work. They pointed out that bulk-fluid based correlations assumed that the thermal conductivity decreased smoothly near the pseudocritical

point; however, this is not the case. Figure 2-6 shows a small peak in the thermal conductivity at the pseudocritical point.

Using an updated library of thermophysical properties of water, Mokry et al. (2011) [36] used the same approach as Bishop et al. (1964) [8].

$$\mathbf{Nu}_b = 0.0061 \cdot \mathbf{Re}_b^{0.904} \cdot \overline{\mathbf{Pr}}_b^{0.684} \left(\frac{\rho_w}{\rho_b}\right)^{0.564} \tag{2.13}$$

This correlation was developed using data from Kirillov et al. (2005) [28] (which had 89 runs with 81 data points per run) for SCW flowing upward for the following experimental parameters: P = 24 MPa, T_{in} = 320 – 350°C, T_{out} = 380 – 406°C, T_w < 700°C, G = 200, 500, 1000, 1500 kg/m^{2}s, q = 70 – 1250 kW/m^2. Mokry et al. (2011) [36] excluded experimental data showing DHT. Furthermore, similar to the correlation developed by Bishop et al. (1964) [8], it included a ratio of wall to bulk-fluid densities. However, it should be noted that the range of the heat flux and mass flux of the Mokry et al. (2011) [36] correlation are significantly smaller than those of the Bishop et al. (1964) [8] correlation.

In a comparison study on the accuracy of SCW correlations, Zahlan et al. (2011) [43] applied several HTC correlations to 5668 data points (of which 1314 were at L/D < 50) at all modes of heat transfer.[34] They concluded that Mokry et al. (2011) [36] showed better agreement with their data than other correlations, even though it does not include an L/D mitigation factor [43].

Gupta et al. (2011) [44] used the same approach as Swenson et al. (1965) [31] to try to predict heat transfer to SCW in bare tubes. Using the same data set as Mokry et al. (2011) [36] and updated thermophysical properties, they developed the following correlation.

$$\mathbf{Nu}_w = 0.0033 \cdot \mathbf{Re}_w^{0.941} \cdot \overline{\mathbf{Pr}}_w^{0.764} \left(\frac{\mu_w}{\mu_b}\right)^{0.398} \left(\frac{\rho_w}{\rho_b}\right)^{0.156} \tag{2.14}$$

This correlation was developed using data from Kirillov et al. (2005) [28] for SCW flowing

[34] L/D < 50 defines the entrance region; refer to Section 2.8 for relation to DHT. Furthermore, the comparison study conducted by Zahlan et al. (2011) [43] used bare tube data (heat transfer in bare tubes is different than in bundles).

upward where the experimental parameters were: P = 24 MPa, T_{in} = 320 – 350°C, T_{out} = 380 – 406°C, T_w < 700°C, G = 200, 500, 1000, 1500 kg/m^{2}s, q = 70 – 1250 kW/m^2 [44]. Due to limited experimental parameters, it should be noted that Gupta et al. (2011) [44] has a smaller range of applicability than its parent correlation, Swenson et al. (1965) [31].

2.11.2. Variable exponent SCW HTC correlations

The correlations presented so far attempt to capture the entirety of their respective experimental data using a single expression. However, as shown in Figure 2-6, there is significant deviation in the thermophysical properties of water in the supercritical region. This is especially true around the pseudocritical point where there is a significant peak in specific heat. Rather than using the same correlation for the entirety of the supercritical region, some authors proposed using a variable that is dependent on wall and bulk-fluid temperatures relative to the pseudocritical temperature. The following section provides an overview of some of these correlations.

Krasnoshchekov et al. (1967) [45] improved their original correlation for forced-convective heat transfer in water and CO_2 at supercritical pressure to account for variation of thermophysical properties around the pseudocritical point.[35]

$$\mathbf{Nu}_b = \frac{\frac{\xi}{8}\mathbf{Re}_b \cdot \overline{\mathbf{Pr}}_b}{12.7\sqrt{\frac{\xi}{8}}\left(\overline{\mathbf{Pr}}_b{}^{2/3} - 1\right) + 1.07} \left(\frac{\rho_w}{\rho_b}\right)^{0.3} \left(\frac{\overline{c_p}}{c_{pb}}\right)^n \tag{2.15}$$

Where n is a function of T_w, T_{pc}, & T_b, which are expressed in Kelvin:

$$n = 0.4; \text{ if } \frac{T_w}{T_{pc}} \leq 1 \text{ or } \frac{T_b}{T_{pc}} \geq 1.2$$

$$n = n_1 = 0.22 + 0.18\,\frac{T_w}{T_{pc}}; \text{if } 1 \leq \frac{T_w}{T_{pc}} \leq 2.5$$

$$n = n_1 + 5(n_1 - 2)\left(1 - \frac{T_b}{T_{pc}}\right); \text{ if } 1 \leq \frac{T_b}{T_{pc}} \leq 1.2$$

Their correlation had a fit of ±20% within the following range: $8{\cdot}10^4 < \mathbf{Re}_b < 5{\cdot}10^5$, 0.85 <

[35] The correlation by Petukhov and Kirillov (1958) [68] is: $\mathbf{Nu}_0 = \frac{\frac{\xi}{8}\mathbf{Re}_b \cdot \overline{\mathbf{Pr}}_b}{12.7\sqrt{\frac{\xi}{8}}\left(\overline{\mathbf{Pr}}_b{}^{2/3} - 1\right) + 1.07}$. Where ξ is the friction factor for turbulent flow: $\xi = (1.82 \cdot \log_{10}\mathbf{Re}_b - 1.64)^{-2}$ [68].

$\overline{\mathbf{Pr}}_b < 65$, $0.9 < \rho_w / \rho_b < 1.0$, $0.02 < \bar{c_p}/c_{pb} < 4.0$, $0.9 < T_w / T_{pc} < 2.5$, $46 < q < 2\ 600$ kW/m^2, $x/D \geq 15$ [45].

Yamagata et al. (1972) [34] applied the concept of the Eckert number discussed in Section 2.10.1 for forced-convection heat transfer to SCW in bare tubes.

$$\mathbf{Nu}_b = 0.0135 \cdot \mathbf{Re}_b^{0.85} \cdot \mathbf{Pr}_b^{0.8} \cdot F_c \tag{2.16}$$

Where F_c is a function of the Eckert number:

$$F_c = 1.0; \text{ for } \mathbf{E} > 1$$

$$F_c = 0.67 \cdot \mathbf{Pr}_{pc}^{-0.05} \left(\frac{\bar{c_p}}{c_{pb}}\right)^{n_1}; n_1 = -0.77\left(1 + \frac{1}{\mathbf{Pr}_{pc}}\right) + 1.49; \text{ for } 0 \leq \mathbf{E} \leq 1$$

$$F_c = \left(\frac{\bar{c_p}}{c_{pb}}\right)^{n_1}; n_2 = -1.44\left(1 + \frac{1}{\mathbf{Pr}_{pc}}\right) - 0.53; \text{ for } \mathbf{E} < 0$$

Rather than specify a range based on the experiment that this correlation was based, Yamagata et al. (1967) [34] recommended using a range as specified by the Eckert number.

Jackson (2002) [3] modified the correlation proposed by Krasnoshchekov et al. (1967) [45] for forced-convection heat transfer in SCW to match that of the format used by Dittus-Boelter (1930) [2] giving it a simpler form, and making it easier to use.

$$\mathbf{Nu}_b = 0.0183 \cdot \mathbf{Re}_b^{0.82} \cdot \mathbf{Pr}_b^{0.5} \left(\frac{\rho_w}{\rho_b}\right)^{0.3} \left(\frac{\bar{c_p}}{c_{pb}}\right)^{n} \tag{2.17}$$

Where n is a function of T_w, T_{pc}, & T_b, which are expressed in Kelvin:

$$n = 0.4; \text{ if } T_b < T_w < T_{pc} \text{ or } 1.2 \cdot T_{pc} < T_b < T_w$$

$$n = 0.4 + 0.2\left(\frac{T_w}{T_{pc}} - 1\right); \text{if } T_b < T_{pc} < T_w$$

$$n = 0.4 + 0.2\left(\frac{T_w}{T_{pc}} - 1\right)\left[1 - 5\left(\frac{T_b}{T_{pc}} - 1\right)\right]; \text{ if } T_{pc} < T_b < 1.2 \cdot T_{pc} \text{ and } T_b < T_w$$

Jackson (2002) [3] recommended using this correlation for the entirety of the supercritical region as the different exponents are meant to account for the variation of thermophysical properties.

2.11.3. SCW HTC correlations developed for Bundles

While the correlations presented in the previous sections provide a conservative estimate of heat transfer inside channels (as they were developed using predominantly bare tube data), they would not capture enhancement of heat transfer due to appendages present in bundle geometries. Dyadyakin and Popov (1977) [13] developed a correlation for a tight 7-element bundle, which fit ±20% of the 504 experimental data set.[36]

$$\mathbf{Nu}_b = 0.021 \cdot \mathbf{Re}_b^{0.8} \cdot \overline{\mathbf{Pr}}_b^{0.7} \left(\frac{\rho_w}{\rho_b}\right)^{0.45} \left(\frac{\mu_b}{\mu_{in}}\right)^{0.2} \left(\frac{\rho_b}{\rho_{in}}\right)^{0.1} \left(1 + 2.5\frac{D_{hy}}{x}\right) \qquad (2.18)$$

The experimental setup used short, finned bundles (L_h = 0.5 m) at the following parameters: P = 24.5 MPa, T_b = 90 – 570°C, G = 500 – 4000 g/m^{2}s, q < 4.7 MW/m^2 [13].

This correlation was developed for application in transport (naval) reactors and not for power reactors. Correlations developed for certain bundle geometries are very inaccurate when applied to other geometries. However, since this correlation was developed specifically for a 7-rod bundle with helical fins, it will be interesting to apply to the experimental data used in this work (single- and 3-rod bundles with helical fins).

2.12. Objectives

In light of the literature review, the objectives of this work are listed below:

1. Propose and verify a universal method to accurately predict wall temperatures and HTCs using HTC correlation(s) for various annular- and bundle-flow geometries cooled with upward flow of SCW.
2. Investigate onset of DHT and IHT regimes in various annular- and bundle-flow geometries cooled with SCW compared to bare tubes.

[36] Hexagonal bundle design; 7-rods (6 peripheral +1 central; D_{rod} = 5.2 mm, L = 0.5m), each rod is equipped with 4 helical fins (fin height = 0.6 mm, thickness = 1mm, helical pitch = 400mm) [13].

Chapter 3. Methodology and Experimental Datasets

This chapter outlines the methodology used to complete the heat transfer analysis, which was conducted to meet the objectives discussed in the Introduction and in Section 2.12. In this work, empirical HTC correlations were used to model heat transfer in several simple bundle flow geometries.[37] This was performed by writing one-dimensional heat transfer numerical models in Matlab and comparing the RMS errors of each correlation.

The methodology presented in this chapter is broken down into several sections with each section detailing a different experiment and model.

Section 3.1 outlines the test facility and test sections of the single and 3-rod bundle trials, conducted at the National Technical University of Ukraine "Kiev Polytechnic Institute" (KPI) in 2009, and the methodology used to develop a numerical model [46]. For these trials, experimental wall temperatures were used to calculate the thermal conductivity of the heated rod(s).

Section 3.2 outlines the methodology used to calculate resultant UO_2 fuel temperature profiles of the single-rod channel experiments discussed in Section 3.1 using both: a spline of the experimentally measured inner wall temperatures (shown in Table A-1) and outer wall temperatures calculated using Jackson (2002) [3].

Section 3.3 outlines the test facility and test section of the 2×2 rod bundle trials, conducted in the SWAMUP test facility at Shanghai Jiao Tong University in 2015, and the methodology used to develop the numerical model is presented [47]. Outer wall temperatures, calculated from experimentally measured inner wall temperatures, were transcribed from Zhao et al. (2015) [47].

[37] The Dyadyakin and Popov (1977) [13] correlation was the only non-bare tube correlation used. It was developed for a short 7-rod bundle with helical fins.

3.1. Heat Transfer to SCW Flowing Upward in Vertical Single-Rod and 3-Rod Bundles

The following section outlines the experimental setup and methodology used to model the experimental setup of SCW flowing upward in a single-rod and 3-rod bundle flow geometry obtained in an SCW loop at the National Technical University of Ukraine "Kiev Polytechnic Institute" in 2009 [48].

3.1.1. Test Facility

The SCW experimental setup is an "open" Stainless-Steel (SS) loop operating at pressures up to 28 MPa and at temperatures up to 700°C. Chemically desalinated water (pH = 7.5 and an average hardness of 0.2 μg-equiv/kg) was used as a coolant. Test sections were installed vertically with an upward flow of SCW and were directly heated with a 90 kW AC power supply, as shown in Figure 3-1.

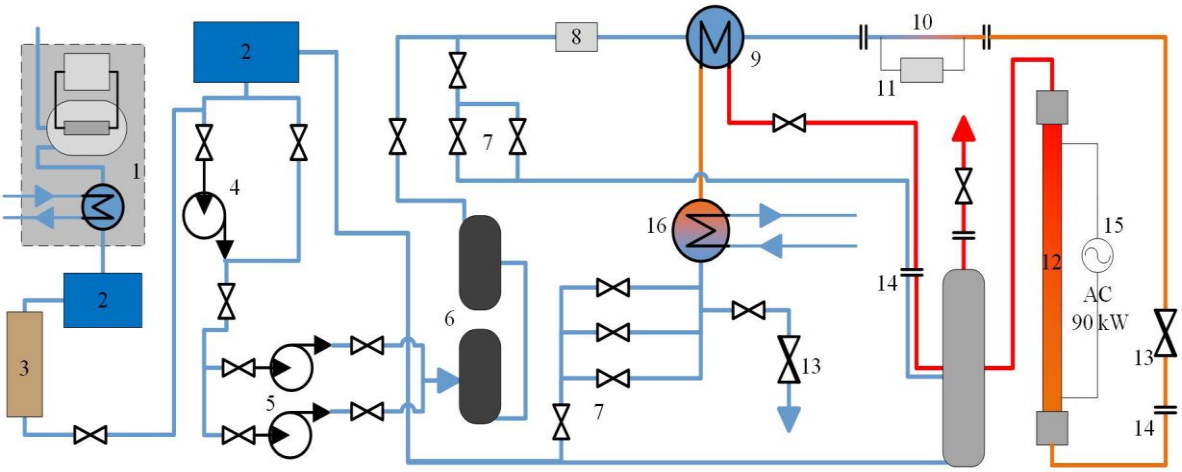

Figure 3-1. A general schematic of SCW experimental setup at KPI [49].

1	Electro-distillator	5	Plunger pump	9	Heat exchanger	13	Throttling valve
2	Accumulator reservoir	6	Damping reservoir	10	Electrical preheater	14	Electro-isolating valve
3	Ion-exchange filter	7	Regulating valve	11	Dynamotor	15	Main power supply
4	Boosting pump	8	Turbine flow meter	12	Test section	16	Cooler

3.1.2. Test-Section Design

Heated elements in each flow geometry consist of a hollow rod that has a 485 mm heated length (rods are actually thin-wall tubes) with four helical ribs wound over a 400 mm pitch, as shown in Figure 3-2 & Figure 3-3. SCW flows in the gap between a heated rod and a cylindrical flow tube (displacer).

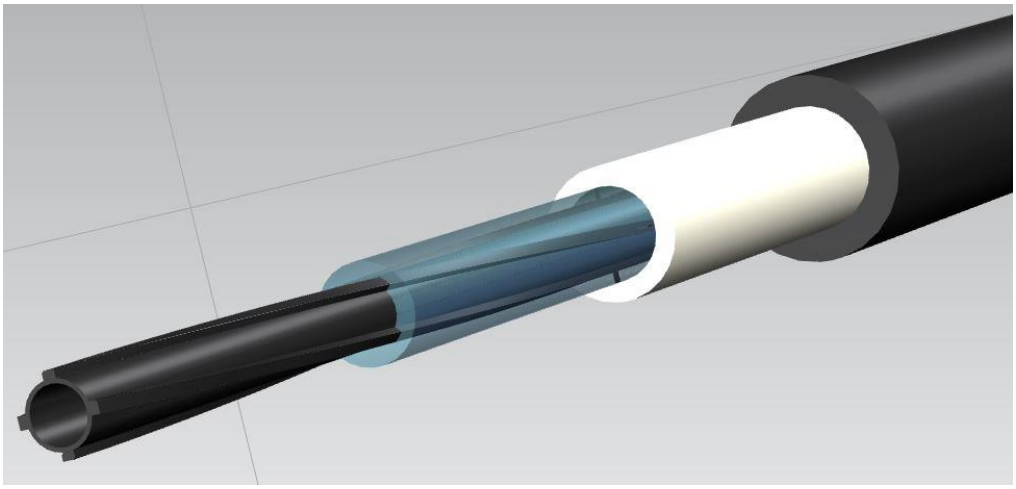

Figure 3-2. 3-D image of a heated single-rod annular channel [49].

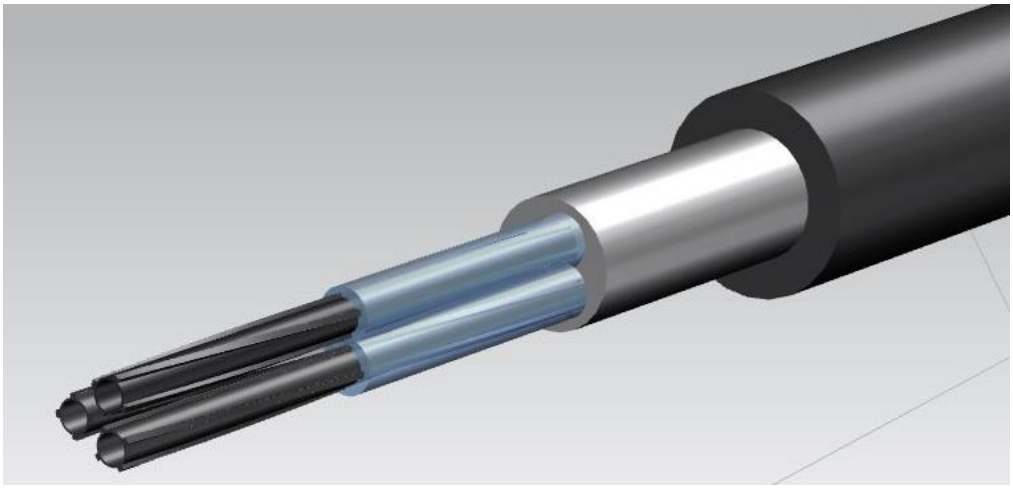

Figure 3-3. 3-D image of a heated 3-rod bundle channel [49].

The single-rod annular channel setup allowed the formation of a peripheral sub-channel, whereas the flow geometry in the channel with the 3-rod bundle allowed the formation of central and peripheral sub-channels, as shown in Figure 3-2 & Figure 3-3, respectively. Rods were heated through direct heating with an Alternating Current (AC) going through the wall(s) of the rod (tube).

Calibrated SS fins of 0.1 mm thickness welded to the rods provided a 1 mm gap between the rod ribs and a shaped dielectric displacer, as shown in Figure 3-4. The displacers were inserted into pressure tubes of 18/12 mm (annular channel) and 32/20 mm (3-rod bundle channel) OD/ID diameters, respectively.

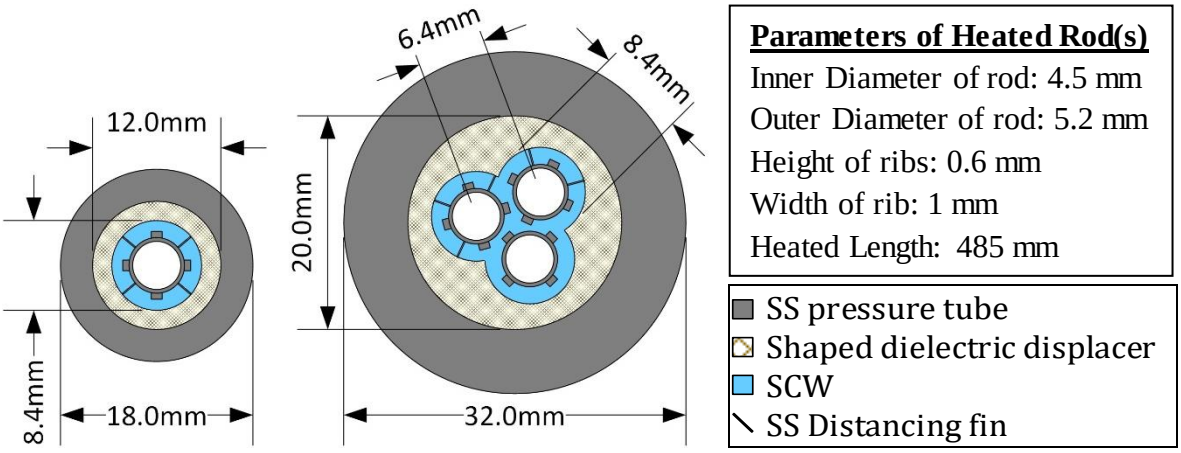

Figure 3-4. Radial cross-section of an annular channel and a 3-rod bundle [49].[38]

Hydraulic equivalent diameters were determined to be 2.67 mm for the single-rod channel and 2.40 mm for the 3-rod bundle channel. The hydraulic-equivalent diameters are calculated using Equation (2.7).

Wall temperatures in the test sections were measured using seven thermocouples installed along the heated length on the inner surface of a heated rod (tube) at 95, 195, 255, 315, 375, 415, and 475 mm from the inlet of the heated section (the first thermocouple is located beyond the entrance region ($L/D_{hy} > 25$). Each thermocouple was tightly engraved into a copper plug of a diameter equal to the inner diameter of the rod (tube). The plugs were covered with heat-resistant silicone resin that provided electrical insulation. Good contact and high thermal conductivity of the copper plugs allowed the measurement of an average temperature in each cross section with good response time. This was verified by isothermal tests.

Bulk-fluid temperatures were measured by using chromel-alumel ungrounded sheathed thermocouples of 0.2 mm diameter (wire) inserted into the fluid flow inside mixing chambers.

[38] SS-304 properties are used to approximate the electrical resistivity and thermal conductivity of the Ukrainian stainless steel: $^{12}Cr^{18}Ni^{10}Ti$ Stainless Steel (which is used in this experiment) as they have similar content and the material properties of SS-304 are publicly available.

These chambers were used to minimize non-uniformity in a cross-sectional temperature distribution and to dampen pressure pulsations within the test sections. Inlet and outlet sections of hydrodynamic stabilization were provided.

3.1.3. Instrumentation and Test Matrix

The following test section parameters were measured or calculated in the experiments (text matrix is listed in Table 2-1):

- Test-section current and voltage, which were used to calculate the power.
- Pressure at the test section inlet.
- Bulk-fluid temperatures at the test section inlet and outlet.
- Thermocouples were calibrated within the temperature range of 20°C – 450°C.
- Inner-wall temperatures of the heated rod(s) were measured by using a probe with seven thermocouples.

Table 3-1. General test matrix for annular channel and 3-rod bundle trials.

Flow Geometry	General test matrix		
	T_{in},°C	q, MW/m^2	G, kg/m^{2}s
Single-rod channel	125 – 352	1.03 – 3.45	800 – 3000
3-rod bundle channel	125 – 337	1.25 – 4.58	1000 – 2700

The instrumentation used to measure the loop parameters was thoroughly checked and calibrated. The maximum uncertainties of primary parameters are listed in Table 3-2.

Table 3-2. Uncertainties of measured and calculated parameters [49].

	Parameters	Maximum Uncertainty
Measured Parameters	**Inlet pressure**	± 0.2%
	Bulk-fluid temperature	± 3.4%
	Wall temperature	± 3.2%
Calculated Parameters	**Mass flow rate**	± 2.3%
	Heat flux	± 3.5%
	HTC	± 12.7%
	Heat loss	≤ 3.4%

Experimental data was recorded using a Data Acquisition System once required power levels and flow conditions were reached and stabilized (steady-state conditions). Increases in power

were limited by the wall temperature; a power trip was set up at a wall-temperature of 620°C. Heat-loss characteristics of the test sections were determined prior to performing experiments, as shown in Table 3-2.

3.1.4. Experimental Data Sets

The experimental inner wall temperatures for single-rod and 3-rod bundle trials are presented in Appendix A. The data set is analyzed using a program written in Matlab, shown in Appendix B, which called properties of water from NIST REFPROP at each iteration [1].[39]

3.1.5. Variable Heat Flux along the Heated Length

Since the rods (tubes) were electrically heated, the electrical resistance of a rod (tube) is directly dependent on local wall temperatures through the electrical resistivity (an intrinsic property),[40] which can be obtained from a reference table specific to the rod material [50].

$$R_{el} = \frac{\rho_{el}(T) \cdot L_h}{A} \tag{3.1}$$

Linear interpolation is used to approximate electrical resistivity between the seven measured wall temperature points. Variation in electrical resistivity along the heated length in the single and 3-rod bundle trials is illustrated in Figure 3-5; data points in Figure 3-5 are determined using experimentally measured inner wall temperature values, and the lines connecting them represent linearly interpolated values.

---

[39] Thermal and transport properties of water were retrieved from NIST REFPROP version 9.0 software [63]. The properties of water in NIST are based on the 1995 formulation by the International Association for the Properties of Water and Steam [60, 61, 62].

[40] An intrinsic property is a property of the material itself, independent of how much of the material is present or its form.

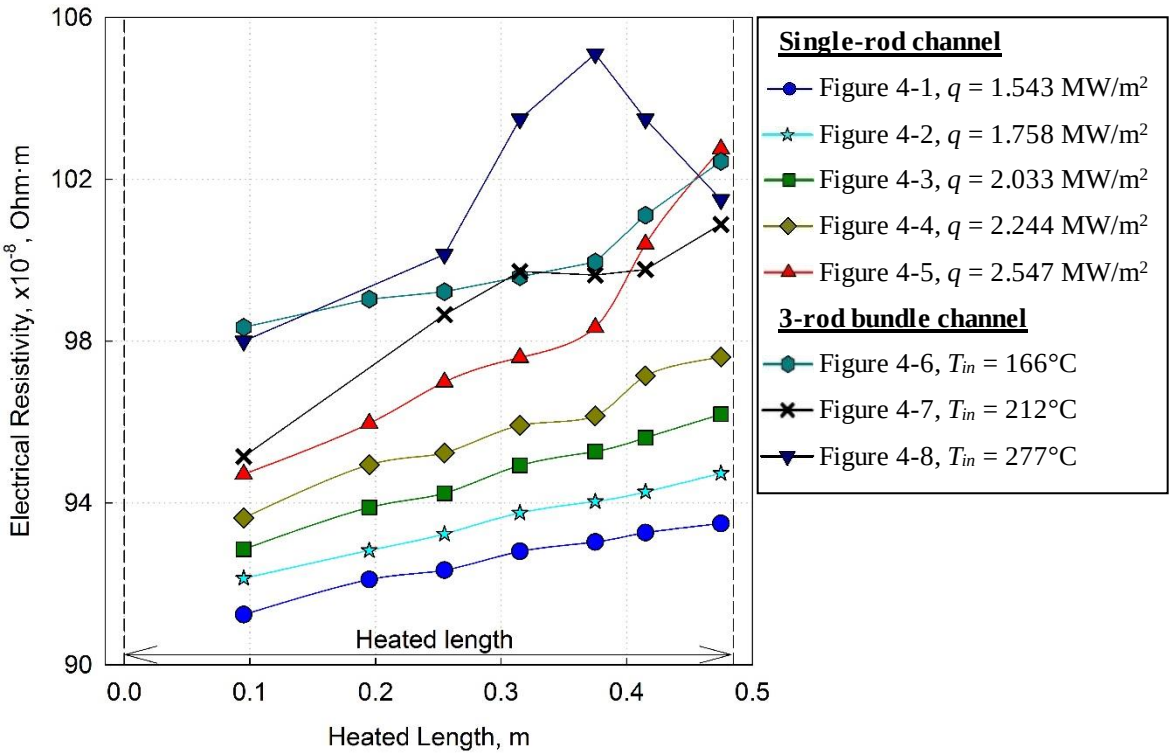

Figure 3-5. Variation of electrical resistivity for SS-304 along the heated length.

Changes in electrical resistivity across the heated length in the single-rod annular channel trials were less than 5% for $q \leq 2.244$ MW/m^2, and ~ 9% for $q = 2.547$ MW/m^2. This is due to a large spike in wall temperatures at the outlet region due to onset of DHT (discussed in Section 4.1.5). Variations in electrical resistivity were greater than 5% for all 3-rod bundle tests.

The electrical resistance of a single, electrically heated, (hollow) rod (where the cross-section illustrated in Figure 3-4), is determined using the following equation:

$$R_{el} = \frac{4 \cdot L_h \cdot \rho_{el}(T)}{\pi (D_{w,o}^2 - D_{w,i}^2)} \tag{3.2}$$

However, the electrical resistance of three electrically heated, (hollow) rods in parallel (the cross-section illustrated in Figure 3-4), is determined using the following equation:

$$R_{el} = \frac{12 \cdot L_h \cdot \rho_{el}(T)}{\pi (D_{w,o}^2 - D_{w,i}^2)} \tag{3.3}$$

Electric current flowing through a rod is a function of both: the power generated and the electrical resistance.

$$I = \sqrt{\frac{Q}{R_{el}}} \tag{3.4}$$

Therefore, the electric current flowing through the (hollow) rod(s) in either experiment can be expressed in terms of the power and average resistance over all axial positions.[41]

$$I = \sqrt{\frac{q_{ave} \cdot L_h \cdot p_h}{\frac{\int_0^n R_{el}(i)\, di}{n}}} \tag{3.5}$$

Finally, local heat flux (assuming variable heat flux) is a function of electric current and local electrical resistance.

$$q = \frac{I^2 \cdot R_{el}}{p_h \cdot L_h} \tag{3.6}$$

The equation above illustrates that the resultant power in a rod will be dependent on its local wall temperature, and thus the heat flux will vary slightly along the heated length.

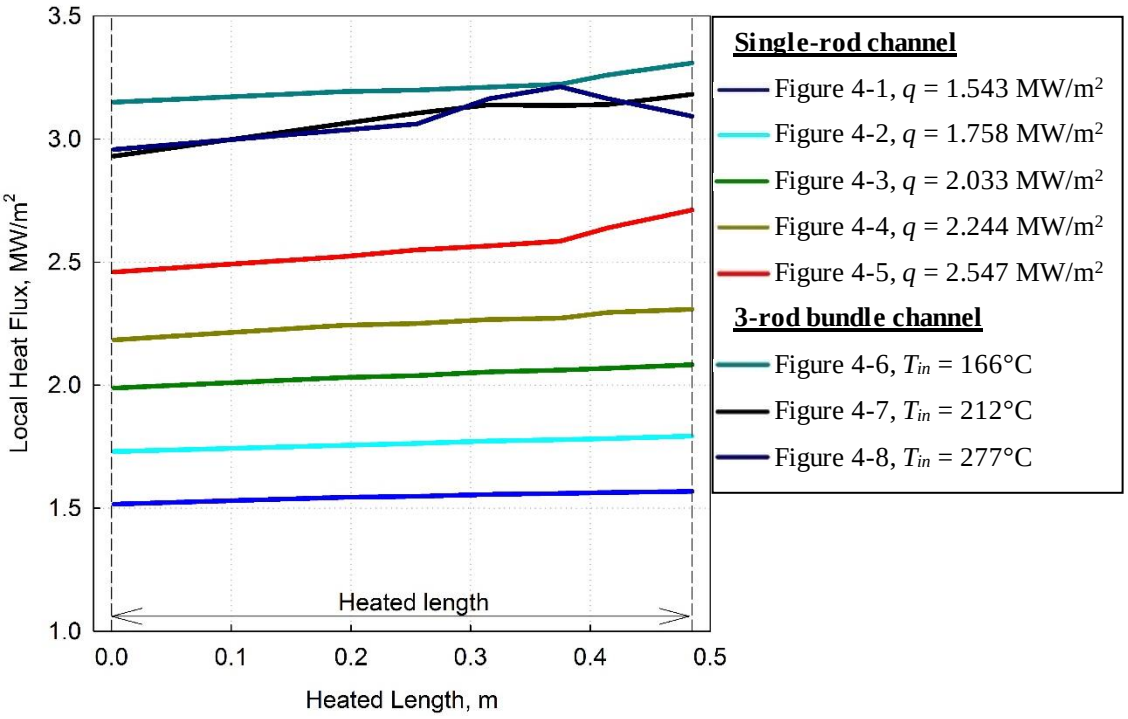

Figure 3-6. Variation of heat flux along the heated length.

[41] The average resistance is calculated by taking an integral of the resistances over all sections, *i*, then dividing by the total number of sections, *n*.

The heat flux along the heated length in the annular channel data set, as shown in Figure 3-6, mirrors the trends of the electrical resistance (Figure 3-5).

Volumetric (electric) heat generation in the hollow rod can be derived from the heat flux equation for a given geometry.

$$q \cdot p_h \cdot L_h = q_v \frac{\pi\left(D_{w,o}^2 - D_{w,i}^2\right)}{4} L_h \tag{3.7}$$

Which simplifies to the following equation for a hollow rod geometry:

$$q_v = \frac{4 \cdot q \cdot p_h}{\pi\left(D_{w,o}^2 - D_{w,i}^2\right)} \tag{3.8}$$

3.1.6. Determination of Experimental HTCs

By applying a heat balance to the test section with an axial-step increase set to 1 mm, and assuming negligible heat losses, the change in the specific enthalpy between two axial positions, can be determined [51].

$$\Delta h_b = \frac{q \cdot dx \cdot p_h}{A_{fl} \cdot G} \tag{3.9}$$

In both test sections, pressure losses along the heated length were considered negligible. The bulk-fluid temperature can be determined based on a calculated specific-enthalpy value and a corresponding pressure in a particular cross section [51].

$$T_b = f(h_b, P) \tag{3.10}$$

Thermophysical properties of SCW at each cross section were calculated based on the inlet pressure and the local bulk-fluid temperature using NIST REFPROP [1] software. Outer wall temperatures, at the rod surface (disregarding fins), are determined by deriving a general solution for the temperature distribution in a tube with uniform volumetric heat generation [51]. Steady state conditions and one-dimensional radial heat conduction were assumed.

$$T_{w,o,sur} = T_{w,i} + \frac{q_v}{8 \cdot k(T)} \left[\frac{D_{w,o}^2 - D_{w,i}^2}{2} - D_{w,o}^2 \cdot \ln\left(\frac{D_{w,o}}{D_{w,i}}\right) \right] \tag{3.11}$$

However, due to the presence of ribs on the surface of the rods, as shown in Figure 3-4, there

was a change in the outer diameter depending on location causing a variation in temperature at the surface of the rod. Thus, the temperature at the rib tip must also be determined.

$$T_{rib} = T_{w,i} + \frac{q_v}{8 \cdot k(T)} \left[\frac{\left(D_{w,o} + H_{rib}\right)^2 - D_{w,i}^2}{2} - \left(D_{w,o} + H_{rib}\right)^2 \cdot \ln\left(\frac{D_{w,o} + H_{rib}}{D_{w,i}}\right) \right] \quad (3.12)$$

Given these two temperatures, a perimeter-weighted temperature was used to determine the average temperature of the outer wall.

$$T_{w,o} = \frac{T_{rib} \cdot W_{rib} + T_{w,o,sur} \cdot (p_h - 4 \cdot W_{rib}) + \frac{T_{w,o,sur} + T_{rib}}{2} (8 \cdot H_{rib})}{p_h} \quad (3.13)$$

Using the average outer wall temperature, Newton's law of Cooling can be used to express the experimental HTC, as the rate of convection per unit area is inversely proportional to the temperature difference between the wall and the bulk-fluid.

$$HTC_{exp} = \frac{q}{T_{w,o} - T_b} \quad (3.14)$$

3.1.7. Determination of Calculated Inner Wall Temperatures

The calculated inner wall temperature was determined by determining the outer wall temperature using HTC correlations and then applying Fourier's law of conduction in a concentric cylinder geometry. Section 2.11 summarizes SCW HTC correlations used to predict outer wall temperatures by determining the HTC at each axial iteration [52].[42]

$$T_{w,o} = \frac{q}{HTC} + T_b \quad (3.15)$$

Outer wall temperatures calculated using HTC correlation do not account for the presence of ribs (which act like fins; i.e. improve heat transfer). The efficiency of a rib is dependent on the ratio of actual to maximum temperature between the rib base and the bulk-fluid [51].[43]

[42] The calculated outer temperature is not the perimeter weighted as the presence of ribs is accounted for later in the section using fin equations.

[43] Maximum heat transfer from the fin can be achieved by having infinite thermal conductivity ($k \rightarrow \infty$); this allows the temperature at the base of the fin to reach the bulk-fluid temperature.

$$\eta_f = \frac{q}{q_{max}} = \frac{q}{HTC \cdot A_{rib} \cdot (T_{w,o} - T_b)} \tag{3.16}$$

Equation (3.16) can be simplified if the tip of a single rectangular rib is assumed to be adiabatic [51].[44]

$$\eta_{fin} = \frac{tanh(m \cdot L_c)}{m \cdot L_c} \tag{3.17}$$

Where:

$$m = \sqrt{\frac{2 \cdot HTC}{k_{SS}(T) \cdot W_{rib}}} \tag{3.18}$$

Given that convection from a fin tip is rather complex, it is prudent to approximate heat loss from the fin tip by assuming it is insulated, and using a corrected fin length [51].

$$L_c = H_{rib} + \frac{W_{rib}}{2} \tag{3.19}$$

The overall surface efficiency of a rod equipped with four ribs attached is characterized by the following equation [51]:

$$\eta_o = \frac{q}{q_{max}} = \frac{q}{HTC \cdot A_t \cdot (T_{w,o} - T_b)} \tag{3.20}$$

Given that:

$$A_t = N \cdot A_{rib} + A_b \tag{3.21}$$

Where N represent the number of ribs attached to the rod, A_b represents the area of the rod that is not covered by the ribs, and A_{rib} represents the total surface area of a rib.

Equation (3.20) can be simplified if the rib tips are assumed to be adiabatic [51].

$$\eta_o = 1 - \frac{4 \cdot A_{rib}}{A_t}\left(1 - \eta_{fin}\right) \tag{3.22}$$

Once the overall fin efficiency is determined, the effect of all four ribs on wall temperature is

[44] An adiabatic process is a process where no heat or matter is transferred between a thermodynamic system and its surroundings.

captured by the following equation.[45]

$$T_{w,o-calc} = \frac{q}{\eta_o \cdot HTC} + T_b \tag{3.23}$$

The error at each measured point is defined as:

$$\text{Error} = \frac{\text{calc}-\text{exp}}{\text{exp}} \tag{3.24}$$

Root Mean Squared (RMS) Error analysis was used to determine the deviation of experimental inner wall temperatures from their calculated counterparts.[46]

$$\text{RMS Error} = \sqrt{\frac{\sum_{i=1}^{n}(\text{Error})^2}{n}} \cdot 100\% \tag{3.25}$$

3.1.8. Flowchart of Method for Section 3.1

Figure 3-7 illustrates the methodology presented above as a flowchart to better explain the steps taken in this section.

[45] It should be noted that ribs in this experiment are helical. However, there is no explicit way to implement the twisting of the ribs into the model. Since a helical scenario would increase turbulence, and thus improve heat transfer, the model is assumed to provide a conservative estimate of the experiment.

[46] RMS error is used in this thesis instead of Mean Absolute Error as it gives a greater weight to large errors, since in this case, they are particularly undesired.

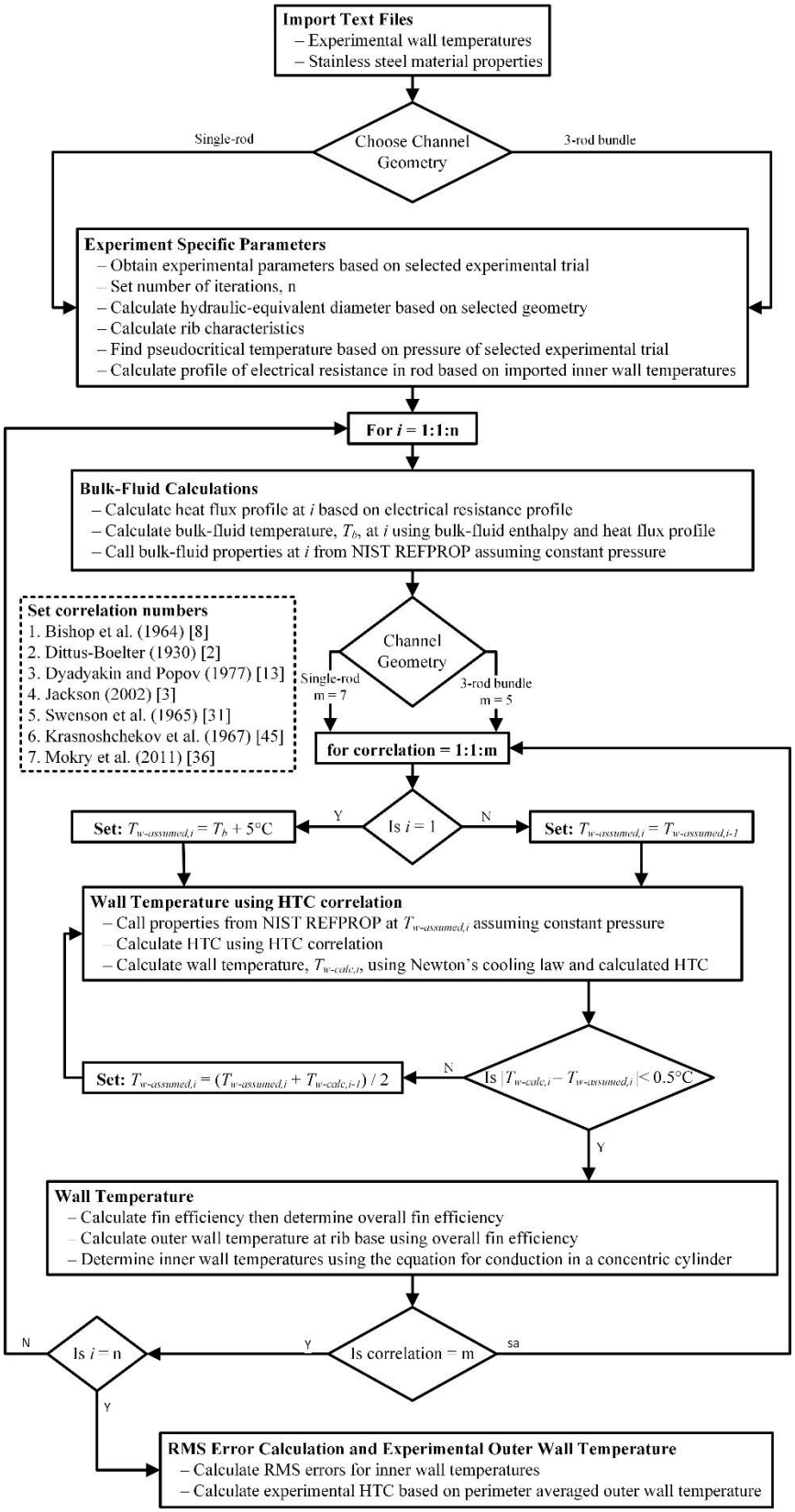

Figure 3-7. Method used to calculate inner wall temperature for the experiment outlined in Section 3.1.

3.2. UO_2 Fuel Temperature Profiles of Single-Rod Annular Channels

The relevance of the experimental data detailed in Section 3.1 to nuclear engineering can be illustrated by modelling heat generation in the single-rod annular channel trials by UO_2 fuel pellets rather than by electrical resistance.

3.2.1. Design of Nuclear Fuel Model

To obtain a more representative model, the same channel geometry, pressure, mass flux, and heat fluxes as the experimental trials was used. The possibility of applying these experimental conditions in non-research applications is dependent on ensuring that the maximum UO_2 fuel temperature does not exceed the industry accepted operating limit of 1850°C [53].

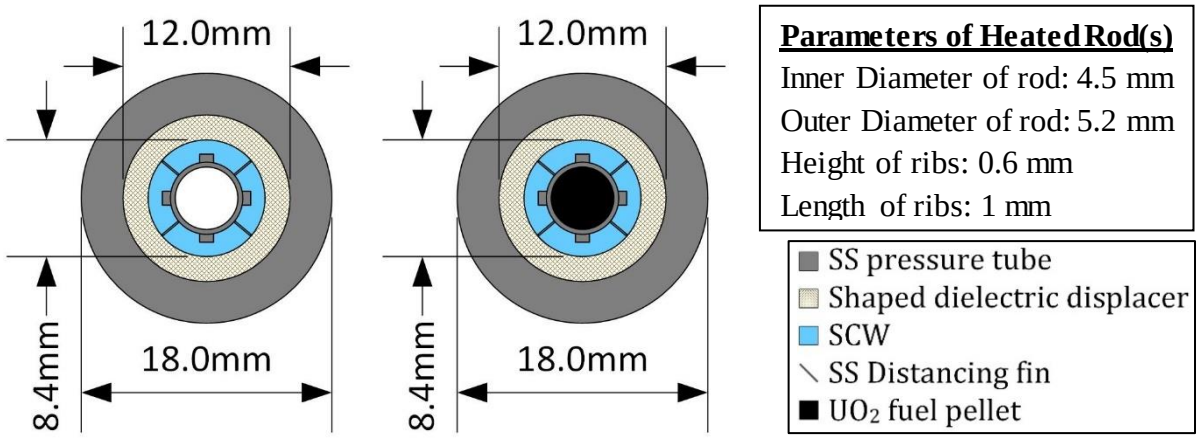

Figure 3-8. Cross-sectional view of: an electrically heated and UO_2 filled single-rod channel [54].

In the experimental test section, wall temperatures were measured using seven thermocouples installed along the heated length on the inner surface of the heated rod (tube); the first thermocouple was located beyond the entrance region ($L/D_{hy} > 25$) [48]. A spline of the seven experimental inner wall temperatures was used to obtain an outer wall temperature profile.

3.2.2. Heat conduction through Stainless Steel-304 sheath

Since experimental electrical heat generation was given in terms of heat flux, the equivalent value of volumetric heat generation in UO_2 fuel is a function of the geometry.[47]

[47] It was assumed that there was no gap; the fuel pellet diameter is equal to the inner SS sheath diameter.

$$q_v = \frac{4 \cdot q \cdot p_h}{\pi \cdot D_{sh,i}^2} \tag{3.26}$$

Table 3-3 relates given experimental heat fluxes to equivalent volumetric heat generation values based on the rod geometry shown in Figure 3-8. It should be noted that the values in Table 3-3 are averaged (for easier readability), however the calculations accounted for a variation of heat flux due to changes in electrical resistance along the heated length.

Table 3-3. Experimental heat fluxes versus their corresponding volumetric heat generation values [54].

Trial	Heat Flux, MW/m^2	Volumetric Heat Generation, MW/m^3
1	1.543	2048
2	1.758	2334
3	2.033	2699
4	2.244	2979
5	2.547	3381

The wall temperature of the SS-304 sheath is determined by calculating the HTC using the Jackson (2002) [3] correlation and then compensating for the presence of ribs using the overall fin efficiency, η_o. The Jackson (2002) [3] correlation was used as it has some sensitivity of wall conditions, and thus can capture, to a limited extent, onset of DHT.

$$T_{sh,o} = \frac{q_v \cdot \pi \cdot D_{sh,i}^2}{4 \cdot p_h \cdot \eta_o \cdot HTC} + T_b \tag{3.27}$$

Given the thickness of the SS-304 sheath (0.7 mm) compared to the diameter of the UO_2 fuel (4.5 mm), and the thermal conductivity of SS-304 sheath (~ 21 W/m·K as shown in Figure 3-9) compared to that of UO_2 (~ 2.5 W/m·K as shown in Figure 3-10), it was deemed unnecessary to conduct an iterative approach on the radial change in temperature of the SS-304 sheath. Rather, the inner sheath temperature is determined using a modified form of Fourier's law for conduction in concentric cylinders [52].

$$T_{sh,i} = T_{sh,o} + q_v \frac{\pi \cdot D_{sh,i}^2 \cdot D_{sh,o}}{16 \cdot p_h \cdot k(T)} \ln\left(\frac{D_{sh,o}}{D_{sh,i}}\right) \tag{3.28}$$

Since thermal conductivity in the literature is only available for some temperatures for SS-304 (data points illustrated in Figure 3-9), interpolation is used [55].

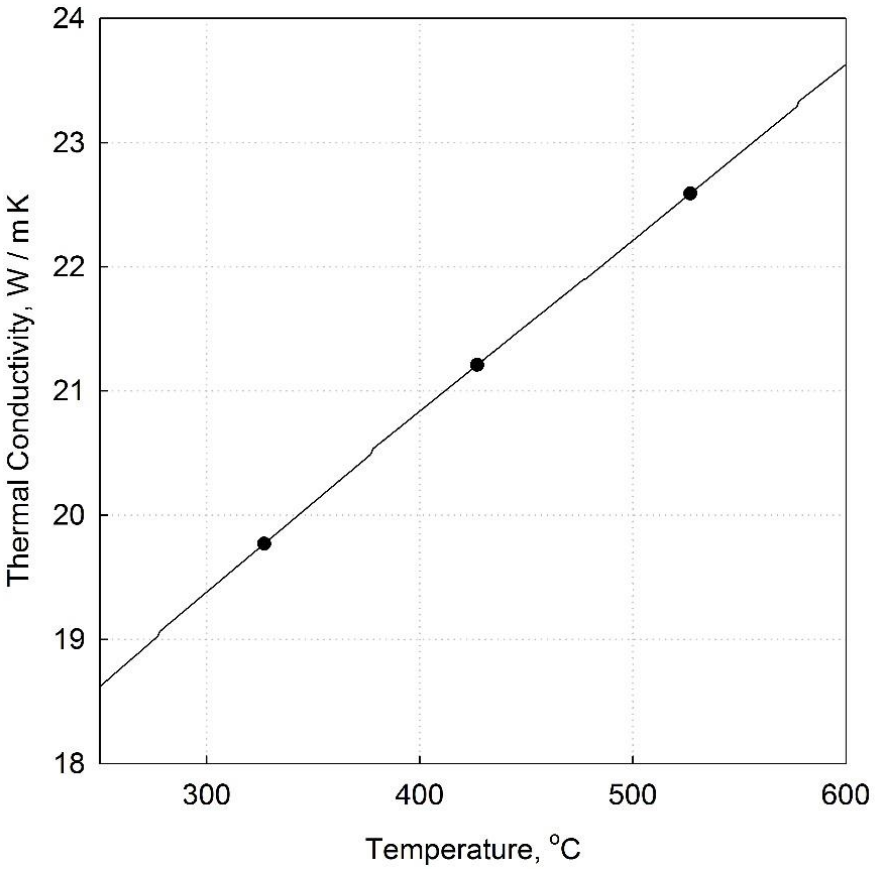

Figure 3-9. Thermal Conductivity variation of SS-304 between 250°C – 600°C

As shown in Figure 3-9, the thermal conductivity of the SS-304 varies linearly between 250°C and 600°C.

The change in the thermal conductivity both axially and radially can be determined by assuming uniform heat generation rate in the fuel pellet. The thermal conductivity for 95% dense UO_2 is defined by the correlation shown in Figure 3-10 [56].

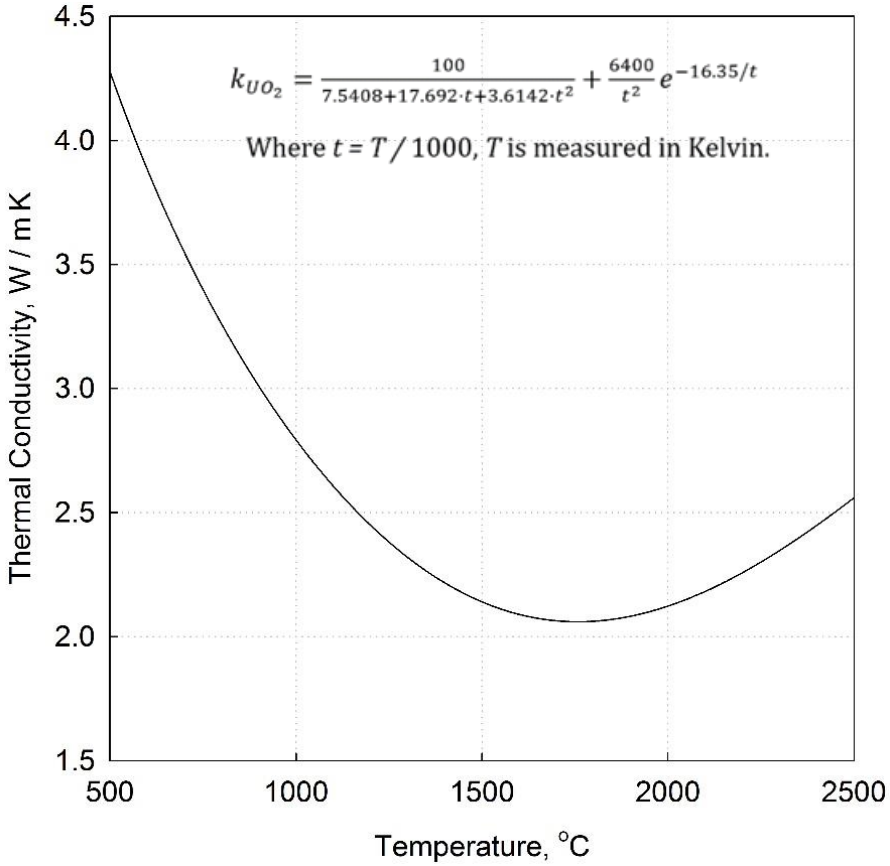

Figure 3-10. Thermal Conductivity variation of 95% dense UO_2 between 500°C – 2500°C.

Heat conduction is proportional to the thermal conductivity and temperature [55]. The fuel temperature was calculated using an analytical solution to temperature distribution in a solid with uniform heat generation. It was assumed that the temperature, at the outer surface of the fuel was equal to the inner sheath temperature, and that there was no gap [57].

$$T_f(r) = T_{sh,i} + \frac{q_v}{4k_f(T)}\left({r_f}^2 - r^2\right) \tag{3.29}$$

3.3. Heat Transfer to SCW flowing upward in a vertical 2×2 Rod Bundle

The experimental data of SCW flowing upward in a 2×2 rod bundle flow geometry was obtained in an SWAMUP test facility at Shanghai Jiao Tong University in 2015 for a wide range of operating conditions [47].

3.3.1. Test Facility

The SWAMUP facility consists of the main test loop, a cooling water loop, a water purification loop, and I&C system [47]. The main test loop consists of a circulating pump, pre-heater, mixing chamber, two heat exchangers, accumulator and test sections, as shown in Figure 3-11.

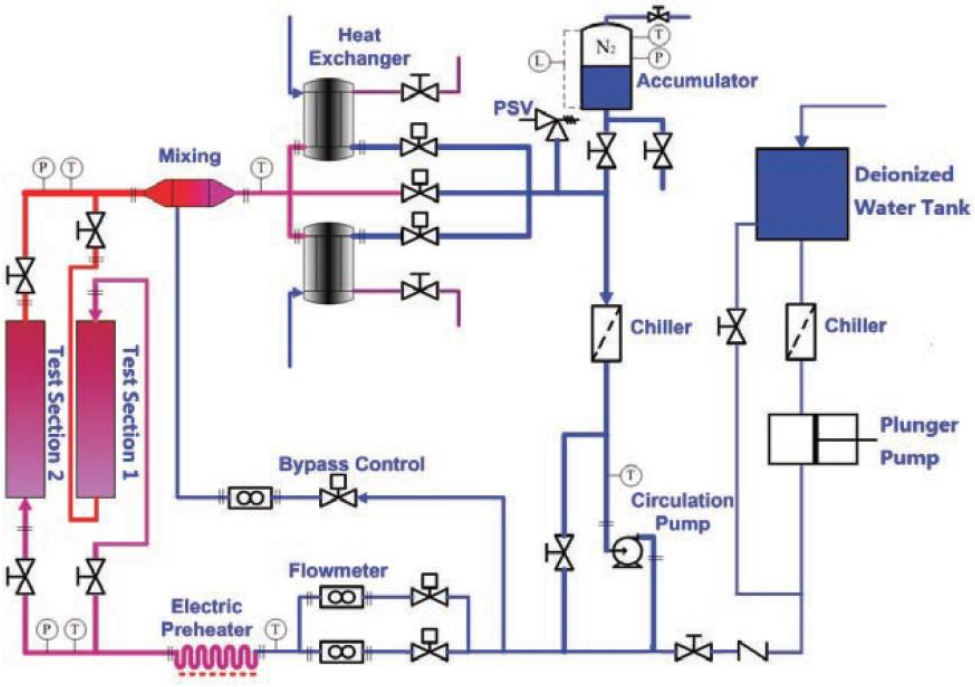

Figure 3-11. Scheme of the SWAMUP test facility (Courtesy of Zhao et al. (2015) [47]).

The main technical parameters of the test facility are listed in Table 3-4.

Table 3-4. Technical specification of the SWAMUP test facility [47].

Parameters	
Design pressure	30 MPa
Design temperature	550°C
DC power for test section	0.9 MW
Heating power for pre-heater	0.3 MW
Heat exchanger capacity	1.2 MW
Max. flow rate	1.39 kg/s
Pump head at maximum flow rate	80 m

3.3.2. Test-Section Design

The channel consists of four (2×2) Inconel-718 heated tubes (channel is 20.32 mm by 20.32 mm) and a ceramic square tube (23.20 mm thickness). The hydraulic diameter was determined to be 6.98 mm using Equation (2.7) [47]. The channel length is 1328 mm and is supported by 5 or 6 spacer grids [47]. The outer square tube is unheated and covered with fiberglass insulation to minimize heat loss [47].

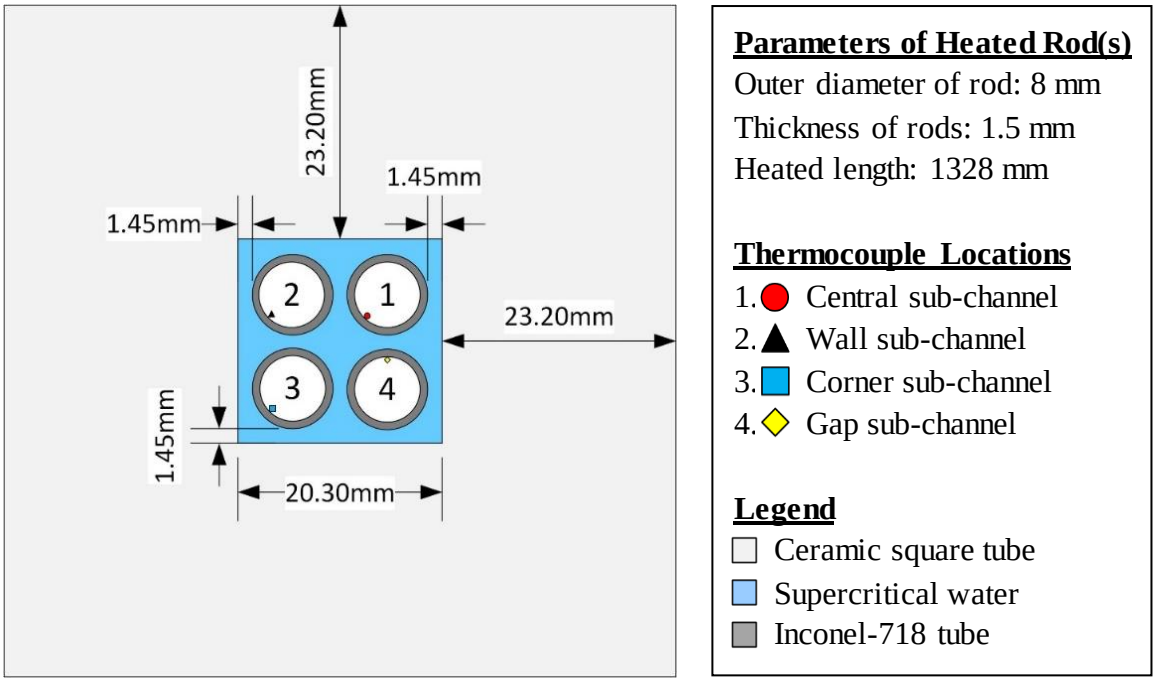

Figure 3-12. Radial cross-section of a 2×2 rod bundle channel.

3.3.3. Instrumentation and Test Matrix

More than 500 measurement points were recorded. Experiments were carried out with test parameters shown in Table 3-5.

Table 3-5. Range of test parameters [47].

Pressure, MPa	Mass Flux, kg/m^{2}s	Heat Flux, MW/m^2	Bulk-Fluid Temperature, °C
23, 25, 26	500 – 1500	0.40 – 1.50	310 – 390

The figures from which the data was transcribed calculated the outer rod temperatures using experimentally measured inner wall temperatures (the thermal conductivity's dependence on temperature was considered) [47]. Furthermore, Zhao et al. (2015) [47] assumed that the

volumetric power density in the tube was uniform and axial heat conduction was negligible. The uncertainties of test parameters are shown in Table 3-6.

Table 3-6. Uncertainties of primary parameters.

Parameter	Maximum Uncertainty
Pressure	± 0.2%
Mass flow rate	± 0.4%
Fluid temperature	± 1.5°C
DC current	± 1.0%
DC voltage	± 1.0%
Heated tube diameter	± 0.04 mm
Heated tube thickness	± 0.02 mm

3.3.4. Experimental Data Sets

The outer wall temperatures transcribed from Zhao et al. (2015) [47] for 2×2-rod bundle trials are presented in Appendix E. The data set was analyzed using a program written in Matlab, shown in Appendix E, which called properties of water from NIST REFPROP [1] software at each iteration.[48]

3.3.5. Determination of Calculated Inner Wall Temperatures

By applying a heat balance to the test section with an axial-step increase set to 1 mm, and assuming negligible heat losses, the change in the specific enthalpy between two axial positions can be determined using Equation (3.9) [51]. The bulk-fluid temperature can be determined based on a calculated specific-enthalpy value and a corresponding pressure in a particular cross section [51].[49] Thermophysical properties of SCW at each cross section were calculated based on the inlet pressure and the local bulk-fluid temperature using NIST REFPROP [1] software.

Section 2.11 summarizes SCW HTC correlations used to predict outer wall temperatures by determining the HTC at each axial iteration [52].

---

[48] Thermal and transport properties of water were retrieved from NIST REFPROP version 9.0 software [63]. The properties of water in NIST are based on the 1995 formulation by the International Association for the Properties of Water and Steam [60, 61, 62].

[49] Pressure losses along the heated length were considered negligible.

$$T_{w,o} = \frac{q}{HTC} + T_b \tag{3.30}$$

Newton's law of Cooling was used to express the experimental HTC (Equation (3.14)), as the rate of convection per unit area is inversely proportional to the temperature difference between the wall and the bulk-fluid.

RMS error analysis was used to determine the deviation of the transcribed outer wall temperatures from their calculated counterparts. RMS error values were determined using Equations (3.24) & (3.25).

3.3.6. Flowchart of Method for Section 3.1

Figure 3-13 illustrates the methodology presented above as a flowchart to better explain the steps taken in this section.

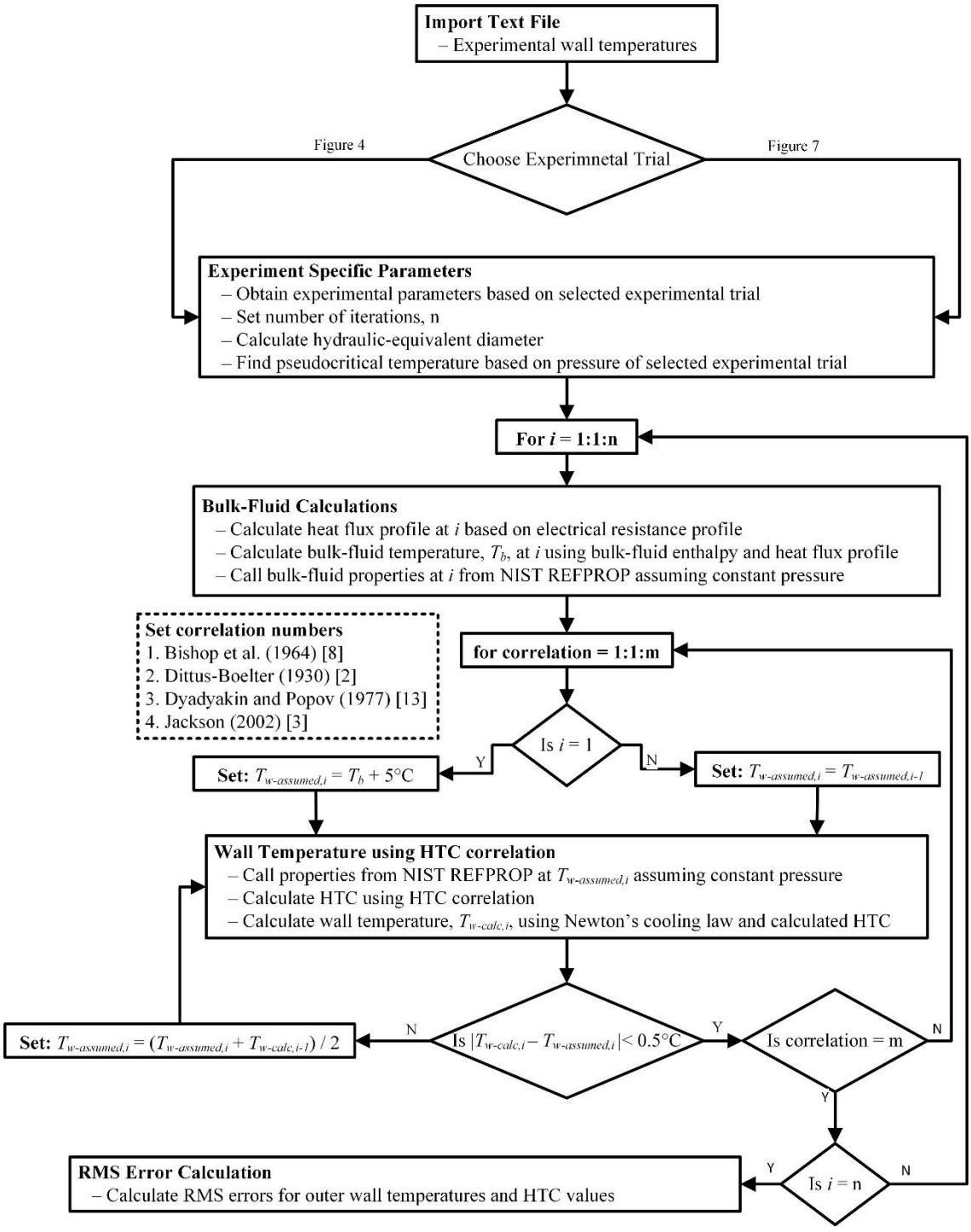

Figure 3-13. Method used to calculate inner wall temperature for the experiment outlined in Section 3.3.

Chapter 4. Analysis of Single-Rod and 3-Rod Bundle Trials

This chapter analyzes heat transfer to SCW flowing upward in annular- and 3-rod bundle flow geometries. Measured inner wall temperatures are compared against values calculated using bare tube HTC correlations. To reduce errors that may arise due to non-uniformity of outer wall temperatures, calculated inner wall temperatures will be compared to the experimental data.[50] HTC profiles are shown as a reference to other experiments; however, the accuracy of the HTC values is less than that of inner wall temperature values, as HTCs calculated using bare tube HTC correlations do not account for the presence of ribs.[51]

The range of heat fluxes in this experiment (outlined in Section 3.1) is higher than those applied in long bare tubes (1 – 6 m) due to the short length of the rods (only 0.485 m) [4, 11, 58, 16, 36].

4.1. Bulk-fluid and Inner Wall Temperatures and HTC Profiles of Single-Rod Channel Trials

Bulk-fluid temperatures were well below the pseudocritical temperature despite high heat fluxes for all single-rod channel trials. Outer wall temperatures exceeded the pseudocritical temperature only for trials with a heat flux greater than 2.2 MW/m^2.

- Constant pressure in all trials: P = 22.6 MPa; $P_{cr\text{-}water}$ = 22.064 MPa
    - Pseudocritical temperature: $T_{pc@22.6MPa}$ = 376°C
- Constant mass flux in all trials: G = 2000 kg/m^{2}s
- Variable inlet temperature: T_{in} = 205°C – 214°C [52]
- Variable heat flux: q = 1.543 – 2.547 MW/m^2

HTC correlations shown include those proposed by: Bishop et al. (1964) [8], Dittus-Boelter

[50] For this geometry, errors may arise due to the unclear definition of outer wall temperature. For rods equipped with fins, this thesis will take a weighted average of outer wall temperatures based on the perimeter.
[51] Since correlations do not account for ribs, the error associated with the inner wall temperature will differ from that of the error associated with the HTC. This is because, while the experimental HTC is calculated using an outer temperature that is corrected for ribs using Equation (3.23), the HTC determined using correlations is not, which skews the plot of the experimental versus calculated HTC values.
[52] The small variation of inlet temperatures between trials is not significant (less than 5%), and thus, for the purposes of this thesis, the inlet temperature can be considered a controlled variable.

(1930) [2], Dyadyakin and Popov (1977) [13], Jackson (2002) [3], Krasnoshchekov et al. (1967) [45], Mokry et al. (2011) [36], and Swenson (1965) [31]. It should be noted that the maximum heat flux trial is outside the Mokry et al. (2011) [36] correlation's range of applicability. However, it was still included as it was based on the Bishop et al. (1964) [8] correlation, which is valid at this heat flux range. Furthermore, although the Dyadyakin and Popov (1977) [13] correlation was developed for bundles, not bare tubes, the majority of correlations presented in this work were developed for bare tubes.

4.1.1. Single-Rod Channel Trial; q = 1.543 MW/m2

Figure 4-1 shows bulk-fluid temperatures, inner wall temperatures, and HTC profiles as functions of the heated length for upward flow of SCW in a single-rod annular channel for a heat flux of 1.543 MW/m^2 (q/G = 0.77 kJ/kg), and an inlet temperature of 205°C.[53]

[53] The q/G ratio is shown here, as all other parameters in the following trials are kept constant.

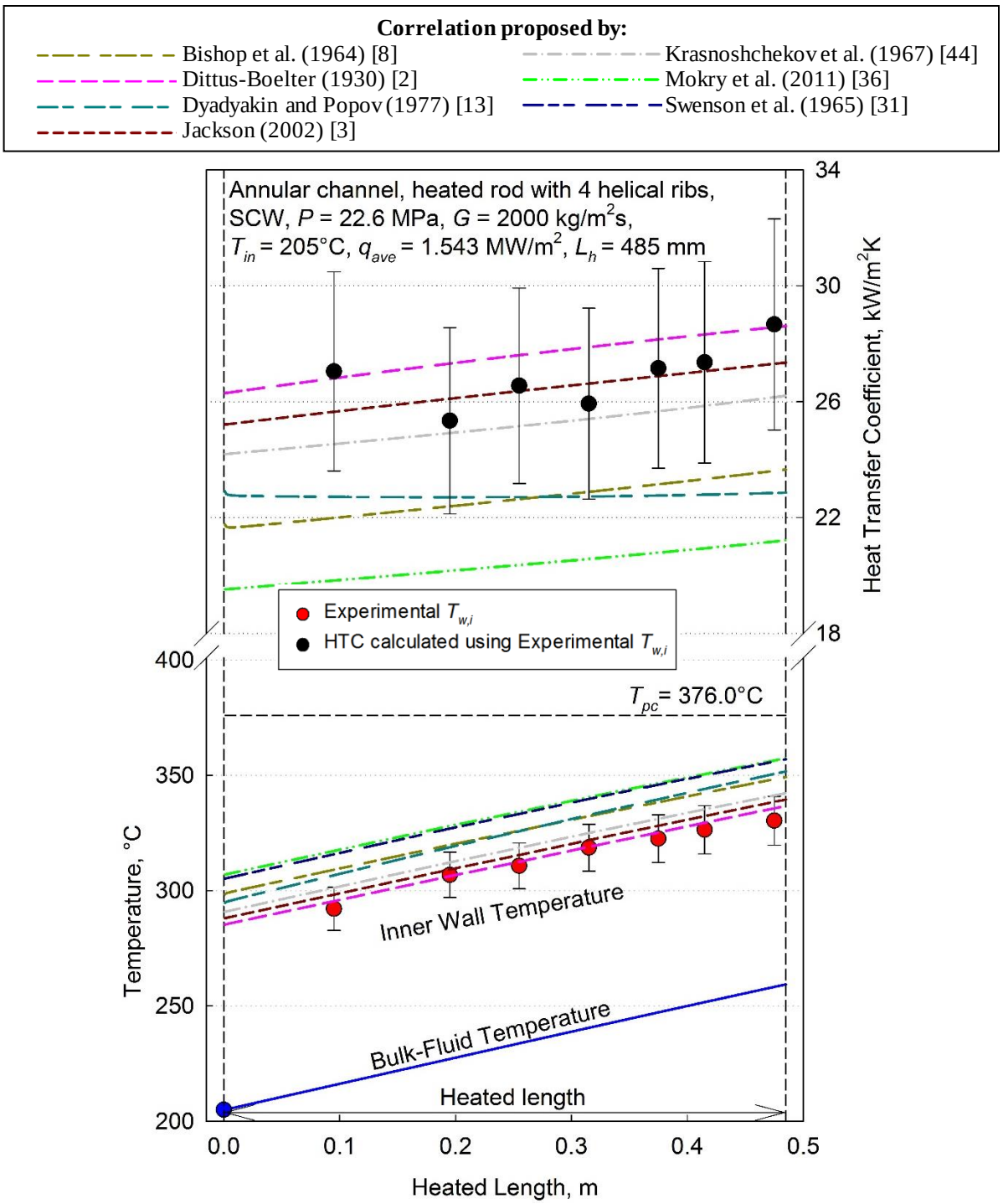

Figure 4-1. Bulk-fluid temperature, wall temperature, and HTC profiles along the heated length of a single-rod annular channel; q = 1.543 MW/m^2.

All correlations illustrated in Figure 4-1 gave a conservative estimate of the inner wall

temperature.[54] The error bars shown are based on values shown in Table 3-2. Enhancements in heat transfer of experimental values as compared to HTC correlation predicted values is most likely due to channel geometry and rod appendages.[55] At a heat flux of 1.543 MW/m^2, bulk-fluid and wall temperatures were significantly lower than the pseudocritical temperature, i.e. there was no significant deviation in thermophysical properties across any cross section, which allowed accurate prediction of inner wall temperatures. Experimental HTC values ranged between 25 – 29 kW/m^{2}K. Table 4-1 lists RMS errors calculated using experimental inner wall temperature measured at each of the seven-thermocouple positions and the corresponding values obtained using each correlation.[56]

Table 4-1. Inner wall temperature RMS errors in a single-rod annular channel; q = 1.543 MW/m^2.

Correlation Proposed by	Inner Wall Temperature RMS Error
Bishop et al. (1964) [8]	5.0%
Dittus-Boelter (1930) [2]	0.9%
Dyadyakin and Popov (1977) [13]	5.1%
Jackson (2002) [3]	1.7%
Krasnoshchekov et al. (1967) [45]	2.6%
Mokry et al. (2011) [36]	7.6%
Swenson et al. (1965) [31]	7.3%

Most correlations accurately predicted the inner wall temperature. The Dittus-Boelter (1930) [2] correlation showed the lowest RMS error for inner wall temperature with the Jackson (2002) [3] correlation having the second lowest. The Mokry et al. (2011) [36] correlation and the Swenson et al. (1965) [31] correlation showed the largest RMS errors.

4.1.2. Single-Rod Channel Trial; q = 1.758 MW/m^2

Figure 4-2 shows bulk-fluid temperatures, inner wall temperatures, and HTC profiles as

[54] A conservative estimate in this thesis means that the wall temperature was overestimated; even if the accuracy is not high, the rod will not expectantly melt due to underestimating the wall temperature.
[55] Enhancements in heat transfer are characterized by lower experimental wall temperatures than those predicted using bare tube HTC correlations.
[56] HTC RMS errors will not be shown because the perimeter averaged outer wall temperature is greater than the outer wall temperature calculated using a correlation. The lower correlation-obtained outer wall temperature causes a slight increase in HTC, which results in deceptively lower RMS error values.

functions of the heated length for upward flow of SCW in a single-rod annular channel for a heat flux of 1.758 MW/m^2 (q/G = 0.88 kJ/kg), and an inlet temperature of 207°C. All other parameters remained constant from the previous trial.

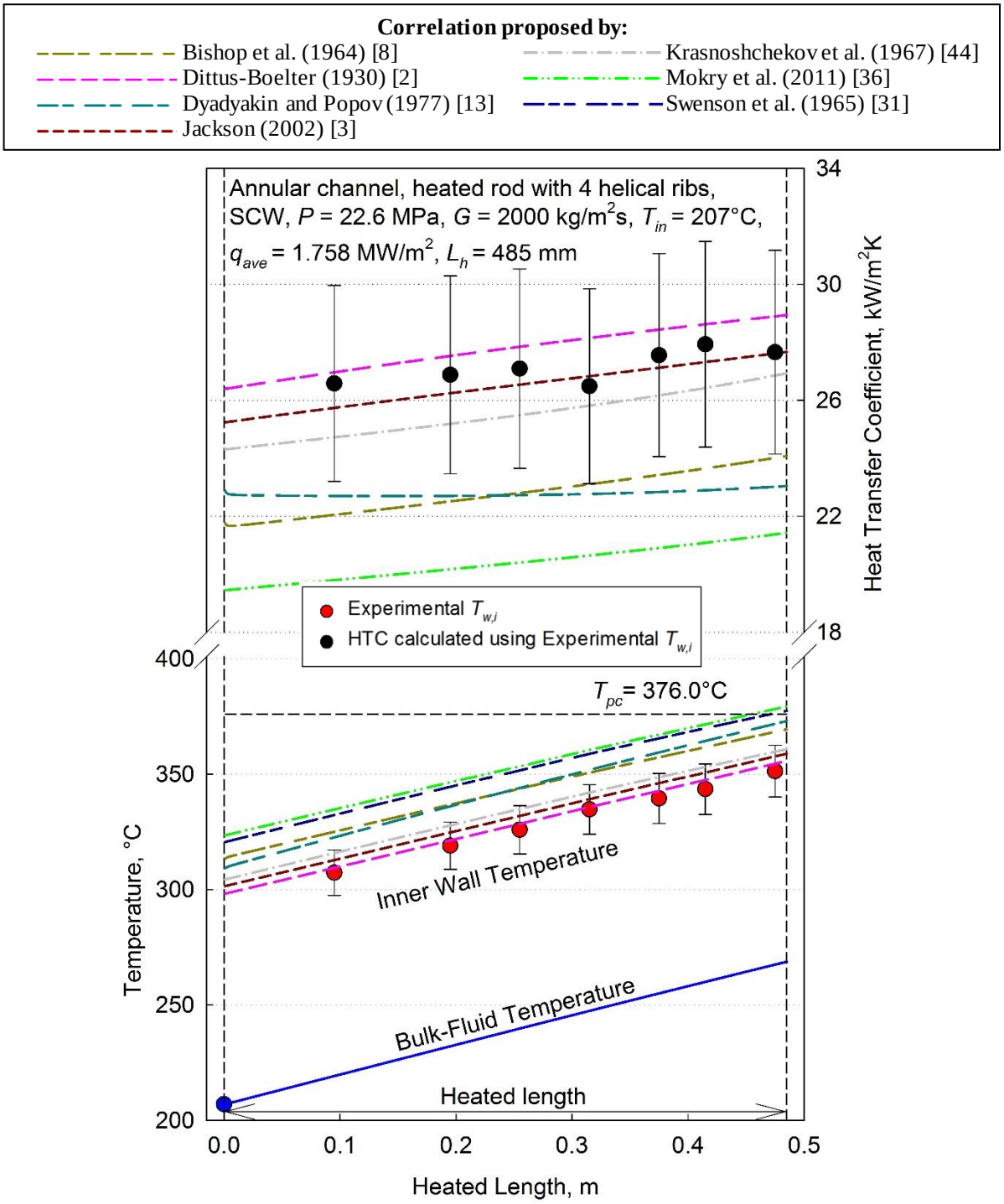

Figure 4-2. Bulk-fluid temperature, wall temperature, and HTC profiles along the heated length of a single-rod annular channel; q = 1.758 MW/m^2.

All correlations illustrated in Figure 4-2 gave a conservative estimate of the inner wall temperature. The error bars shown are based on values shown in Table 3-2. Bulk-fluid and wall temperatures were well below the pseudocritical temperature for the entire heated length, which is reflected by a linear calculated inner wall temperature profile. Experimental HTC values ranged between 26 – 28 kW/m^{2}K. Table 4-2 lists RMS errors calculated using experimental inner wall temperature measured at each of the seven-thermocouple positions and the corresponding values obtained using each correlation.

Table 4-2. Inner wall temperature RMS errors in a single-rod annular channel; q = 1.758 MW/m^2.

Correlation Proposed by	Inner Wall Temperature RMS Error
Bishop et al. (1964) [8]	5.3%
Dittus-Boelter (1930) [2]	0.8%
Dyadyakin and Popov (1977) [13]	5.6%
Jackson (2002) [3]	1.8%
Krasnoshchekov et al. (1967) [45]	2.6%
Mokry et al. (2011) [36]	8.3%
Swenson et al. (1965) [31]	7.7%

Similar to the trial with a heat flux of 1.543 MW/m^2, most correlations predicted the wall temperature within 5% RMS error. Again, the Dittus-Boelter (1930) [2] correlation showed the lowest RMS error and the Jackson (2002) [3] correlation had the second lowest RMS error. The Mokry et al. (2011) [36] correlation and the Swenson et al. (1965) [31] correlation showed the largest RMS errors.

4.1.3. Single-Rod Channel Trial; q = 2.033 MW/m^2

Figure 4-3 shows bulk-fluid temperatures, inner wall temperatures, and HTC profiles as functions of the heated length for upward flow of SCW in a single-rod annular channel for a heat flux of 2.033 MW/m^2 (q/G = 1.02 kJ/kg), and an inlet temperature of 208°C. All other parameters remained constant from the previous trial.

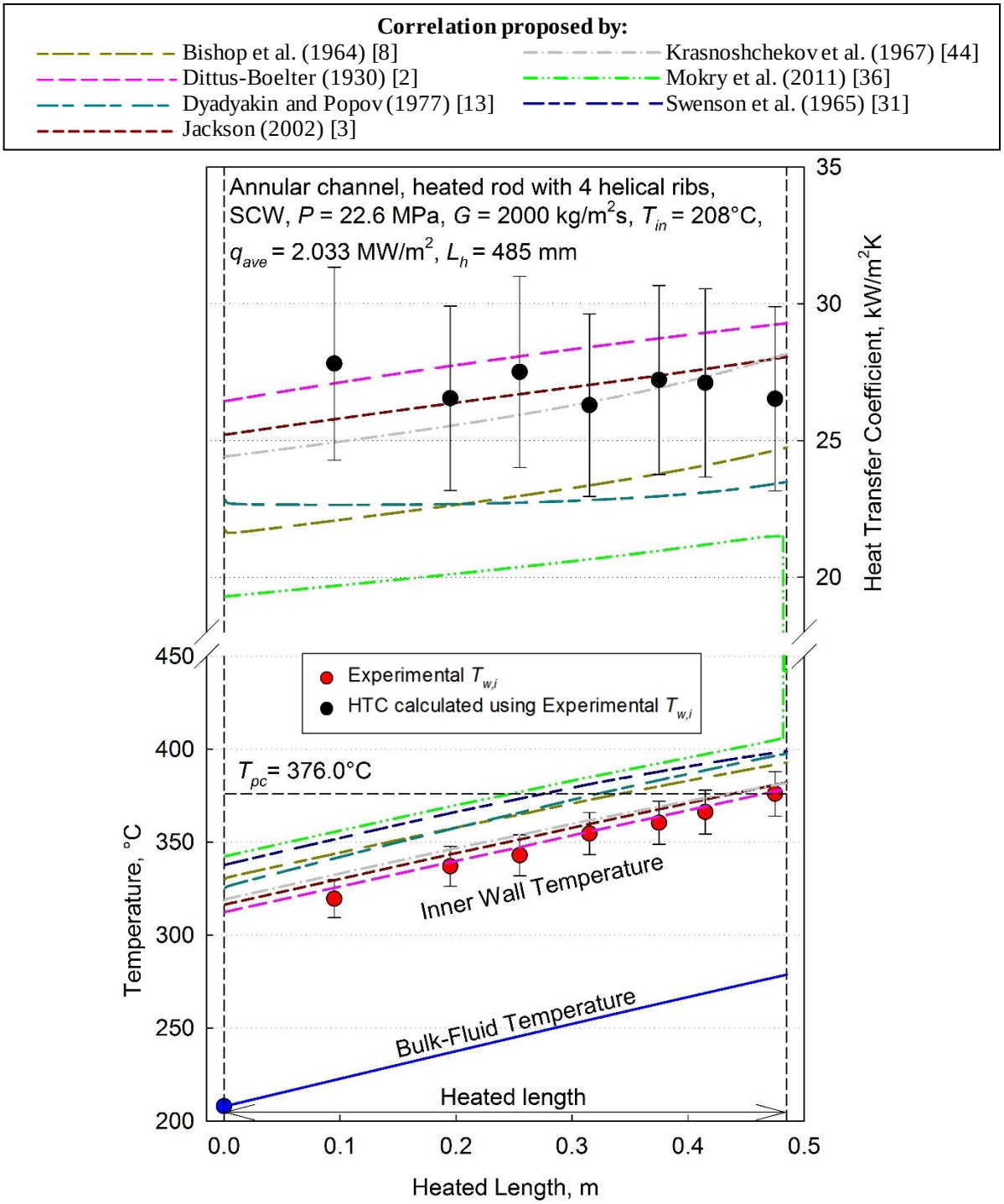

Figure 4-3. Bulk-fluid temperature, wall temperature, and HTC profiles along the heated length of a single-rod annular channel; q = 2.033 MW/m^2.

All correlations illustrated in Figure 4-3 gave a conservative estimate of inner wall temperature. The error bars shown are based on values shown in Table 3-2. While bulk-fluid temperatures were well below the pseudocritical temperature, outer wall temperatures

approached the pseudocritical region, causing a discontinuity in correlations that significantly overestimated wall temperatures.[57] While applying the Mokry et al. (2011) [36] correlation to this trial, the convergence criterion (based on Newton's law of Cooling) was not met at a heated length of 0.480 m. This caused a rapid rise in the predicted wall temperature: ~150°C rise in wall temperature for a 1 mm axial step (and a corresponding drop in HTC). Given that the Dittus-Boelter (1930) [2] correlation did not take into account wall conditions, it was unaffected by the wall temperature's proximity to the pseudocritical temperature. Experimental HTC values ranged between 26 – 28 kW/m^{2}K, which is consistent with the previous trials. Table 4-3 lists RMS errors calculated using experimental inner wall temperature measured at each of the seven-thermocouple positions and the corresponding values obtained using each correlation.

Table 4-3. Inner wall temperature RMS errors in a single-rod annular channel; q = 2.033 MW/m^2.

Correlation Proposed by	Inner Wall Temperature RMS Error
Bishop et al. (1964) [8]	5.8%
Dittus-Boelter (1930) [2]	1.0%
Dyadyakin and Popov (1977) [13]	6.2%
Jackson (2002) [3]	2.1%
Krasnoshchekov et al. (1967) [45]	2.7%
Mokry et al. (2011) [36]	9.3%
Swenson et al. (1965) [31]	8.0%

At higher heat fluxes, there was an increase in RMS error for most correlations, as shown in Table 4-3 versus Table 4-1. The Dittus-Boelter (1930) [2] correlation continued to show the lowest RMS error. Even though it accounted for properties at wall temperature, the Jackson (2002) [3] correlation came in a close second due to its variable exponent on the ratio of specific heat. The Mokry et al. (2011) [36] correlation and the Swenson et al. (1965) [31] correlation continued to show the largest RMS errors.

[57] While wall temperatures illustrated in Figure 4-3 seem to be crossing the pseudocritical temperature, this is somewhat misleading, as those are actually inner wall temperatures. The temperature of the fluid near the wall is ~20°C less than those at the inner wall. Correlations that significantly overestimated the outer wall temperature predicted values near and/or equal to the pseudocritical temperature (which is a problem region for many correlations) exhibited a discontinuity in the temperature profile.

4.1.4. Single-Rod Channel Trial; q = 2.244 MW/m²

Figure 4-4 shows bulk-fluid temperatures, inner wall temperatures, and HTC profiles as functions of the heated length for upward flow of SCW in a single-rod annular channel for a heat flux of 2.244 MW/m² (q/G = 1.12 kJ/kg) and an inlet temperature of 210°C. All other parameters remained constant from the previous trial.

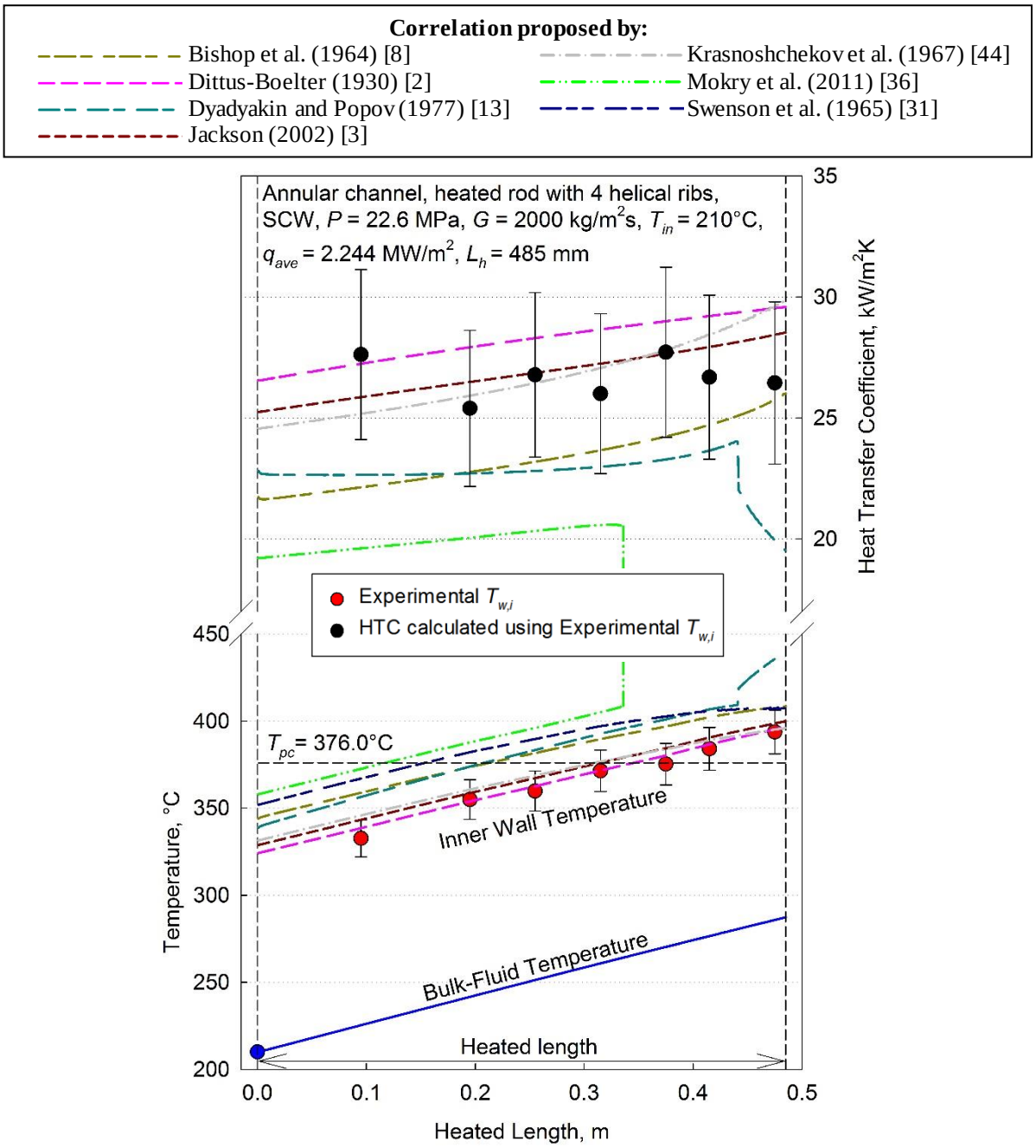

Figure 4-4. Bulk-fluid temperature, wall temperature, and HTC profiles along the heated length of a single-rod annular channel; q = 2.244 MW/m².

All correlations illustrated in Figure 4-4 gave a conservative estimate of the inner wall temperature. The error bars shown are based on values shown in Table 3-2. In this trial, the outer wall temperature exceeded the pseudocritical temperature causing many correlations to exhibit the discontinuous behaviour first observed in Figure 4-3. This discontinuity in wall temperature prediction was observed for the Dyadyakin and Popov (1977) [13] correlation and the Mokry et al. (2011) [36] correlation at a heated length of 0.443 m and 0.338 m, respectively. Furthermore, at a heated length of 0.483 m, the Swenson et al. (1965) [31] correlation did not converge at all, resulting in a lack of a predicted wall temperature for the remainder of the heated length. Although the Dyadyakin and Popov (1977) [13] correlation showed a step increase in wall temperature, it was not as severe as that of the Mokry et al. (2011) [36] correlation. However, it was still unexpected to observe a break in predicted wall temperature, given that the Dyadyakin and Popov (1977) [13] correlation was developed using short 7-rod bundles with rod appendages similar to those used in this experiment. It should be noted that while the Bishop et al. (1964) [8] correlation uses the same form as the Mokry et al. (2011) [36] correlation, it did not exhibit a discontinuity in wall temperature prediction. Experimental HTC values ranged between 25 – 28 kW/m^{2}K. Table 4-4 lists RMS errors calculated using experimental inner wall temperature measured at each of the seven-thermocouple positions and the corresponding values obtained using each correlation.

Table 4-4. Inner wall temperature RMS errors in a single-rod annular channel; q = 2.244 MW/m^2.

Correlation Proposed by	Inner Wall Temperature RMS Error
Bishop et al. (1964) [8]	5.6%
Dittus-Boelter (1930) [2]	1.0%
Dyadyakin and Popov (1977) [13]	7.1%
Jackson (2002) [3]	2.0%
Krasnoshchekov et al. (1967) [45]	2.2%
Mokry et al. (2011) [36]	44.8%
Swenson et al. (1965) [31]	N/A

The Dittus-Boelter (1930) [2] correlation continued to show the lowest RMS error with the Jackson (2002) [3] correlation in a close second. The RMS error for the Swenson et al. (1965) [31] correlation in Table 4-4 is shown as not applicable as the correlation was unable to predict a wall temperature.

4.1.5. Single-Rod Channel Trial; q = 2.547 MW/m²

Figure 4-5 shows bulk-fluid temperatures, inner wall temperatures, and HTC profiles as functions of the heated length for upward flow of SCW in a single-rod annular channel for a heat flux of 2.547 MW/m² (q/G = 1.27 kJ/kg) and an inlet temperature of 214°C. All other parameters remained constant from the previous trial.

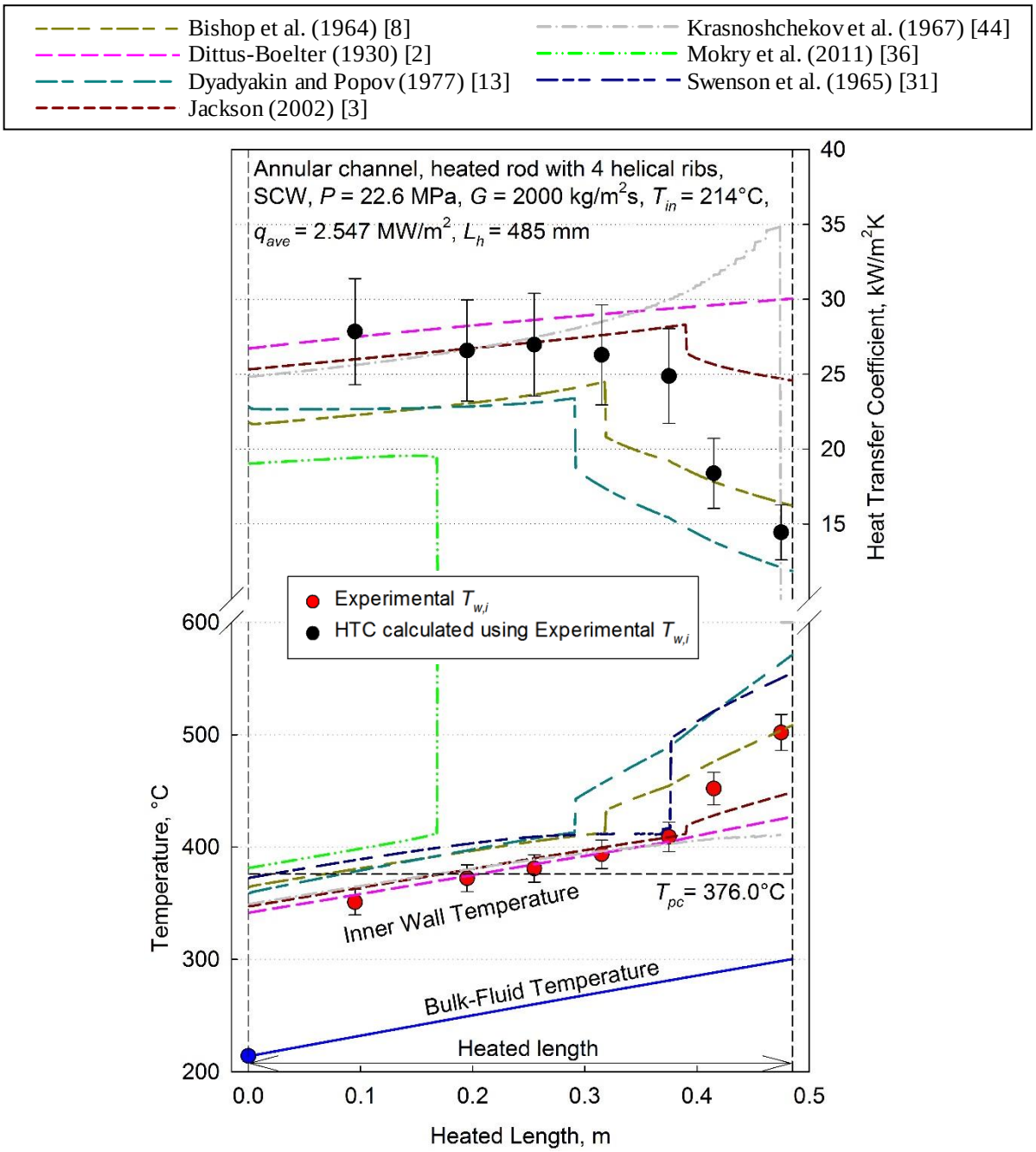

Figure 4-5. Bulk-fluid temperature, wall temperature, and HTC profiles along the heated length of a single-rod annular channel; q = 2.547 MW/m².

Unlike previous trials, at a heat flux of 2.547 MW/m^2 there is significant deterioration of heat transfer near the outlet of the test section, which resulted in a rapid increase in wall temperature, as shown in Figure 4-5. The error bars shown are based on values shown in Table 3-2. The correlations proposed by Bishop et al. (1964) [8], Dyadyakin and Popov (1977) [13], Mokry et al. (2011) [36], and Swenson et al. (1965) [31] all exhibited some level of discontinuity in wall temperature prediction. While, the Mokry et al. (2011) [36] correlation showed the largest discontinuity, the Swenson et al. (1965) [31] correlation did not converge at all for some sections of the heated length. The Jackson (2002) [3] correlation showed a small discontinuity that actually somewhat followed the trend of the wall temperature; however, the wall temperature was underestimated. Experimental HTC values ranged between 18 – 28 kW/m^{2}K due to onset of DHT.

While the Krasnoshchekov et al. (1967) [45] correlation has not been explicitly mentioned in the subsections above, it was predicting results only a few tenths of a percent greater than those of the Jackson (2002) [3] correlation.[58] However, in this trial, bulk-fluid and wall conditions caused the Krasnoshchekov et al. (1967) [45] correlation to predict one wall temperature in an iteration using one exponent, then in the next iteration, predict one vastly different, due to the use of a different exponent. This would result in an endless loop as the predicted temperature would simply alternate between these two temperatures. Furthermore, since the temperature range was not complete, this correlation could not predict wall temperature for the majority of the region near the test section outlet. Table 4-5 lists RMS errors calculated using experimental inner wall temperature measured at each of the seven-thermocouple positions and the corresponding values obtained using each correlation.

[58] This is to be expected as the Jackson (2002) [3] correlation is in fact an improved version of the Krasnoshchekov et al. (1967) [45] correlation.

Table 4-5. Inner wall temperature RMS errors in a single-rod annular channel; q = 2.547 MW/m^2.

Correlation Proposed by	Inner Wall Temperature RMS Error
Bishop et al. (1964) [8]	7.8%
Dittus-Boelter (1930) [2]	6.7%
Dyadyakin and Popov (1977) [13]	13.0%
Jackson (2002) [3]	5.0%
Krasnoshchekov et al. (1967) [45]	N/A
Mokry et al. (2011) [36]	91.1%
Swenson et al. (1965) [31]	13.7%

Interestingly, due to the Jackson (2002) [3] correlation's variable exponents, it showed the lowest RMS error in this trial with the Dittus-Boelter (1930) [2] correlation this time coming second. While the RMS error using the Dittus-Boelter (1930) [2] correlation was low, it was completely insensitive to the region of DHT near the test channel outlet. The RMS error for the Krasnoshchekov et al. (1967) [45] correlation was shown in Table 4-5 as not applicable, as the correlation was unable to provide a predicted wall temperature at these channel conditions.

4.1.6. Discussion on Correlation Accuracy in Single-Rod Trials

Experimental HTC values ranged between 25 – 30 kW/m^{2}K for all single-rod experimental trials, except in the region of DHT in Figure 4-5 (q/G = 1.27 kJ/kg) where it decreased significantly to ~ 18 kW/m^{2}K. Onset of DHT in single-rod channels occurred at a significantly greater value of heat to mass flux than in bare tubes (q/G = 0.7 kJ/kg), discussed in Section 2.8. For trials with a heat flux greater than 2 MW/m^2, most correlations had a discontinuity in the calculated wall temperature profile. This occurred because the convergence criterion was not met without an abrupt increase in wall temperature; the difference between two consecutive calculated wall temperature values at the point of discontinuity (a 1 mm axial step) was ~150°C. Therefore, it seems prudent to discuss the ability of these SCW correlations at predicting heat transfer to SCW flowing upward in single-rod channels.

Table 4-6. Summary RMS error for all single-rod annular channel trials

Correlation Proposed by	Inner Wall Temperature RMS Error				
	q = 1.543 MW/m^2	q = 1.758 MW/m^2	q = 2.033 MW/m^2	q = 2.244 MW/m^2	q = 2.547 MW/m^2
Bishop et al. (1964) [8]	5.0%	5.3%	5.8%	5.6%	7.8%
Dittus-Boelter (1930) [2]	0.9%	0.8%	1.0%	1.0%	6.7%
Dyadyakin and Popov (1977) [13]	5.1%	5.6%	6.2%	7.1%	13.0%
Jackson (2002) [3]	1.7%	1.8%	2.1%	2.0%	5.0%
Krasnoshchekov et al. (1967) [45]	2.7%	2.7%	2.7%	2.2%	N/A
Mokry et al. (2011) [36]	7.6%	8.3%	9.3%	44.8%	91.1%
Swenson et al. (1965) [31]	7.3%	7.7%	8.0%	N/A	13.7%

RMS error for the Bishop et al. (1964) [8] correlation varied between 5 – 8% for almost all trials, which is significant. However, it had lower RMS error values than many of the other correlations shown in Table 4-6. Unlike other correlations, which grossly overestimated wall temperatures, the Bishop et al. (1964) [8] correlation gave a realistic conservative estimate even in regions of DHT (although only just, as shown in Figure 4-5).

The Dittus-Boelter (1930) [2] correlation was the easiest correlation to use, as it did not require an assumption of wall temperature. It had the lowest RMS error for all trials except in Figure 4-5. This is because once wall temperatures neared the pseudocritical point, there was a total lack of response from the correlation, as it is dependent solely on bulk-fluid conditions. Part of the reason why the RMS error is so low is perhaps due to the fact the coolant in the first four trials is a compressed fluid as discussed in Section 2.6, which means it behaves similar to subcritical water.

Although the Dyadyakin and Popov (1977) [13] correlation was developed using a short 7-rod bundle with rod appendages similar to those of this experiment, it was unable to accurately predict wall temperature. The RMS error ranged between 5 – 13%, which is relatively high when compared to the Dittus-Boelter (1930) [2] correlation. Furthermore, the correlation exhibited a discontinuity as shown in Figure 4-5.

The Jackson (2002) [3] correlation showed good agreement with experimental values for all

single-rod channel trials; RMS error ranged around 2% except in Figure 4-5 where it was ~5%. Although the Jackson (2002) [3] correlation was developed for bare tubes, the variable exponents allowed accurate prediction of heat transfer even when wall temperatures approached the pseudocritical temperature. Unlike the Dittus-Boelter (1930) [2] correlation which was insensitive to areas of rapid rise in wall temperature (DHT), wall temperature was incorporated into the correlation which allowed some sensitivity to wall conditions, as shown in Figure 4-5. It should be noted that while the Jackson (2002) [3] correlation did experience a discontinuity in wall temperature, it was very small.

The Krasnoshchekov et al. (1967) [45] correlation showed good results for Figure 4-1 – Figure 4-4 with RMS error only slightly greater than the Jackson (2002) [3] correlation. However, the ranges of the exponents were not holistic (it did not account for some wall temperatures); this caused an inability in the calculation of wall temperature for some part of the test section, as shown in Figure 4-5. Due to this, the Krasnoshchekov et al. (1967) [45] correlation will not be further analyzed in this thesis, as the correlation seems to be incomplete for these experimental conditions.

The Mokry et al. (2011) [36] correlation had the largest RMS errors; it was unable to accurately predict wall temperature, even at the lowest heat flux, as shown in Figure 4-1. It should be noted that all heat fluxes presented lie outside its range of applicability. However, the Bishop et al. (1964) [8] correlation which shares the same form with similar exponents, had RMS errors less than half those of the Mokry et al. (2011) [36] correlation. The Mokry et al. (2011) [36] correlation will also not be used in the 3-rod bundle trials as it significantly overestimated wall temperatures.

The wall temperature approach used by the Swenson et al. (1965) [31] correlation was not able to predict wall temperature; it had one of largest RMS errors in every trial. Furthermore, the convergence criterion could not be satisfied in Figure 4-4. Therefore, the Swenson et al. (1965) [31] correlation will also not be used in the 3-rod bundle trials as it significantly overestimated wall temperatures.

To summarize, the correlations proposed by Dittus-Boelter (1930) [2] and Jackson (2002) [3] showed the best agreement with the experimental results of SCW flowing upward in a single-

rod channel.

4.2. Bulk-fluid and Inner Wall Temperatures, and HTC Profiles of 3-Rod Bundle Trials

Bulk-fluid temperatures were well below the pseudocritical temperature despite high heat fluxes for all 3-rod bundle trials. However, unlike the single-rod trials, wall temperatures regularly exceeded the pseudocritical temperature along the heated length.

- Variable pressure: P = 24.5, 27.5 MPa; $P_{cr\text{-}water}$ = 22.064 MPa
    - Pseudocritical temperature: $T_{pc@24.5MPa/27.5MPa}$ = 383.1/393.7°C
- Variable mass flux: G = 1500, 2700 kg/m^{2}s
- Variable inlet temperature: T_{in} = 166, 212, 277°C
- Variable heat flux: q = 3.07, 3.2 MW/m^2

HTC correlations that will be shown include those proposed by Bishop et al. (1964) [8], Dittus-Boelter (1930) [2], Dyadyakin and Popov (1977) [13], and Jackson (2002) [3]. Krasnoshchekov et al. (1967) [45] is not illustrated for this experiment, as the exponent range was discontinuous; i.e. not all bulk-fluid and wall temperatures could be defined by the criteria defined by the exponents, as discussed in Section 4.1.5. The Mokry et al. (2011) [36] correlation was also removed as it consistently predicted results that were unrealistic as these experimental parameters lie outside its range of applicability.

4.2.1. 3-Rod Bundle Channel Trial; q = 3.07 MW/m^2, G = 1500 kg/m^{2}s, T_{in} = 166°C

Figure 4-6 shows bulk-fluid temperatures, inner wall temperatures, and HTC profiles as functions of the heated length for upward flow of SCW in a 3-rod bundle channel for a heat flux of 3.07 MW/m^2 (q/G = 2.05 kJ/kg), an inlet temperature of 166°C, and a mass flux of 1500 kg/m^{2}s.

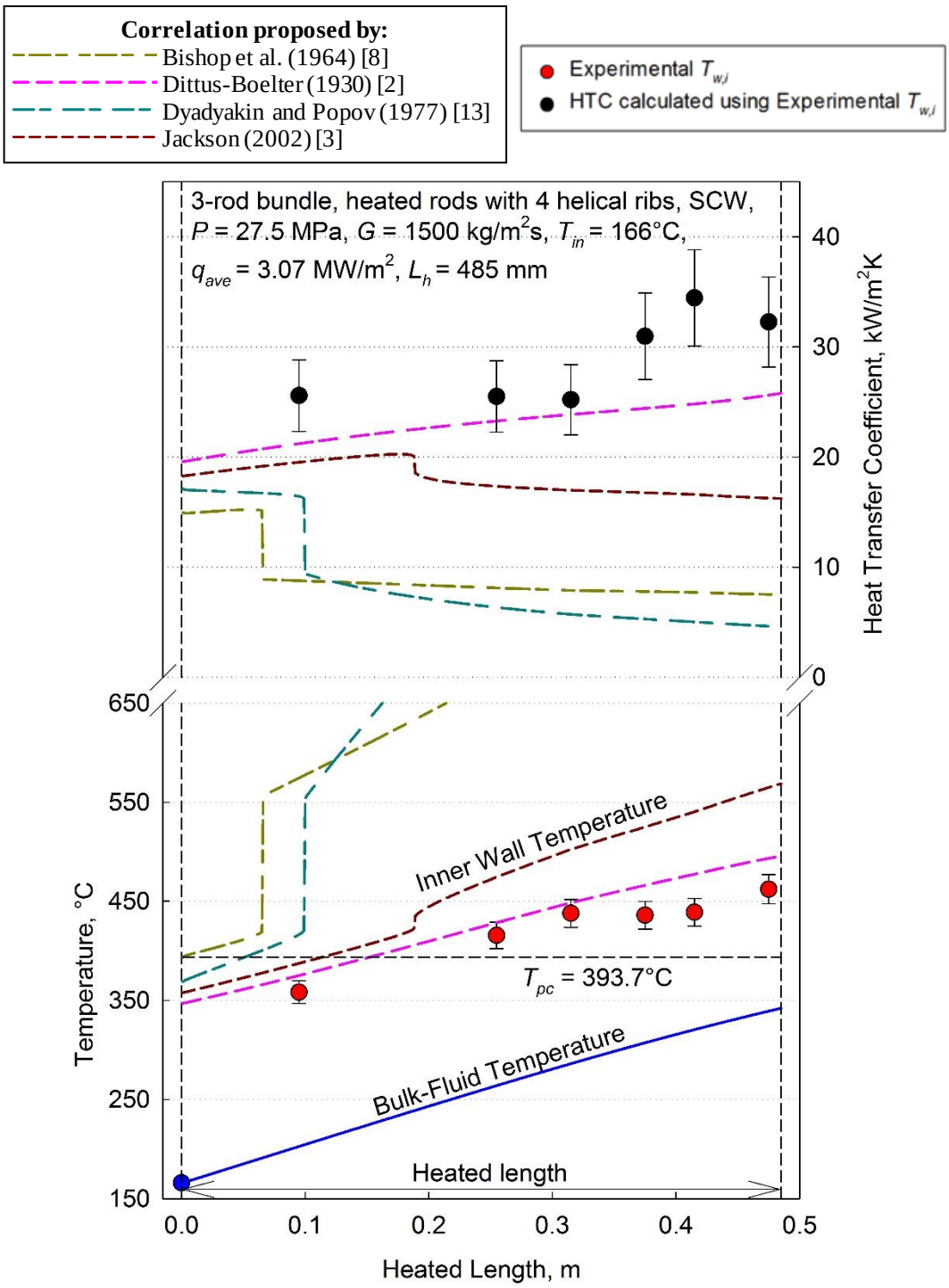

Figure 4-6. Bulk-fluid temperature, wall temperature, and HTC profiles along the heated length of a 3-rod bundle channel; q = 3.07 MW/m^2, G = 1500 kg/m^{2}s, T_{in} = 166°C.

All correlations illustrated in Figure 4-6 gave a conservative estimate of the inner wall temperature. While bulk-fluid temperatures were well below the pseudocritical temperature,

outer wall temperatures approached the pseudocritical region, causing a discontinuity in most correlations and a significant overestimation of wall temperatures. At such high heat and mass fluxes, channel conditions are extreme, which makes predicting heat transfer more difficult. There is significant enhancement of heat transfer as compared to bare tubes due to the complex channel geometry, which would increase turbulence. The correlations proposed by Bishop et al. (1964) [8] and Dyadyakin and Popov (1977) [13] experienced discontinuities, as shown in Figure 4-6 at 0.66 m, and 0.1 m, respectively. Experimental HTC values ranged between 25 – 35 kW/m^{2}K, which are greater than those of the single-rod channel trials (Figure 4-1 – Figure 4-5). Table 4-7 lists RMS errors calculated using experimental inner wall temperature measured at each of the seven-thermocouple positions and the corresponding values obtained using each correlation.

Table 4-7. Inner wall temperature RMS errors in a 3-rod bundle trial; q = 3.07 MW/m^2, G = 1500 kg/m^{2}s, T_{in} = 166°C.

Correlation Proposed by	RMS Error for Inner Wall Temperature
Bishop et al. (1964) [8]	66.8%
Dittus-Boelter (1930) [2]	5.9%
Dyadyakin and Popov (1977) [13]	100.8%
Jackson (2002) [3]	17.9%

The Dittus-Boelter (1930) [2] correlation showed the lowest RMS error, while the Jackson (2002) [3] correlation was a distant second. The RMS error for the Dyadyakin and Popov (1977) [13] correlation, shown in Table 4-7, was very high, which is unexpected considering it was developed for short 7-rod bundles with ribs similar to this test section.

4.2.2. 3-Rod Bundle Channel Trial; q = 3.07 MW/m^2, G = 1500 kg/m^{2}s, T_{in} = 212°C

Figure 4-7 shows bulk-fluid temperatures, inner wall temperatures, and HTC profiles as functions of the heated length for upward flow of SCW in a 3-rod bundle channel given an inlet temperature of 212°C (q/G = 2.05 kJ/kg). All other parameters remained constant from the previous trial.

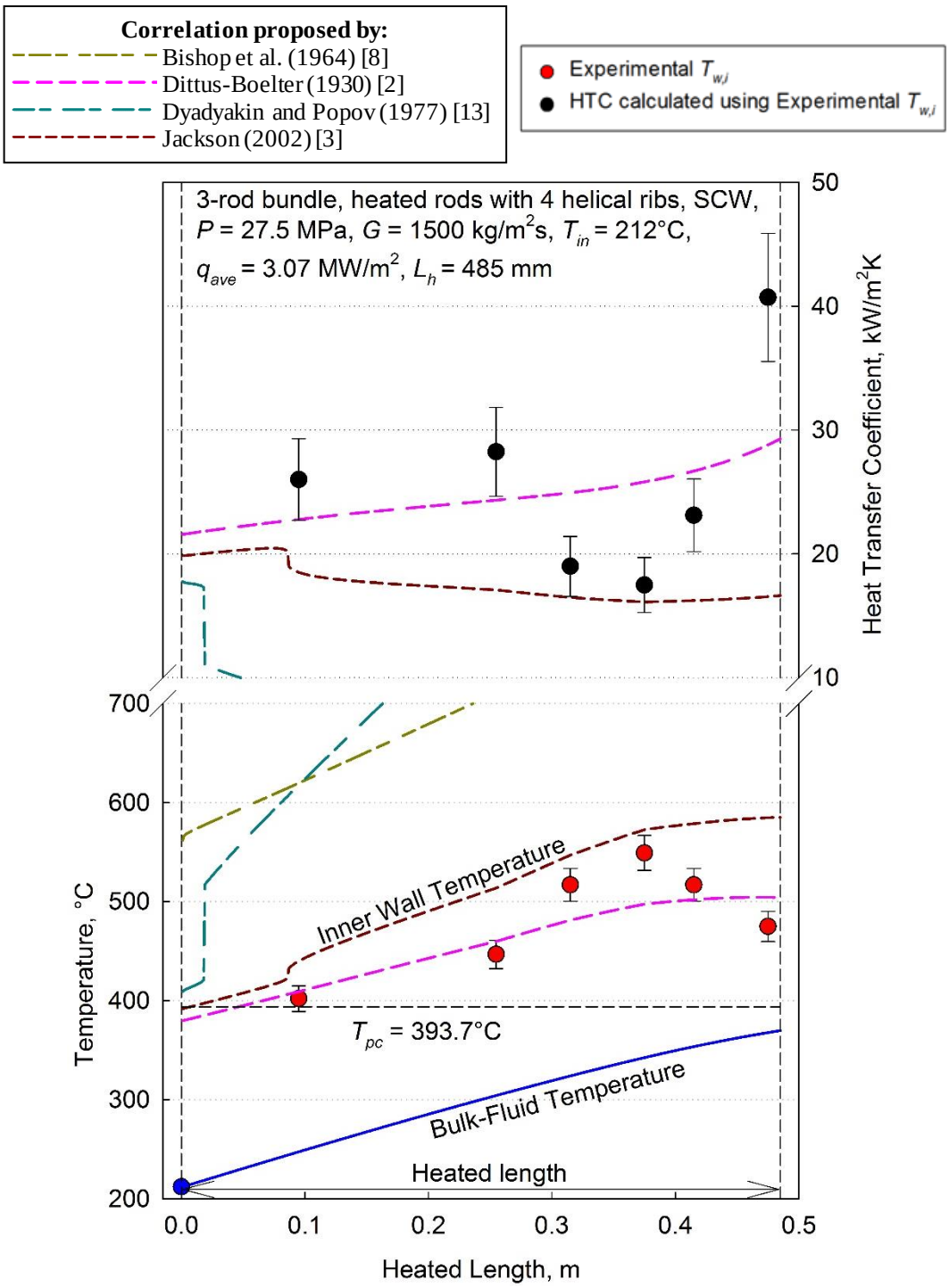

Figure 4-7. Bulk-fluid temperature, wall temperature, and HTC profiles along the heated length of a 3-rod bundle channel; q = 3.07 MW/m^2, G = 1500 kg/m^{2}s, T_{in} = 212°C.

All correlations illustrated in Figure 4-7 gave a conservative estimate of the inner wall temperature, except Dittus-Boelter (1930) [2]. This is because the Dittus-Boelter (1930) [2]

correlation was insensitive to the region of DHT at ~0.3 m, as shown in Figure 4-7. While bulk-fluid temperatures were well below the pseudocritical temperature, outer wall temperatures were above the pseudocritical region. The Dyadyakin and Popov (1977) [13] correlation showed a discontinuity at a heated length of 0.019 m, as shown in Figure 4-7. The Bishop et al. (1964) [8] correlation appeared to overestimate wall temperature significantly, and this caused the calculated HTC to decrease to below the 10 kW/m^{2}K cut-off in Figure 4-7. Experimental HTC values ranged between 17 – 29 kW/m^{2}K, which are similar to Figure 4-5 (single-rod annular channel trial) where there was also onset of DHT regime. Table 4-8 lists RMS errors calculated using experimental inner wall temperature measured at each of the seven-thermocouple positions and the corresponding values obtained using each correlation.

Table 4-8. Inner wall temperature RMS errors in a 3-rod bundle trial; q = 3.07 MW/m^2, G = 1500 kg/m^{2}s, T_{in} = 212°C.

Correlation Proposed by	RMS Error for Inner Wall Temperature
Bishop et al. (1964) [8]	55.5%
Dittus-Boelter (1930) [2]	5.7%
Dyadyakin and Popov (1977) [13]	86.6%
Jackson (2002) [3]	13.2%

The Dittus-Boelter (1930) [2] correlation showed the lowest RMS error, while the Jackson (2002) [3] correlation showed the second lowest value. The RMS errors for the correlations proposed by Bishop et al. (1964) [8] and Dyadyakin and Popov (1977) [13] were very high, so much so that use of these correlations would net meaningless results.

4.2.3. 3-Rod Bundle Channel Trial; q = 3.2 MW/m^2, G = 2700 kg/m^{2}s, T_{in} = 277°C

Figure 4-8 shows bulk-fluid temperatures, inner wall temperatures, and HTC profiles as functions of the heated length for upward flow of SCW in a 3-rod bundle channel for a heat flux of 3.2 MW/m^2 (q/G = 1.19 kJ/kg), an inlet temperature of 277°C, and a mass flux of 2700 kg/m^{2}s.

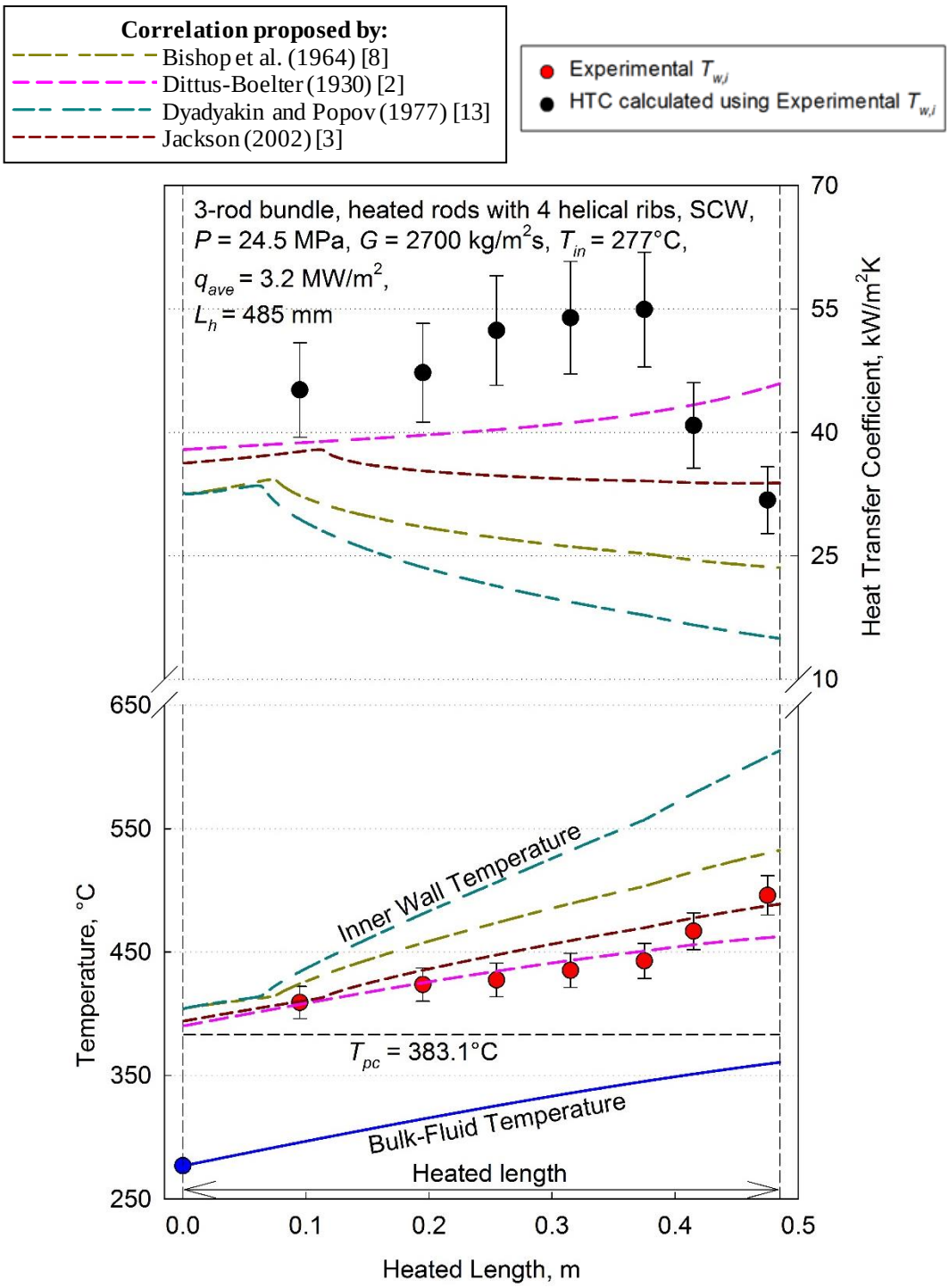

Figure 4-8. Bulk-fluid temperature, wall temperature, and HTC profiles along the heated length of a 3-rod bundle channel; q = 3.07 MW/m^2, G = 2700 kg/m^{2}s, T_{in} = 212°C.

All correlations illustrated in Figure 4-8 gave a conservative estimate of the inner wall temperature, except the Dittus-Boelter (1930) [2] correlation and the Jackson (2002) [3]

correlation. This is characteristic of the Dittus-Boelter (1930) [2] correlation as it was insensitive to the region of DHT near the test section outlet, as shown in Figure 4-8. While bulk-fluid temperatures were well below the pseudocritical temperature, outer wall temperatures were above the pseudocritical temperature for the entirety of the test section. It should be noted that although this heat flux was very high (the highest heat flux of this experiment), the very large mass flux significantly reduced onset of DHT. The correlations proposed by Bishop et al. (1964) [8] and Dyadyakin and Popov (1977) [13] appear to agree with the experimental result better in the trial illustrated in Figure 4-8 than that in Figure 4-7. Experimental HTC values ranged between 32 – 55 kW/m^{2}K, which are significantly greater than those of the single-rod channel trials (Figure 4-1 – Figure 4-5). It should be noted that the HTC values only decreased near the outlet of the channel due to onset of DHT. Figure 4-8 shows how increases in bundle complexity, from single-rod to a 3-rod bundle, can lead to improvements in heat transfer. Table 4-9 lists RMS errors calculated using experimental inner wall temperature measured at each of the seven-thermocouple positions and the corresponding values obtained using each correlation.

Table 4-9. Inner wall temperature RMS errors in a 3-rod bundle trial; q = 3.07 MW/m^2, G = 2700 kg/m^{2}s, T_{in} = 277°C.

Correlation Proposed by	RMS Error for Inner Wall Temperature
Bishop et al. (1964) [8]	10.0%
Dittus-Boelter (1930) [2]	3.0%
Dyadyakin and Popov (1977) [13]	20.1%
Jackson (2002) [3]	3.9%

The Dittus-Boelter (1930) [2] correlation showed the lowest RMS error, while the Jackson (2002) [3] correlation showed the second lowest value; both errors were very low, showing very good agreement with the experimental data. This is in contrast to previous 3-rod bundle trials where lowest error was ~6%. The RMS errors for the Bishop et al. (1964) [8] correlation and the Dyadyakin and Popov (1977) [13] correlation where still significantly high, but, again, less than those of the previous trials.

4.2.4. Discussion on Correlation Accuracy in 3-Rod Bundle Trials

For trials with relatively lower mass flux, there was a discontinuity in the calculated wall

temperatures because the convergence criterion was not met without an abrupt increase in wall temperature.[59] Some trials even appeared to have reached a point of discontinuity even before the heated length (as shown by the Bishop et al. (1964) [8] correlation in Figure 4-7) as they significantly overestimated wall temperature along the entire cross section. Therefore, it seems prudent to discuss the ability of these SCW bare tube correlations at predicting heat transfer to SCW flowing upward in 3-rod bundle channels.

Table 4-10. RMS error of inner wall temperature for all 3-rod bundle trials.

Correlation Proposed by	Inner Wall Temperature RMS Error		
	T_{in} = 166°C q = 3.2 MW/m^2 G = 1500 kg/m^{2}s	T_{in} = 212°C q = 3.2 MW/m^2 G = 1500 kg/m^{2}s	T_{in} = 277°C q = 3.07 MW/m^2 G = 2700 kg/m^{2}s
Bishop et al. (1964) [8]	66.8%	55.5%	10.0%
Dittus-Boelter (1930) [2]	5.9%	5.7%	3.0%
Dyadyakin and Popov (1977) [13]	100.8%	86.6%	20.1%
Jackson (2002) [3]	17.9%	13.2%	3.9%

RMS error is notably lower in the final trial compared to the first two due to the lower q/G ratio, as shown in Table 4-6. The increase in mass flux in the trial shown in Figure 4-8 showed significantly better HTC values compared to all other previous trials (3-rod bundle or otherwise). Thus, lower q/G ratios for a given channel geometry reduce onset of DHT. Furthermore, trials with lower q/G had lower RMS errors, as correlations were better able to predict heat transfer. Onset of DHT in 3-rod bundle channels occurred at a significantly greater value of heat to mass flux than in bare tubes, discussed in Section 2.8.

RMS error for the Bishop et al. (1964) [8] correlation varied between 10 – 68%, which is a very large range, as shown in Table 4-10. The Bishop et al. (1964) [8] correlation experienced a discontinuity in wall temperatures in almost all trials, with the exception of the last trial where it overestimated the wall temperature near the channel outlet by a significant margin. These experiments show that, for these experimental conditions, the Bishop et al. (1964) [8]

[59] The difference between two consecutive calculated wall temperature values at the point of discontinuity (a 1 mm axial step) was ~150°C as shown in Figure 4-6.

correlation is not a viable correlation to use.

The Dittus-Boelter (1930) [2] correlation was the easiest correlation to use, as it did not require the setup of a loop to assume wall temperatures. It had the lowest RMS error for all trials, as shown in Table 4-10. However, once wall temperatures approached the pseudocritical temperature, there was a lack of response from the correlation, as it is dependent solely on bulk-fluid conditions, as shown in Figure 4-7. Part of the reason why the RMS error is so low is perhaps due to the fact the bulk-fluid is a compressed fluid, as shown in Figure 2-4, which means it behaves similar to subcritical water.

Although the Dyadyakin and Popov (1977) [13] correlation was developed using a 7-rod bundle with rod appendages similar to those used in this experiment, it was unable to predict wall temperature as the RMS errors ranged between 20 – 100%. Furthermore, there was a discontinuity in the wall temperature profile for this correlation as illustrated in Figure 4-7.

The Jackson (2002) [3] correlation showed good agreement with experimental values for all 3-rod bundle channel trials; RMS errors ranged between 4 – 18%. Unlike the Dittus-Boelter (1930) [2] correlation which was insensitive to areas of rapid rise in wall temperature (DHT), the Jackson (2002) [3] correlation incorporated wall conditions into the correlation which allowed some sensitivity (though it showed higher RMS errors), as shown in Table 4-10. It should be noted that while the Jackson (2002) [3] correlation did experience a discontinuity in wall temperature, as shown in Figure 4-8, it was very small, and it followed the trend of the wall temperature.

4.3. Mechanism of Convection and Onset of DHT in Section 4.1 & 4.2 Data

Increases in the $\frac{\overline{\mathbf{Gr}_b}}{\mathbf{Re}_b^{2.7}}$ ratio discussed in Section 2.9 for trials shown in Section 4.1 & 4.2 parallel onset of DHT [38]. While the ratio was not developed for this purpose, buoyancy effects seem to increase at onset of DHT, as shown in Figure 4-9.

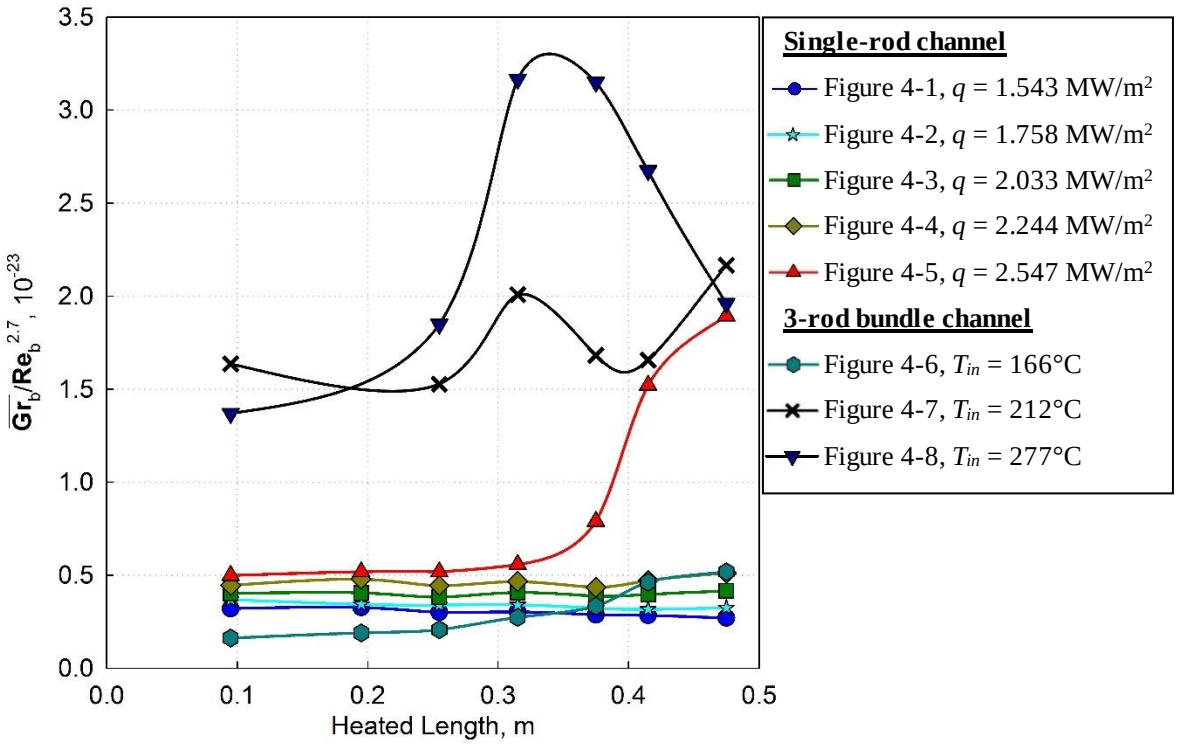

Figure 4-9. The $\frac{\overline{Gr_b}}{Re_b^{2.7}}$ ratio across the heated length for heat flux and channel geometries presented in Section 4.1 & 4.2.

The $\frac{\overline{Gr_b}}{Re_b^{2.7}}$ ratio is significantly less than $2.4 \cdot 10^{-5}$ across the heated length for all heat fluxes, which indicates that this is predominantly forced-convection flow. There is an increase in buoyancy effects represented by the Grashof number in the numerator, at onset of DHT as shown in Figure 4-5 – Figure 4-8. It should be noted that an increase in wall temperature does not simply cause an increase in buoyancy effects. Although there is a steady rise in temperature along the heated length, the ratio of the trials illustrated in Figure 4-1 – Figure 4-4 does not significantly change.

4.4. Analysis of Section 4.1 & 4.2 data based on the Eckert Number

The Eckert number (Equation (2.3)) was introduced in Section 2.10.1 to describe the degree of divergence of wall and bulk-fluid conditions. Figure 4-10 applies this concept to the data set discussed in in Section 4.1 & 4.2.

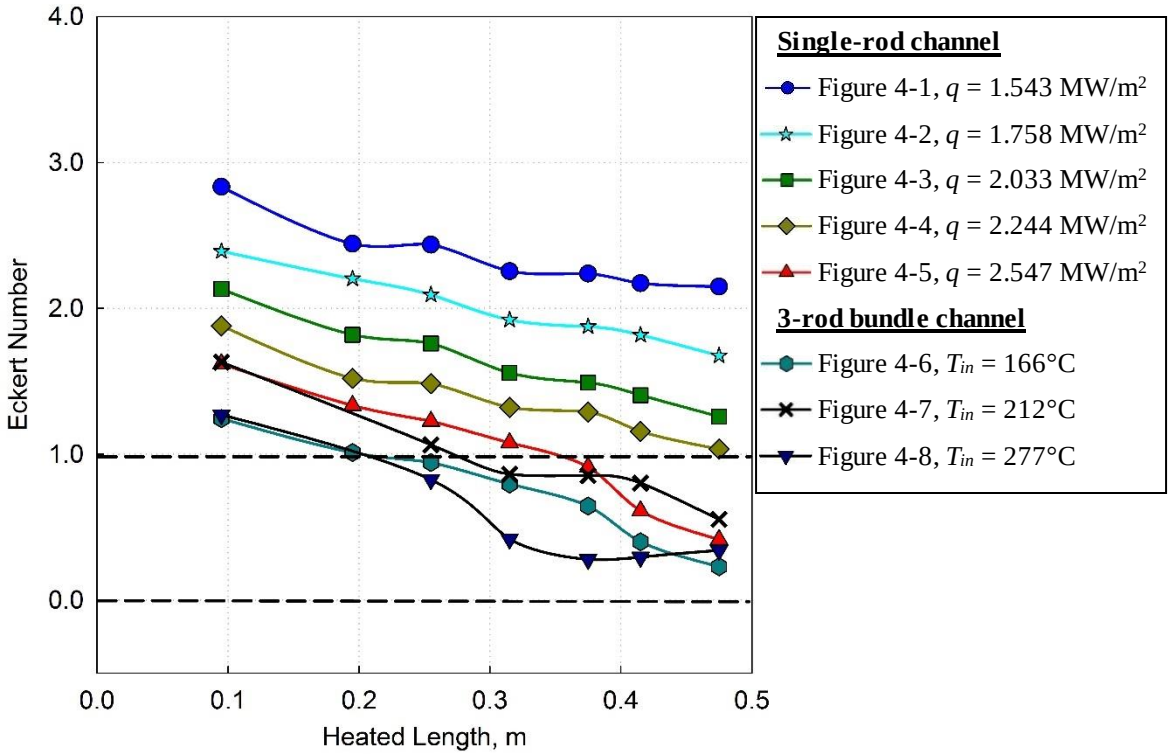

Figure 4-10. The Eckert number across the heated length for single-rod and 3-rod bundle trials.

In the first four annular channel trials, Figure 4-1 – Figure 4-4, SCW is liquid-like (**E** > 1) at each of the 7-measured points along the heated length, as shown in Figure 4-10. All correlations were able to predict the wall temperature in these trials (some more accurately than others). The correlations proposed by Dittus-Boelter (1930) [2] and Jackson (2002) [3] were the most accurate in predicting the wall temperature in this region

However, once there was a large deviation in densities in a cross-section ($0 \leq \mathbf{E} \leq 1$), there was a discontinuity in most correlations that had a ratio of thermophysical properties. Furthermore, there was a universal inability to predict wall temperatures as $\mathbf{E} \rightarrow 0$ (especially when $\mathbf{E} < 0.3$), as shown in Figure 4-5 – Figure 4-8. It should be noted that although there was no discontinuity in the Dittus-Boelter (1930) [2] correlation when $0 \leq \mathbf{E} \leq 1$, it was insensitive to the changes in the wall temperature along the heated length as it was solely dependent of the bulk-fluid properties.[60]

[60] It cannot take into account the effect on heat transfer as the wall temperature approached the pseudocritical temperature.

A closer look at the 3-rod bundle trials in Figure 4-6 – Figure 4-8 indicates that, initially, even though **E** > 1; the Jackson (2002) [3] correlation (and other correlations) were unable to accurately predict HTC in that region. Since most of those correlations were designed to predict HTC in bare tubes, this inability to predict HTC might be due to appendages in the channel geometry and the increased complexity of flow; however, more data is needed to arrive at a clear conclusion. It should be noted that at the higher mass flux, lower ratio of q/G, of the third 3-rod bundle trial (Figure 4-8), correlations were able to more accurately predict wall temperature with lower RMS errors.

4.5. Analysis of Section 4.1 & 4.2 data based on the Modified Boiling Number

The modified boiling number (Equation (2.4)) was introduced in Section 2.10.2 as a unique method to correlate heat transfer data without needing to distinguish the mode of heat transfer. Figure 4-11 applies this concept to the data set discussed in in Section 4.1 & 4.2.

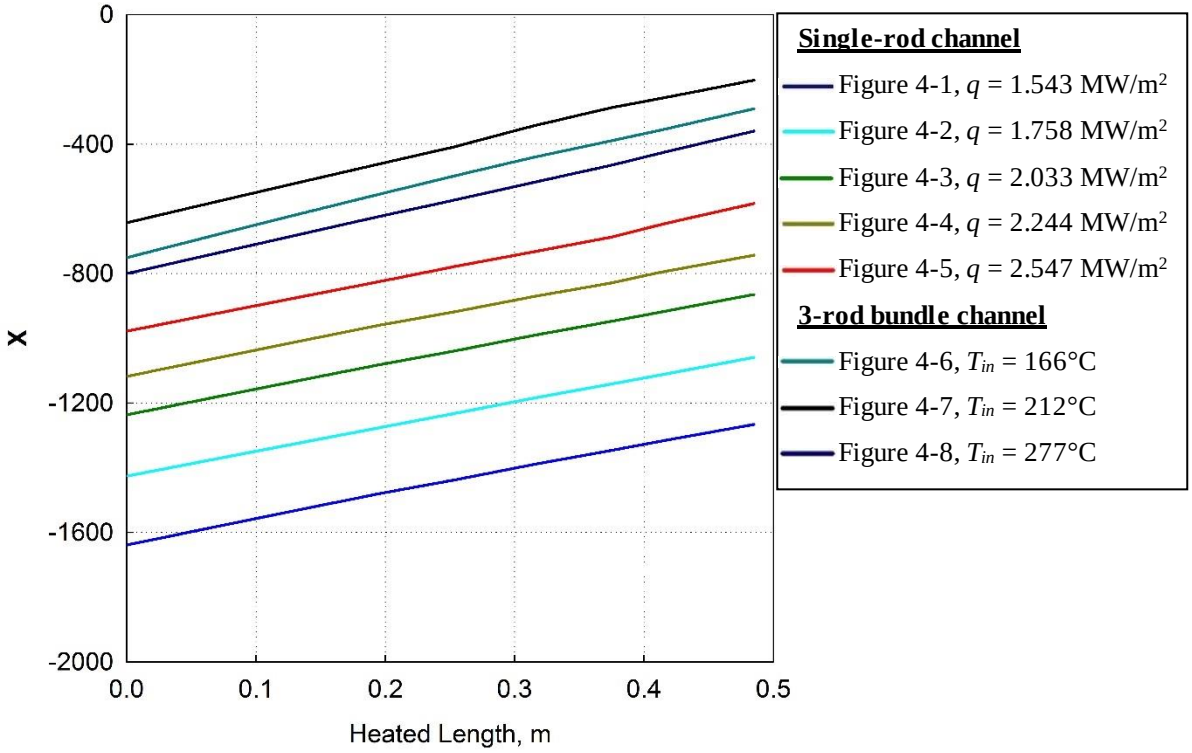

Figure 4-11. The Modified Boiling number across the heated length for single-rod and 3-rod bundle trials.

However, since the modified boiling number is solely dependent on bulk-fluid conditions, it lacks any sensitivity to wall condition; regions of DHT observed in Figure 4-5 – Figure 4-8

are not reflected in Figure 4-11. In fact, there does not seem to be any effect on the modified boiling number regardless of the heat transfer regime, as it remained linear across the heated length in all trials.

Many authors have compared the heat flux to the mass flux as a method of characterization of heat transfer. However, the heat transfer regime is dependent on much more than simply the heat and mass flux, as the geometry of flow plays a very large role. One hypothesis is that there would be a different threshold for onset of DHT for each flow geometry. However, a concluding statement using the single-rod channel data is not possible as there is onset of DHT in only one trial (Figure 4-5). Furthermore, there does not appear to be any trends in the 3-rod bundle trials either.

4.6. Discussion

Table 4-11 compares q_{DHT} in bare tubes (calculated values) using Equation (2.1) and q_{DHT} in the annular channel and 3-rod bundle (experimental values).

Table 4-11. Comparison of DHT values in bare tube, annular channel, and 3-rod bundle.

Test section	Mass Flux	q_{DHT}, MW/m^2
Bare-tube	G = 2000 kg/m^{2}s	1.43
Single-rod annular channel	G = 2000 kg/m^{2}s	2.55
Bare-tube	G = 1500 kg/m^{2}s	1.06
3-rod bundle	G = 1500 kg/m^{2}s	3.07

Analysis of the data listed in Table 4-11 shows that q_{DHT} values in bare tubes are significantly lower (up to three times) than those in the single-rod and 3-rod bundle channels. This difference can be due to the following three reasons:

1. Different flow geometries than bare tubes.
2. Rods were equipped with helical ribs, which can be considered as an enhanced heat transfer surface and as an additional flow-turbulization device.
3. The single-rod and 3-rod bundle data were of a relatively short heated length (485 mm). Therefore, even at high heat fluxes bulk-fluid temperatures were always below the pseudocritical temperature, i.e., a liquid-like cooling took place.

However, it should be noted that once the wall temperature crossed the pseudocritical line, DHT regime was observed in both test sections.

This analysis shows that a simple function such as q_{DHT} vs. G is not sufficient to cover various flow geometries and different heated lengths. Therefore, more experimental data on these flow geometries should be collected and analyzed to make more general "solid" conclusions.

There seems to be a threshold for onset of DHT regime in single-rod channels. Given that all other parameters are kept constant, onset of DHT is indeed a function of heat flux. In the first four trials (Figure 4-1 – Figure 4-4), there was no rapid increase in wall temperature; temperature profiles were smooth and linear along the heated length. However, in the final trial (Figure 4-5), there is rapid increase in wall temperature at a heated length of 0.37 m which is characteristic of onset of DHT. While the Dittus-Boelter (1930) [2] correlation had the lowest RMS error in most trials, it lacked sensitivity to wall conditions especially around regions of DHT. Although no correlation was able to accurately predict wall temperature in regions of DHT, the Jackson (2002) [3] correlation had low RMS errors and captured the trend around the DHT region in Figure 4-5 sufficiently to be recommended.

The second 3-rod bundle trial (Figure 4-7) showed onset of DHT at a heated length of 0.25 m even though it was at a lower heat flux and inlet temperature than the third 3-rod bundle trial (Figure 4-8). However, the third 3-rod bundle trial had a significantly greater mass flux (almost double the first two), which allowed more accurate prediction of heat transfer than the first two trials; however, there onset of DHT was observed near the channel outlet at a heated length of 0.42 m. The 3-rod bundle trials had significantly higher HTC values even in regions of DHT than single-rod trials. In 3-rod bundle trials where there was DHT, HTC values were almost double those of single-rod trials.

4.7. Temperature Distribution in Modeled UO_2 Fuel for a Single-Rod Flow Geometry

Assuming heat is generated in UO_2 fuel rather than by electrical resistance (discussed in Section 4.1), projected UO_2 fuel temperatures at such conditions can be determined in a single-rod channel.[61] Modelled UO_2 fuel temperature profiles of a single-rod in an annular channel

[61] The heat flux that is quoted in Section 4.1 is based on the outside surface of the rod (which includes the ribs).

cooled with upward flow of SCW are determined using:[62]

1. A spline of the seven experimentally measured inner wall temperatures shown in Appendix A (electrically heated experiment discussed in Section 4.1)
2. Inner wall temperatures obtained using the conduction in a concentric cylinder equation based on outer wall temperatures calculated using the Jackson (2002) [3] correlation.

The percent error calculations between the centerline temperatures derived from the experimental data and those calculated using the Jackson (2002) [3] correlation are determined using Equation (3.24).

4.7.1. Single-Rod Heated by UO_2 fuel; q = 1.543 MW/m^2

Figure 4-12 shows a contour of fuel temperature at the axial position of maximum temperature for a single-rod annular channel at a heat flux of 1.543 MW/m^2 and an SCW inlet temperature of 205°C.

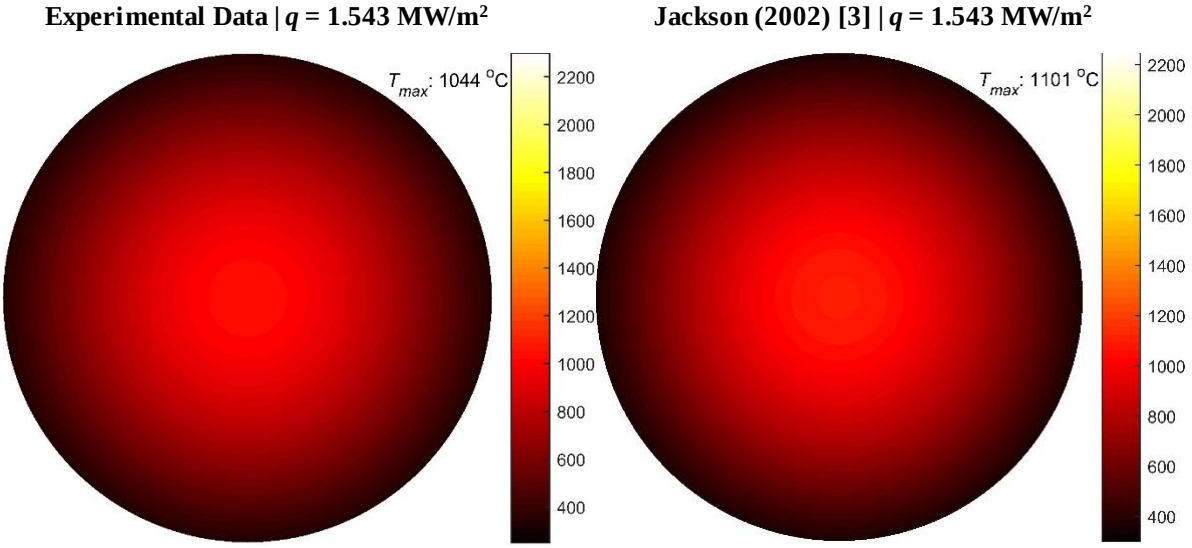

Figure 4-12. Contour of maximum UO_2 temperature cross section; q = 1.543 MW/m^2.

For q = 1.543 MW/m^2, the Jackson (2002) [3] correlation overestimated the fuel centerline

Therefore, the heat flux in this section given that heat generated in the fuel is not in fact equal to that in Section 4.1, however, for the sake of continuity, the same heat flux will be quoted; however, the corrected heat flux is used in the calculations.

[62] Fuel temperatures are assumed radially isotropic.

temperature by 57°C: a percent error of ~ 5%. The maximum fuel temperature was well below the industry accepted operating limit of 1850°C [53].

4.7.2. Single-Rod Heated by UO_2 fuel; q = 1.758 MW/m^2

Figure 4-13 shows a contour of fuel temperature at the axial position of maximum temperature for a single-rod annular channel at a heat flux of 1.758 MW/m^2 and an SCW inlet temperature of 207°C.

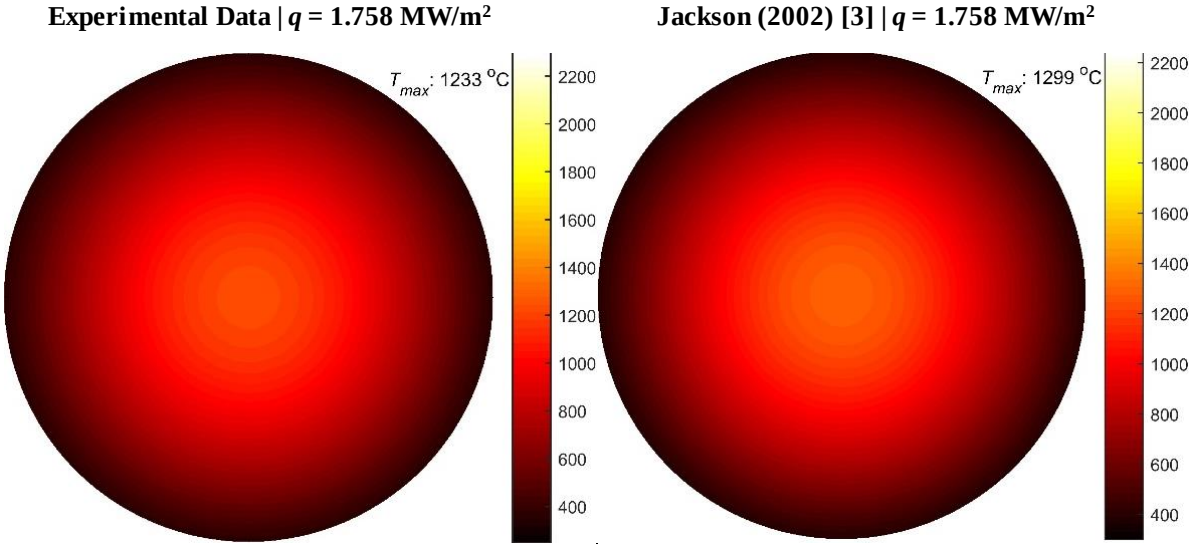

Figure 4-13. Contour of maximum UO_2 temperature cross section; q = 1.758 MW/m^2.

For q = 1.758 MW/m^2, the Jackson (2002) [3] correlation overestimated the fuel centerline temperature by 66°C: a percent error of ~ 5%.[63] The maximum fuel temperature was well below the industry accepted operating limit of 1850°C.

4.7.3. Single-Rod Heated by UO_2 fuel; q = 2.033 MW/m^2

Figure 4-14 shows a contour of fuel temperature at the axial position of maximum temperature for a single-rod annular channel at a heat flux of 2.033 MW/m^2 and an SCW inlet temperature of 208°C.

[63] Even though the difference between the experimental fuel temperature and the one obtained using the Jackson (2002) [3] correlation is increasing, the error remains around 5%. This is because the temperature is larger, which negates the significance of a small increase in difference.

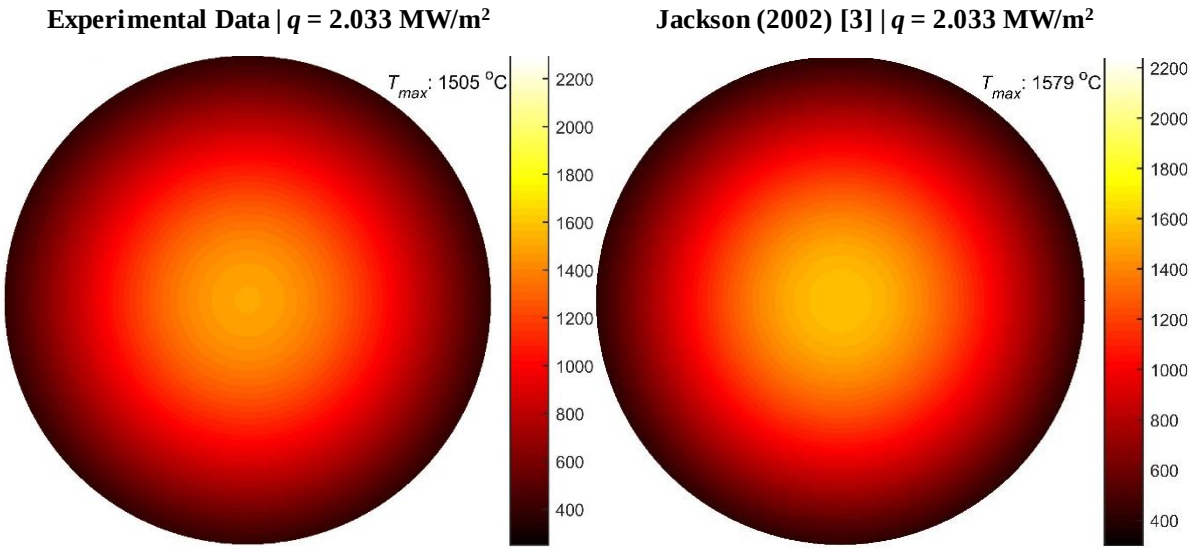

Figure 4-14. Contour of maximum UO_2 temperature cross section; q = 2.033 MW/m^2.

For q = 2.033 MW/m^2, the Jackson (2002) [3] correlation overestimated the fuel centerline temperature by 74°C: a percent error of ~ 5%. The maximum fuel temperature approached industry accepted operating limit of 1850°C when compared to earlier trials.

4.7.4. Single-Rod Heated by UO_2 fuel; q = 2.244 MW/m^2

Figure 4-15 shows a contour of fuel temperature at the axial position of maximum temperature for a single-rod annular channel at a heat flux of 2.244 MW/m^2 and an SCW inlet temperature of 210°C.

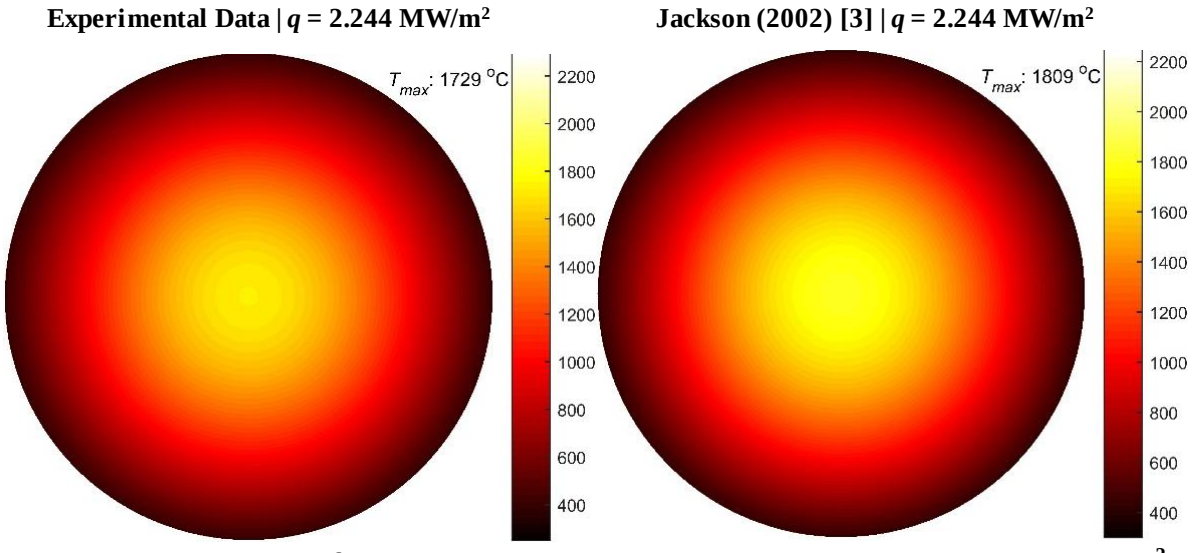

Figure 4-15. Contour of maximum UO_2 temperature cross section; q = 2.244 MW/m^2.

For q = 2.244 MW/m^2, the Jackson (2002) [3] correlation overestimated the fuel centerline temperature by 80°C: a percent error of ~ 5%. Maximum fuel temperature was almost equal to the industry accepted operating limit of 1850°C.

4.7.5. Single-Rod Heated by UO_2 fuel; q = 2.547 MW/m^2

Figure 4-16 shows a contour of fuel temperature at the axial position of maximum temperature for a single-rod annular channel at a heat flux of 2.547 MW/m^2 and an SCW inlet temperature of 214°C.

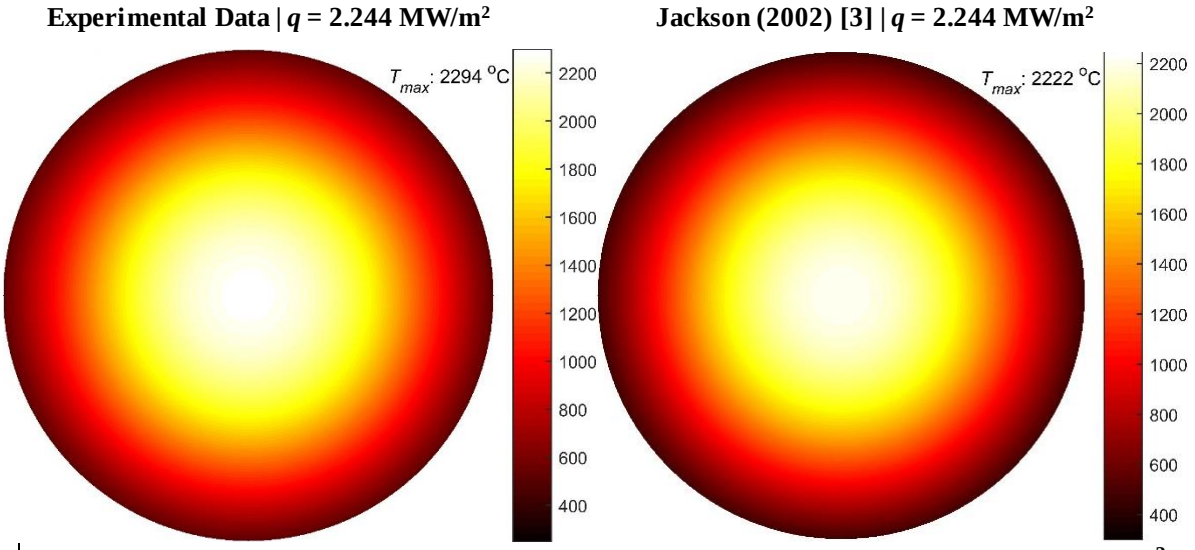

Figure 4-16. Contour of maximum UO_2 temperature cross section; q = 2.547 MW/m^2.

For q = 2.547 MW/m^2, the Jackson (2002) [3] correlation underestimated the fuel centerline temperature by 72°C: a percent error of ~ 3%. The maximum fuel temperature was significantly greater than the industry accepted operating limit of 1850°C. Unlike the previous trials, the significant increase in wall temperature is due to the region of DHT near the channel outlet, as shown in Figure 4-5.

4.7.6. Discussion

As shown in Figure 4-12 – Figure 4-16, the Jackson (2002) [3] correlation provided a conservative estimate of fuel temperature for the first four trials. Figure 4-17 illustrates the radial temperature profile of maximum centerline temperature and provides a summary of Section 4.7.

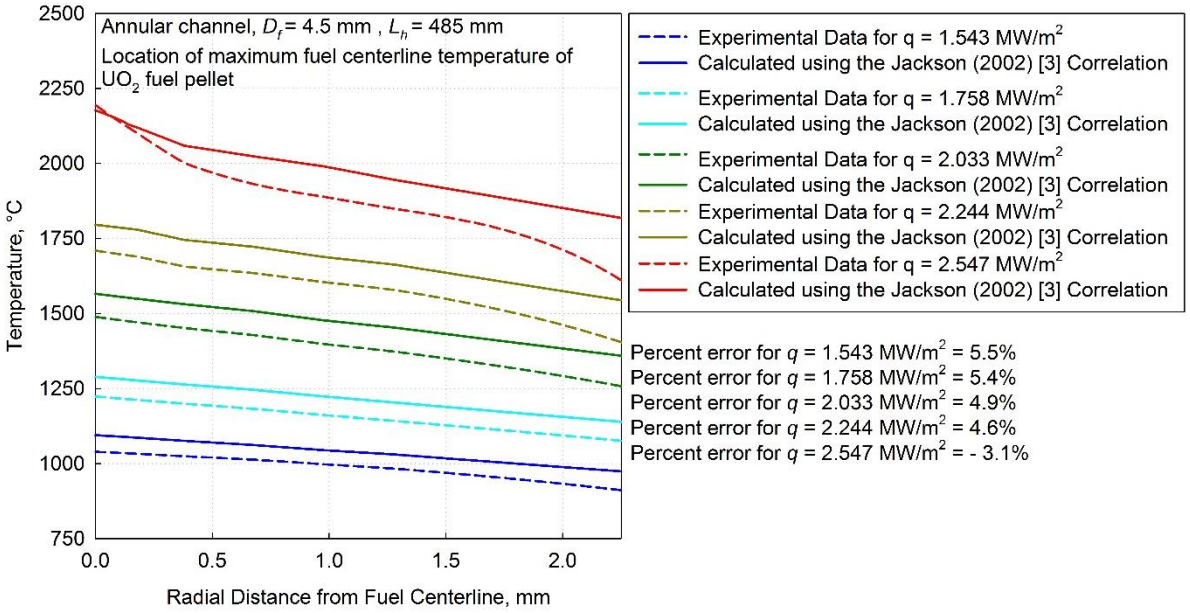

Figure 4-17. Radial UO_2 fuel temperature distribution and summary of percent error for all single-rod channel trials with heat generated by UO_2 fuel.

The Jackson (2002) [3] correlation showed good agreement with the experimental data (giving a conservative estimate) for the first four trials. Only at the trial with the highest heat flux (2.547 MW/m^2) did fuel temperatures exceed the industry accepted limit of 1850°C (although the percentage error was still only 3.1%). It should be noted that at that heat flux, there was a region of significant DHT not fully captured by the Jackson (2002) [3] correlation, as shown in Figure 4-5. Although only a small data set was used, this is an attempt to show preliminary results of using such a geometry, especially for its applicability in transport reactors, and the resultant effects of using bare tube HTC correlations to predict fuel centerline temperatures.

Chapter 5. Analysis of 2×2 Rod Bundle Trials

This chapter analyzes heat transfer to SCW flowing upward in a 2×2 rod bundle-flow geometry. Outer wall temperatures transcribed from Zhao et al. (2015) [47] are compared against values calculated using HTC correlations [47].[64] The unique flow geometry of a 2×2 rod bundle caused the development of several sub-channels each with slightly different wall and bulk-fluid conditions; wall temperatures were measured at the resulting: center, wall, corner, and gap sub-channels, as shown in Figure 3-12.[65] The presence of spacers caused significant local turbulence of the coolant.[66] Heat fluxes found in this experiment were significantly lower than those found in Section 4.1 due to the longer heated length.

5.1. First 2×2 Rod Bundle Trial; G = 900 kg/m^{2}s, q = 1.2 MW/m^2

Bulk-fluid temperatures were almost equal to the pseudocritical temperature near the outlet of the test section; most HTC correlations had difficulty in accurately predicting heat transfer in this region. Channel parameters in the first 2x2 rod bundle trial are:

- Constant pressure: P = 23 MPa; $P_{cr\text{-}water}$ = 22.064 MPa
    - Pseudocritical temperature: $T_{pc@23\text{MPa}}$ = 377.5°C
- Mass flux: G = 900 kg/m^{2}s
- Heat flux: q = 1.2 MW/m^2

HTC correlations that are illustrated include those proposed by: Bishop et al. (1964) [8], Dittus-Boelter (1930) [2], Dyadyakin and Popov (1977) [13], Jackson (2002) [3], and Swenson (1965) [31].

---

[64] Since raw experimental data was not used, the percentage error is greater than experimental uncertainties given in Table 3-6. It is difficult to say exactly how much error is caused by transcribing the densely packed data in Figure 5-1; however, every effort was put to ensure accurate results (such as: zooming, confirming using two values).

[65] Due to the limitations of one-dimensional heat transfer correlations, minor differences in bulk-fluid conditions between each sub-channel are not captured; however, the presence of spacers increases mixing of the bulk-fluid significantly (at the expense of pressure head), reducing the deviation of bulk-fluid temperatures.

[66] Regions of high turbulence are indicative of regions of improved heat transfer. This improvement in heat transfer is due to increased turbulence and is not the same phenomenon as IHT (discussed in Section 2.5), which due to variation in thermophysical properties.

5.1.1. Bulk-fluid and Inner Wall Temperatures, and HTC Profiles

Figure 5-1 shows bulk-fluid temperatures, outer wall temperatures, and HTC profiles as functions of the heated length for upward flow of SCW in a 2×2 rod bundle channel at a heat flux of 1.2 MW/m^2 and a mass flux of 900 kg/m^{2}s.

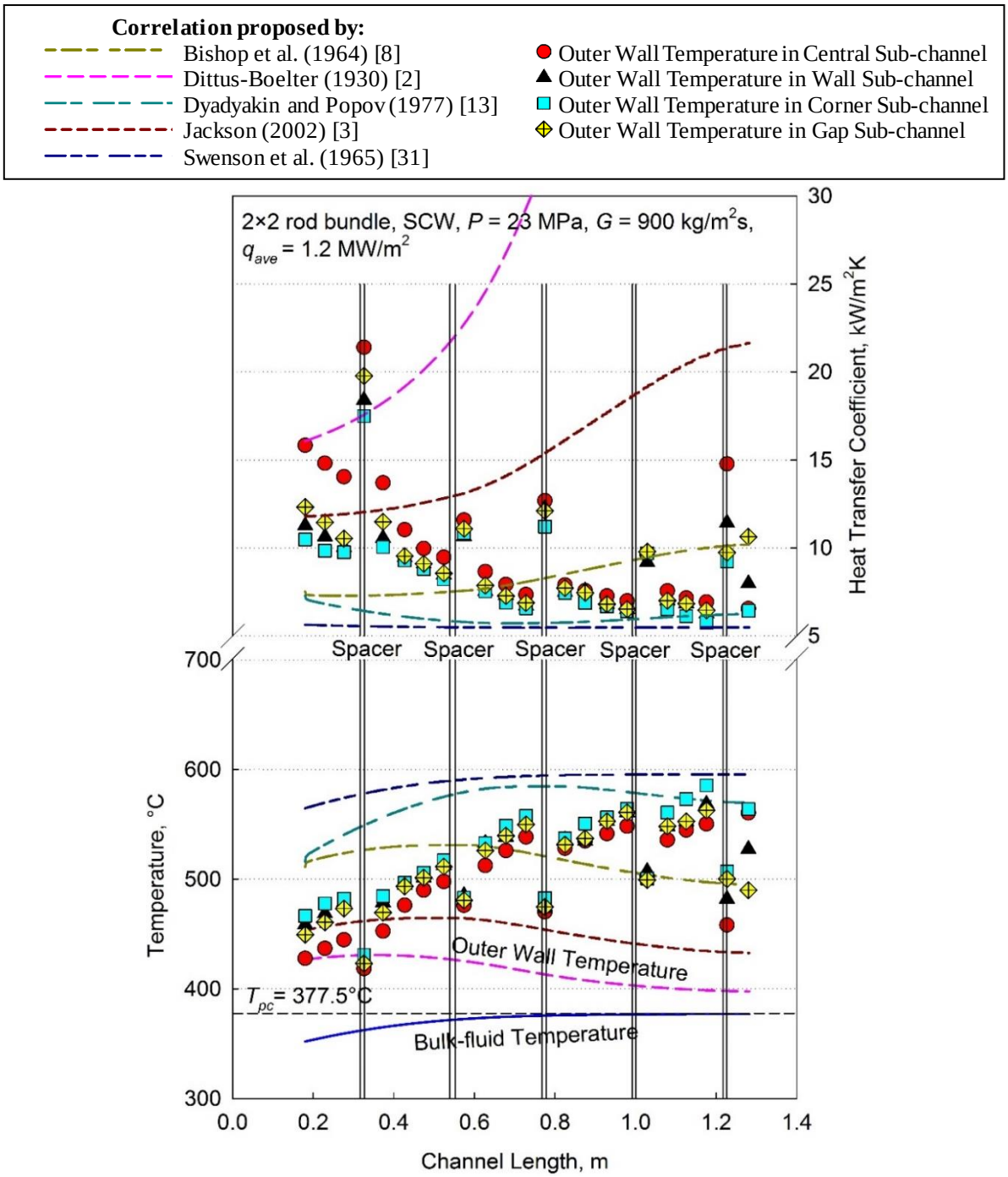

Figure 5-1. Bulk-fluid temperature, wall temperature and HTC profiles along heated length of a 2×2 rod bundle channel; q = 1.2 MW/m^2, G = 900 kg/m^{2}s.

Only the correlations proposed by Swenson et al. (1965) [31] and Dyadyakin and Popov (1977) [13] gave a conservative estimate of the outer wall temperature, however, they did not follow the trend of the experimental data. Almost a third of the heated length had bulk-fluid temperatures almost equal to the pseudocritical temperature; this was problematic for most bulk-fluid dependent correlations due to rapid variation in thermophysical properties. Both correlations proposed by Dittus-Boelter (1930) [2] and Jackson (2002) [3] initially showed good agreement with the experimental data; however, as bulk-fluid temperatures approached the pseudocritical temperature, the accuracy of predicted outer wall temperatures decreased significantly. The Bishop et al. (1964) [8] correlation overestimated the wall temperature initially, and then underestimated it near the outlet.

Rapid drops in wall temperatures were observed at spacer locations, which were not accounted for by any correlation as they cannot account for the local improvement in heat transfer due to spacers. The outer wall temperature in corner sub-channel consistently showed the highest temperature values, possibly due to the low degree of turbulence in the corner region. The central sub-channel had the lowest outer wall temperature values due to the large degree of turbulence in that region. Outer wall temperatures of the gap and wall sub-channels were in between these two extremes. Experimental HTC values ranged between 6 – 12 kW/m^{2}K, which were significantly lower than HTC values obtained in Chapter 4 (due to lower heat and mass fluxes). Table 5-1 lists RMS errors calculated using experimental outer wall temperature transcribed from Zhao et al. (2015) [47] were compared to the corresponding value obtained using each correlation.

Table 5-1. Outer Wall Temperature RMS errors of Central, Wall, Corner, and Gap sub-channels in a 2×2 rod bundle; q = 1.2 MW/m^2 and G = 900 kg/m^{2}s.

Correlation Proposed by	Outer Wall Temperature Sub-channel RMS Error			
	Central	Wall	Corner	Gap
Bishop et al. (1964) [8]	11.5%	9.0%	9.3%	9.4%
Dittus-Boelter (1930) [2]	18.5%	20.0%	21.2%	19.5%
Dyadyakin and Popov (1977) [13]	16.6%	13.3%	12.1%	14.1%
Jackson (2002) [3]	12.9%	13.8%	15.1%	13.4%
Swenson et al. (1965) [31]	21.0%	17.3%	15.9%	18.2%

The Bishop et al. (1964) [8] correlation showed the lowest RMS error in this trial with the

Jackson (2002) [3] correlation coming in a close second.[67] RMS error for the Dittus-Boelter (1930) [2] correlation was high as it gave a completely inaccurate prediction of wall temperature (underestimated). Generally, the central sub-channel had the largest RMS errors, as it had the largest heated length.

5.1.2. Mechanism of Convection and Onset of DHT of Section 5.1.1 data

Variation in the $\frac{\overline{\mathbf{Gr}_b}}{\mathbf{Re}_b^{2.7}}$ ratio discussed in Section 2.9 for the trial shown in Figure 5-1 are shown in Figure 5-2. Since there was no onset of DHT in Figure 5-1, rapid increases in the ratio are not expected except in the spacer regions.

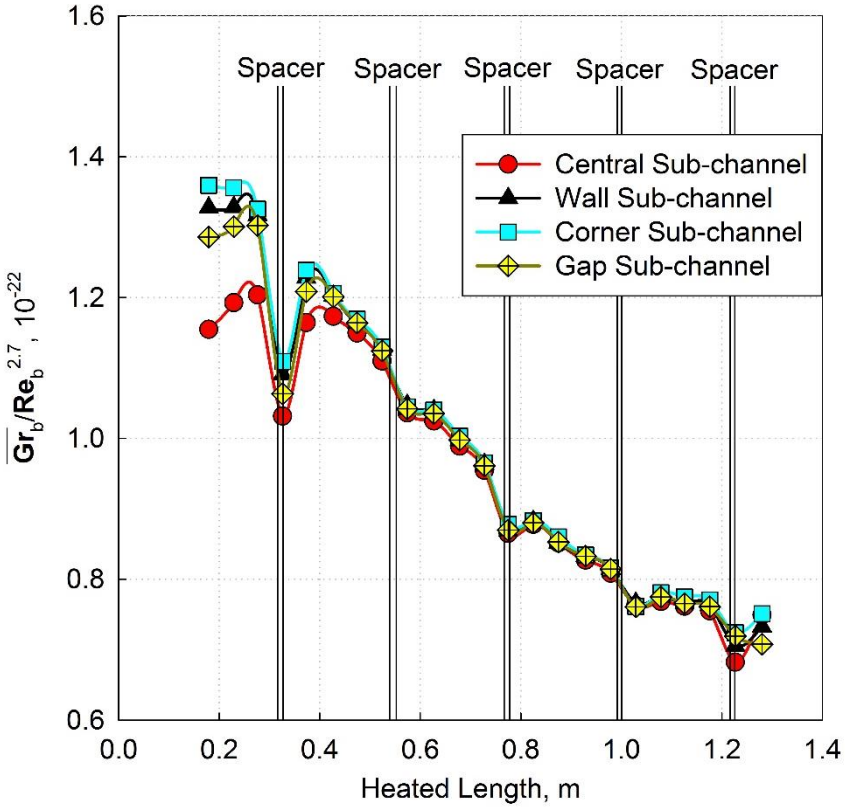

Figure 5-2. The $\frac{\overline{\mathbf{Gr}_b}}{\mathbf{Re}_b^{2.7}}$ ratio across the heated length for q = 1.2 MW/m^2 and G = 900 kg/m^{2}s.

[67] It should be noted that RMS errors in this trial are a bit misleading. The Bishop et al. (1964) [8] correlation gave a significantly overestimated value for the wall temperature near the channel outlet, while giving a significantly underestimated value near the outlet, which resulted in an average line, thus achieving the lowest RMS error.

As shown in Figure 5-2, the $\frac{\overline{\mathbf{Gr}_b}}{\mathbf{Re}_b^{2.7}}$ ratio is significantly less than $2.4 \cdot 10^{-5}$ across the heated length (for all sub-channels) which indicates that this is solely forced-convection flow. There are no increases in buoyancy effects and no onset of DHT. This is because an increase in wall temperature (as in the case of DHT) does not simply cause an increase in buoyancy effects; wall temperature in Figure 5-1 steadily increased along the heated length with no effect on the ratio.

5.1.3. Analysis of Section 4.15.1.1 data based on the Eckert Number

The Eckert number (Equation (2.3)) was introduced in Section 2.10.1 to describe the degree of divergence of wall and bulk-fluid conditions. Figure 5-3 applies this concept to the data set discussed in in Section 5.1.

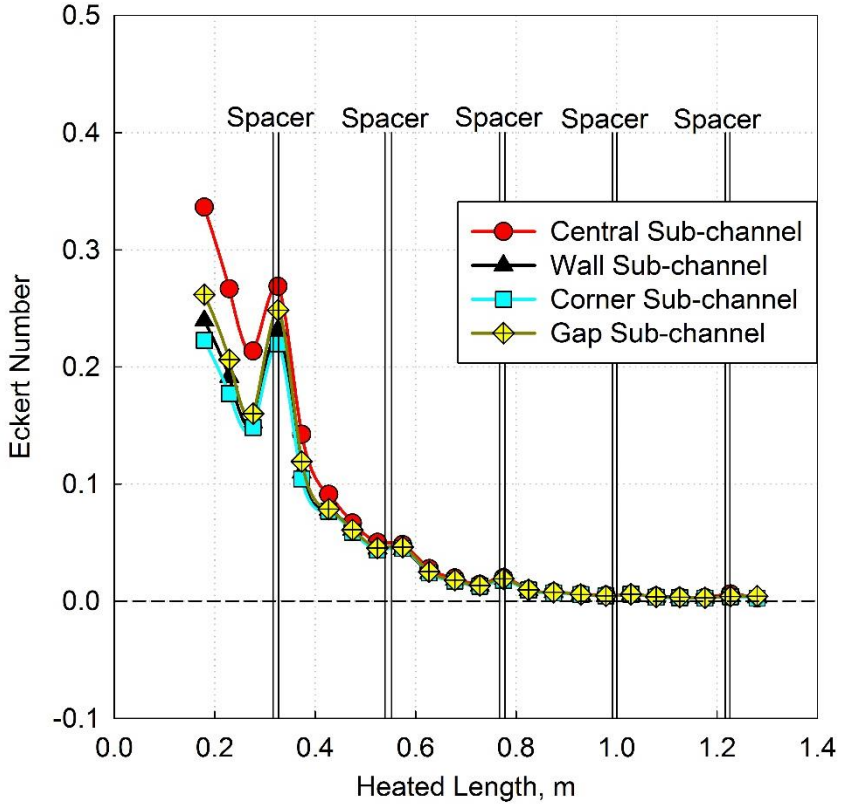

Figure 5-3. The Eckert number across the heated length of a 2×2 rod bundle for q = 1.2 MW/m^2 and G = 900 kg/m^{2}s.

As $\mathbf{E} \rightarrow 0$ in the latter part of the heated length, there was significant decrease in the accuracy of prediction of wall temperature, as shown in Figure 5-1 & Figure 5-3. In fact, once $\mathbf{E} \lesssim 0.2$, the Dittus-Boelter (1930) [2] correlation became unable to predict wall temperature. The

Jackson (2002) [3] correlation was able to predict wall temperature until $\mathbf{E} \lesssim 0.1$, as shown in Figure 5-1 & Figure 5-3.[68] The Eckert number mirrors trends of outer wall temperature. Although the heat and mass flux were significantly lower than the experiment illustrated in Chapter 4, the proximity of the bulk-fluid temperature to the pseudocritical temperature caused large increases in RMS error for all correlations.

5.2. Second 2×2 Rod Bundle Trial; G = 1000 kg/m^{2}s, q = 0.8 MW/m^2

Bulk-fluid temperatures were slightly lower than the pseudocritical temperature near the outlet of the test section, unlike the trial presented in Figure 5-1. Thus, channel parameters in the second 2x2 rod bundle trial are:

- Constant pressure: P = 23 MPa; $P_{cr\text{-}water}$ = 22.064 MPa
    - Pseudocritical temperature: $T_{pc@23\text{MPa}}$ = 377.5°C
- Mass flux: G = 1000 kg/m^{2}s
- Heat flux: q = 0.8 MW/m^2

HTC correlations that are illustrated include those proposed by: Bishop et al. (1964) [8], Dittus-Boelter (1930) [2], Dyadyakin and Popov (1977) [13], Jackson (2002) [3], and Swenson (1965) [31].

5.2.1. Bulk-fluid and Inner Wall Temperatures, and HTC Profiles

Figure 5-4 shows bulk-fluid temperatures, outer wall temperatures, and HTC profiles as functions of the heated length for upward flow of SCW in a 2×2 rod bundle channel at a heat flux of 0.8 MW/m^2 and a mass flux of 1000 kg/m^{2}s.

[68] The other correlations did not follow the trend of outer wall temperatures throughout the heated length, as shown in Figure 5-1, and thus did not warrant further discussion using the Eckert number.

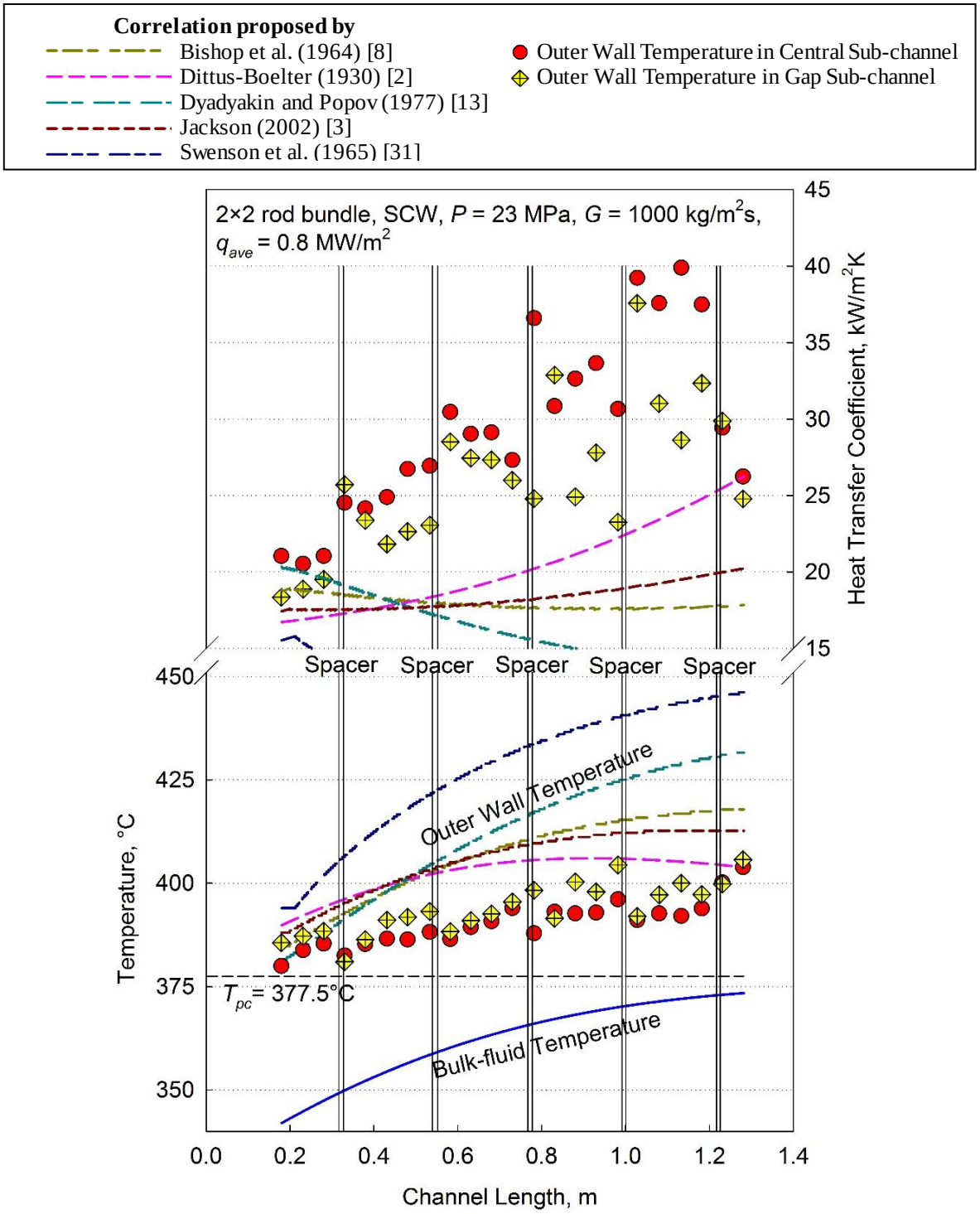

Figure 5-4. Bulk-fluid and outer wall temperature of a 2×2 rod bundle channel along the heated length; q = 0.8 MW/m^2, G = 1000 kg/m^{2}s.

All correlations illustrated in Figure 5-4 gave a conservative estimate of the outer wall temperature. The correlation proposed by Swenson et al. (1965) [31] and Dyadyakin and Popov (1977) [13] significantly overestimated the outer wall temperature. The region near

the test section outlet had bulk-fluid temperatures slightly lower than the pseudocritical temperature; unlike Figure 5-1, both correlations proposed by Dittus-Boelter (1930) [2] and Jackson (2002) [3] showed good agreement with the experimental data.

Rapid drops in wall temperatures were observed at spacer locations, which were not accounted for by any correlation as they cannot account for the presence of spacers. The gap sub-channel showed the highest temperature values, except right after the spacers. This is due to increased mixing and a lower sub-channel heated perimeter compared with the central sub-channel. The central sub-channel had the lowest outer wall temperature values due to the high turbulence. Experimental HTC values ranged between 20 – 40 kW/m^{2}K, which were significantly higher than those observed in Figure 5-1.[69] Table 5-2 lists RMS errors calculated using experimental outer wall temperature transcribed from Zhao et al. (2015) [47] were compared to the corresponding value obtained using each correlation.

Table 5-2. Outer Wall Temperature RMS errors of Central, Wall, Corner, and Gap sub-channels in a 2×2 rod bundle; q = 0.8 MW/m^2 and G = 1000 kg/m^{2}s.

Correlation Proposed by	Outer Wall Temperature Sub-channel RMS Error	
	Central	Gap
Bishop et al. (1964) [8]	4.4%	3.6%
Dittus-Boelter (1930) [2]	3.2%	2.4%
Dyadyakin and Popov (1977) [13]	6.1%	5.3%
Jackson (2002) [3]	4.1%	3.2%
Swenson et al. (1965) [31]	9.9%	8.9%

The Dittus-Boelter (1930) [2] correlation showed the lowest RMS error in this trial with the correlations proposed by Bishop et al. (1964) [8] and Jackson (2002) [3] coming in a close second. The correlations proposed by Swenson et al. (1965) [31] and Dyadyakin and Popov (1977) [13] both had large RMS error values. The Bishop et al. (1964) [8] correlation also managed to give an accurate prediction of wall temperature, however, it was still less accurate than the correlations proposed by Jackson (2002) [3] and Dittus-Boelter (1930) [2]. The gap

[69] Significantly improved HTC values in Figure 5-4 indicate that there was onset of DHT regime in Figure 5-1. This is interesting because the only difference between the two trials is a slightly lower heat flux, and a slightly larger mass flux.

sub-channel was predicted with lower RMS errors than the central sub-channel, as it had a lower sub-channel heated perimeter.

5.2.2. Mechanism of Convection and Onset of DHT of Section 5.2.1 data

Variation in the $\frac{\overline{Gr_b}}{Re_b^{2.7}}$ ratio discussed in Section 2.9 for the trial shown in Figure 5-4 are shown in Figure 5-5. Since there was no onset of DHT in Figure 5-4, rapid increases in the ratio are not expected, except in the spacer regions.

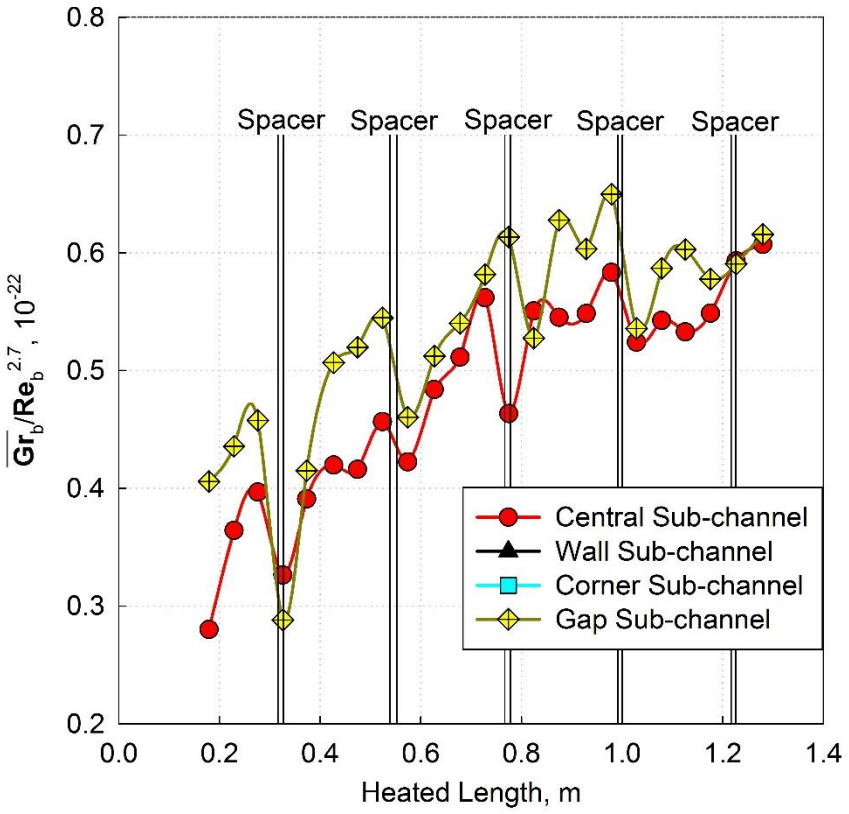

Figure 5-5. The $\frac{\overline{Gr_b}}{Re_b^{2.7}}$ ratio across the heated length for q = 1.2 MW/m^2 and G = 900 kg/m^{2}s.

As shown in Figure 5-5, the $\frac{\overline{Gr_b}}{Re_b^{2.7}}$ ratio is significantly less than $2.4 \cdot 10^{-5}$ across the heated length (for all sub-channels) which indicates that this is solely forced-convection flow. There are no rapid increases in buoyancy effects represented and no onset of DHT. The ratio did increase steadily along the heated length. It should be noted that an increase in wall temperature does not simply cause an increase in buoyancy effects; wall temperature in Figure 5-4 steadily increases along the heated length with no effect on the ratio.

5.2.3. Analysis of Section 5.2.1 data based on the Eckert Number

The Eckert number (Equation (2.3)) was introduced in Section 2.10.1 to describe the degree of divergence of wall and bulk-fluid conditions, and the concept is applied to Figure 5-5. Figure 5-6 applies this concept to the data set discussed in in Section 5.2.

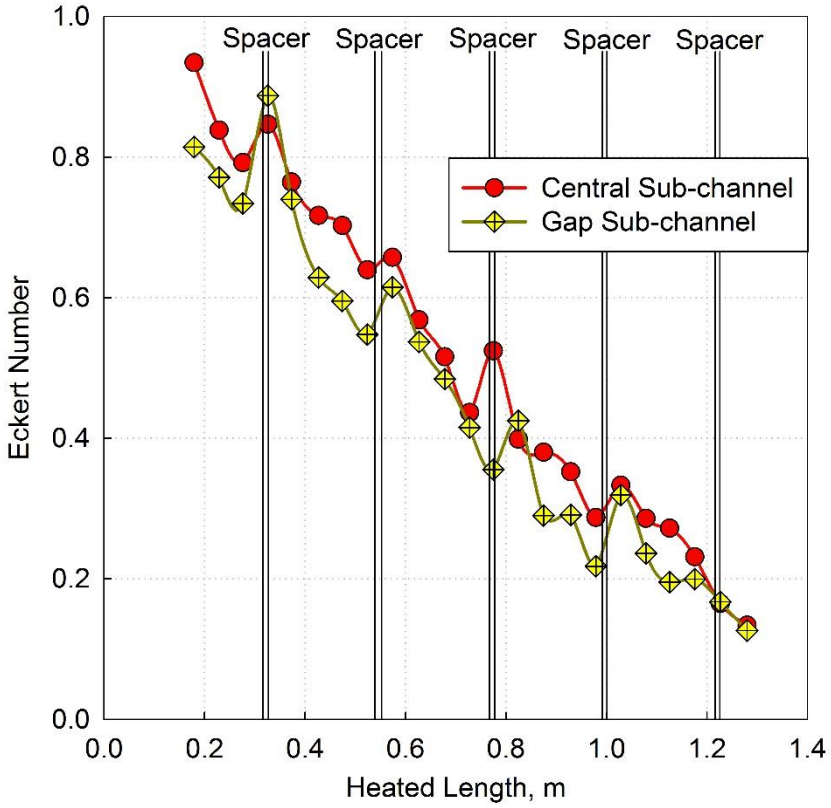

Figure 5-6. The Eckert number across the heated length of a 2×2 rod bundle trials for q = 0.8 MW/m^2 and G = 1000 kg/m^{2}s.

Given that **E** > 0.2 for the majority heat length, most correlations were able to accurately predict heat transfer, as shown in Figure 5-4 & Figure 5-6. There is significant local increase in the Eckert number due to spacers due to the decrease in the denominator of the Eckert number equation.

5.3. Discussion

There was a clear inability to predict outer wall temperatures in Figure 5-1 versus Figure 5-4, even though bulk-fluid temperature profiles were almost identical. Thus, for the same geometry and bulk-fluid conditions, the ratio of heat to mass flux plays a crucial role. The lower q/G ratio illustrated in Figure 5-4 (0.8 kJ/kg versus 1.3 kJ/kg) allowed most correlations

to better predict heat transfer, as shown in Table 5-2 versus Table 5-1. Spacers caused some enhancement in heat transfer, however, their effects were localized, with wall temperatures returning to normal right after the spacer region.

Although the correlations proposed by Dyadyakin and Popov (1977) [13] and Swenson et al. (1965) [31] were unable to predict heat transfer in all trials, the Bishop et al. (1964) [8] correlation showed some accuracy at the lower q/G ratio. The correlations proposed by Dittus-Boelter (1930) [2] and Jackson (2002) [3] continued to show the most accurate predictions, as shown in Table 5-1 and Table 5-2.

Equation (2.1) was not used to analyze this data set, as there were not enough trials to accurately determine onset of DHT, unlike the single-rod and 3-rod bundle trials.

Conclusions

This work assessed the viability of using Heat Transfer Coefficient (HTC) correlations found in the open literature, as a preliminary, but conservative approach to predict HTCs and wall temperatures in bundle-flow geometries cooled with SuperCritical Water (SCW).

A one-dimensional heat-transfer analysis was conducted on three different channel geometries. The first geometry was a single-rod channel, the second was a 3-rod bundle channel, and the third case was a 2×2 rod bundle. There were at least two trials for each case, which allowed some specifics of heat transfer to be explored. Differences in the onset of DHT regime between several channel geometries were explored.

A universal method for accurate prediction of heat transfer in bundle-flow geometries cooled with upward flow of SCW using correlations published by Dittus-Boelter (1930) [2] and Jackson (2002) [3] was proposed and verified. These correlations showed very good agreement with the experimental data when the coolant is a compressed fluid (~2% RMS error). However, there was an inability to predict wall temperatures as the Eckert number approached zero (i.e. as the bulk-fluid temperature approached the pseudocritical temperature). While the Dittus-Boelter (1930) [2] correlation had the lowest RMS error for most trials, it lacked sensitivity to wall conditions in regions of Deteriorated Heat Transfer (DHT). This was due to the sole dependence of the Dittus-Boelter (1930) [2] correlation on bulk-fluid conditions. The Jackson (2002) [3] correlation on the other hand had low RMS errors and, to some extent, followed wall temperature trends in regions of DHT. It was observed that for the same channel geometry, lower q/G ratios showed more accurate predictions of wall temperature. Disregarding regions of DHT, HTC values of more complex bundle geometries were significantly greater than those of single-rod channel trials.

Given all other parameters were kept constant, it was determined that onset of DHT is indeed a function of a ratio of heat flux to mass flux. Analysis of the experimental data showed that q_{DHT} values in bare tubes are significantly lower (up to three times) than those in the single-rod and 3-rod bundle channels. Furthermore, it was found that, in general, bare tube HTC correlations could not be used beyond onset of DHT in bare tubes.

Future Research

Future work should examine a larger data set to verify results shown in this thesis. A larger amount of channel conditions should be used, for a given simple bundle geometry, to better capture specifics of heat transfer.

Furthermore, a two-dimensional or even three-dimensional computational fluid dynamics model should be employed to gain better understanding of fluid behavior and heat transfer mechanisms.

Reference

[1] National Institute of Standards Technology, "NIST Reference Fluid Thermodynamic and Transport Properties-REFPROP: NIST Standard Reference Database 23, Ver. 8.0.," Department of Commerce, Boulder, CO, USA, 2007.

[2] F. Dittus and L. Boelter, "Heat Transfer in Automobile Radiators of the Tubular Type," *Publications on Engineering,* vol. 2, no. 13, pp. 443-461, 1930.

[3] J. Jackson, "Considerations of the heat transfer properties of supercritical pressure water in connection with the cooling of advanced nuclear reactors," in *13th Pacific Basin Nuclear Conference*, Shenzhen City, China, October 21 - 25 2002.

[4] I. Pioro and R. Duffey, Heat Transfer and Hydraulic Resistance at Supercritical Pressures in Power-Engineering Applications, New York: ASME Press, 2007.

[5] J. Levelt Sengers, "Supercritical fluids: Their properties and applications," in *Supercritical Fluids*, vol. 366, E. Kiran and et al., Eds., Kluwer Academic Publishers, 2000, pp. 1-29.

[6] R. Hendricks, R. Simoneau and R. Smith, "Survey of heat transfer to near-critical fluids," NASA,, Cleveland, OH, USA, 1970a.

[7] E. Schmidt, E. Eckert and V. Grigull, "Heat transfer by liquids near the critical state," *Air Materials Command,* vol. 527, April 1946.

[8] A. Bishop, R. Sandberg and L. Tong, "High temperature supercritical pressure water loop: Part IV. Forced convection heat transfer to water at near-critical temperatures and super-critical pressures," Westinghouse Electric Corporation, Pittsburgh, Pa, 1964.

[9] J. Ackerman, "Pseudoboiling heat transfer to supercritical pressure," *Journal of Heat Transfer,* vol. 92, no. 3, pp. 490-498, 1970.

[10] F. Mayinger and M. Scheidt, "Heat transfer in supercritical region with vertical upflow," *Wärme- und Stoffübertragung,* vol. 18, pp. 207-214, 1984.

[11] IAEA, "Heat and Transfer Behaviour and Thermohydraulics Code Testing for SCWR," IAEA, Vienna, Austria, 2014.

[12] Generation-IV International Forum, Handbook of Generation IV Nuclear Reactors, I. Pioro, Ed., New York, NY, USA: Elsevier, 2016, p. 938.

[13] B. Dyadyakin and A. Popov, "Heat Transfer and Thermal Resistance of Tight Seven Rod Bundle Cooled with Water Flow at Supercritical Pressures (In Russian)," *Transactions of VTI,* vol. 11, pp. 244-253, 1977.

[14] V. Razumovskiy, E. Pis'menny, A. Koloskov and I. Pioro, "Heat Transfer to Supercritical Water in Vertical 7-Rod Bundle," in *16th International Conference on Nuclear Engineering (ICONE-16)*, Orlando, Florida, May 11–15, 2008.

[15] G. Richards, G. Harvel, I. Pioro, A. Shelegov and P. Kirillov, "Heat Transfer Profiles of a Vertical, Bare, 7-Element Bundle Cooled with Supercritical Freon R-12," *Nuclear Engineering and Design,* vol. 264, pp. 246-256, 2013.

[16] I. Pioro and S. Mokry, "Heat Transfer. Theoretical Analysis, Experimental Investigations and Industrial Systems," in *Heat Transfer to Fluids at Supercritical Pressures*, A. Belmiloudi, Ed., Rijeka, Croatia, INTECH, 2011, pp. 481-504.

[17] E. Pis'mennyy, V. Razumovskiy, E. Maevskiy, A. Koloskov, I. Pioro and R. Duffey, "Experimental Study on Temperature Regimes to Supercritical Water Flowing in Vertical Tubes at Low Mass Fluxes," in *Nuclear Energy Systems for Future Generation and Global Sustainability, GLOBAL-2005*, Tsukuba, Japan, October 9-13, 2005.

[18] P. Tsvetkov and D. Ames II, "Electrical Generation from Nuclear Power Plants," in *NUCLEAR ENERGY ENCYCLOPEDIA*, New Jersey, Wiley & Sons, 2011, pp. 57-64.

[19] I. Pioro, "Nuclear Power as a Basis for Future Electricity Production in the World:

Generation III and IV Reactors," University of Ontario Institute of Technology (UOIT), Oshawa, 2013.

[20] World Nuclear Association, "World Energy Needs and Nuclear Power," January 2015. [Online]. Available: http://www.world-nuclear.org/information-library/current-and-future-generation/world-energy-needs-and-nuclear-power.aspx. [Accessed 28 March 2016].

[21] A. Chowdhury and N. Kipgen, "Deluge amidst conflict: Hydropower development and displacement in the North-east region of India," *Progress in Development Studies*, vol. 13, no. 3, pp. 195-208, July 2013.

[22] Y. A. Cengel and M. A. Boles, Thermodynamics: An Engineering Approach, New York: McGraw-Hill, 2011.

[23] GIF, "A Technology Roadmap Update for Generation IV Nuclear Energy Systems," OECD Nuclear Energy Agency, January 2014.

[24] D. Wang and S. Wang, "A Preliminary CATHENA Thermalhydraulic Model of the Canadian SCWR for Safety Analysis," *AECL Nuclear Review*, vol. 10, no. 3, pp. 9-16, 2014.

[25] J. Jackson and W. Hall, "Forced Convection Heat Transfer to Fluids at Supercritical Pressure," in *Turbulent Forced Convection in Channels and Bundles*, vol. 2, S. Kakaç and D. Spalding, Eds., New York, New York, USA, Hemisphere Publishing Corp., 1979a, pp. 563-612.

[26] S. Mukherjee and A. Paul, Fundamentals of Mechanical Sciences Engineering Thermodynamics and Fluid Mechanics, New Delhi, : PHI Learning Private Limited, 2009.

[27] J. Fewster and J. Jackson, "Experiments on supercritical pressure convective heat transfer having relevance to SCWR," in *International Congress on Advances in Nuclear*

Power Plants (ICAPP'04), Pittsburgh, PA, USA, June 13–17, 2004.

[28] P. Kirillov, R. Pometko, A. Smirnov, V. Grabezhnaia, I. Pioro, R. Duffey and H. Khartabil, "Experimental study on heat transfer to supercritical water flowing in 1- and 4-m-long vertical tubes," in *GLOBAL 2005 International Conference, Nuclear Energy Systems for Future Generation and Global Sustainability (GLOBAL'05)*, Tsukuba, Japan, 2005.

[29] Y. Vikhrev, Y. Barulin and A. Kon'kov, "A study of heat transfer in vertical tubes at supercritical pressures," *Thermal Engineering (Теплоэнергетика, стр. 80–82),* vol. 14, no. 9, pp. 116-119, 1967.

[30] M. Styrikovich, T. Margulova and Z. Miropol'skii, "Problems in the development of designs of supercritical boilers," *Thermal Engineering (Теплоэнергетика, стр. 4–7),* vol. 14, no. 9, pp. 5-9, 1967.

[31] H. Swenson, J. Carver and C. Kakarala, "Heat transfer to supercritical water in smooth-bore tubes," *Journal of Heat Transfer, Transactions of ASME, Series C,* vol. 87, no. 4, pp. 477-484, 1965.

[32] B. Shiralkar and P. Griffith, "The effect of swirl, inlet conditions, flow direction, and tube diameter on the heat transfer to fluids at supercritical pressure," *Journal of Heat Transfer, Transactions of the ASME,* vol. 92, no. 3, pp. 465-474, 1970.

[33] E. Pis'menny, V. Razumovskiy, E. Maevskiy, A. Koloskov and I. Pioro, "Heat Transfer to Supercritical Water in Gaseous State or Affected by Mixed Convection in Vertical Tubes," in *ICONE,* Miami, Florida, 2006.

[34] K. Yamagata, K. Nishikawa, S. Hasegawa, T. Fujii and S. Yoshida, "Forced Convective Heat Transfer to Supercritical Water Flowing in Tubes," *International Journal of Heat and Mass Transfer,* vol. 15, pp. 2575 - 2593, 1972.

[35] M. Shitsman, "Impairment of the heat transmission at supercritical pressures," *High Temperatures (Теплофизика Высоких Температур, стр. 267–275),* vol. 1, no. 2, pp.

237-244, 1963.

[36] S. Mokry, I. Pioro, A. Farah, K. King, S. Gupta, W. Peiman and P. Kirillov, "Development of supercritical water heat-transfer correlation for vertical bare tubes," *Nuclear Engineering and Design,* vol. 241, no. 4, pp. 1126-1136, 2011.

[37] V. Silin, V. Voznesensky and A. Afrov, "The light water integral reactor with natural circulation of the coolant at supercritical pressure B-500 SKDI," *Nuclear Engineering and Design,* vol. 144, pp. 327-336, 1993.

[38] J. Jackson, M. Cotton and B. Axcell, "Studies of mixed convection in vertical tubes," *Int. J. Heat and Fluid Flow,* vol. 10, no. 1, pp. 2-15, 1988.

[39] T. Rothenfluh, "Heat Transfer Phenomena of Supercritical Water Jets in Hydrothermal Spallation Drilling," ETH Zurich, Zurich Switzerland, 2013.

[40] E. Saltanov, "Specifics of Forced-Convective Heat Transfer to Supercritical CO2 Flowing Upward in Vertical Bare Tubes," University of Ontario Institute of Technology, Oshawa, 2015.

[41] J. Lamarsh and A. Baratta, Introduction to Nuclear Engineering, Third Edition ed., Upper Saddle River, New Jersey: Prentice-Hall Inc, 2001.

[42] B. Petukhov, K. E. and V. Protopopov, "An Investigation of Heat Transfer to Fluids Flowing in Pipes Under Supercritical Conditions," in *International Heat Transfer Conference*, University of Colorado, Boulder, CO, USA, January 8–12, 1961.

[43] H. Zahlan, D. Groeneveld, S. Tavoularis, S. Mokry and I. Pioro, "Assesment of Supercritical Heat Transfer Prediction Methods," in *5th International Symposium on SCWR (ISSCWR-5),* Vancouver, British Columbia, Canada, March 13-16, 2011.

[44] S. Gupta, S. Mokry and I. Pioro, "Developing A heat-transfer correlation for supercritical-water flow in vertical bare tubes and its application in SCWRS," in *19th International Conference On Nuclear Engineering (ICONE-19),* Osaka, Japan, October

24-25, 2011.

[45] E. Krasnoshchekov, V. Protopopov, F. Van and I. Kuraeva, "Experimental investigation of heat transfer for carbon dioxide in the supercritical region,," vol. 1, pp. 26-35, 1967.

[46] V. Razumovskiy, E. Pis'mennyy, A. Koloskov and I. Pioro, "Heat Transfer to Supercritical Water in Vertical Annular Channel and 3-rod Bundle," in *17th International Conference On Nuclear Engineering (ICONE-17)*, Brussels, Belgium, July 12-16, 2009.

[47] M. Zhao, H. Gu, X. Cheng, L. and Q. Yang, "Experimental and Numerical Study on Heat Transfer of Supercritical Water Flowing Upward in 2x2 Rod Bundles," in *Nuclear Reactor Thermal Hydraulics (NURETH-16)*, Chicago,IL, 2015.

[48] V. Razumovskiy, E. Pis'mennyy, A. Koloskov and I. Pioro, "Heat Transfer to Supercritical Water in Vertical Annular Channel and 3-rod Bundle," in *17th International Conference On Nuclear Engineering (ICONE-17)*, Brussels, Belgium, July 12-16, 2009.

[49] K. Sidawi, I. Pioro, V. Razumovskiy, E. Pis'mennyi and A. Koloskov, "HTC Correlation Applications to SuperCritical Water Flowing Upward in a Vertical Annular Channel and 3-rod Bundle," in *23rd International Conference On Nuclear Engineering (ICONE-23)*, Chiba, Japan, May 17 – 21, 2015.

[50] T. Chu and C. Ho, "Electrical Resistivity and Thermal Conductivity of Nine Selected AISI Stainless Steels," CINDAS, West Lafayette, Indiana, USA, 1977.

[51] F. Incropera, D. Dewitt, T. Bergman and A. Lavine, Fundamentals of Heat and Mass Transfer, 6, Ed., Danvers: John Wiley & Sons, 2007.

[52] J. Duderstadt and L. Hamilton , Nulcear Reactor Analysis, United States of America: John Wiley & Sons Inc., 1976.

[53] L. Grande, W. Peiman, S. Mikhael, B. Villamere, A. Rodriguez-Prado, L. Allison and I.

Pioro, "Thermal Aspects of using Uranium Nitride in Supercritical Water-cooled Nuclear Reactors," in *18th International Conference on Nuclear Engineering (ICONE-18)*, Xi'an, China, May 17-21, 2010.

[54] K. Sidawi and I. Pioro, "Modelling of Fuel Temperature Profiles for Upward Flow of SuperCritical Water in Annular Channels," in *36th Annual Conference of the Canadian Nuclear Society (CNS)*, Toronto, Canada, June 19 - 22, 2016.

[55] C. Ho and T. Chu, "Electrical Resistivity and Thermal Conductivity of Nine Selected AISI Stainless Steels," CINDAS, West Lafayette, Indiana, September 1977.

[56] L. Tong and J. Weisman, Thermal Analysis of Pressurized Water Reactors, 3rd ed., La Grange Park, Illinois: American Nuclear Society, 1996.

[57] Y. A. Cengel and A. J. Gharjar, Heat and Mass Transfer: Fundamentals and Applications, New York: McGraw-Hill, 2011.

[58] I. Pioro, S. Mokry and S. Draper, "Specifics of Thermophysical Properties and Forced-Convective Heat Transfer at Critical and Supercritical Pressures," *Reviews in Chemical Engineering*, vol. 27, no. 3-4, pp. 191-214, 2011.

[59] Independent Electricity System Operator, "Supply Overview," 22 March 2016. [Online]. Available: http://www.ieso.ca/Pages/Power-Data/Supply.aspx. [Accessed 5 April 2016].

[60] W. Wagner and A. Prub, "The IAPWS Formulation 1995 for the Thermodynamic Properties of Ordinary Water Substance for General and Scientific Use," *Journal of Physical Chemistry*, vol. 31, no. 2, pp. 387-535, 7 June 2002.

[61] M. Huber, R. Perkins, A. Laesecke and D. Friend, "New International Formulation for the Viscosity of H2O," *Journal of Physical Chemistry*, vol. 38, no. 2, pp. 101-125, 21 April 2009.

[62] IAPWS, "Release on the IAPWS Formulation 2008 for the Viscosity of Ordinary Water

Substance," International Association for the Properties of Water and Steam, Berlin, Germany, 2008.

[63] E. Lemmon, M. Huber and M. McLinden, "NIST Reference Fluid Thermodynamic and Transport Properties—REFPROP Version 9.0," U.S. Department of Commerce , Gaithersburg, Maryland, 2010.

[64] M. Kazimi, "Actinide Burning in Reactors: Options and Outcomes," in *American Nuclear Society*, Boston, June 26, 2007.

[65] R. Winterton, "Where did the Dittus and Boelter equation come from?," *International Journal of Heat and Mass Transfer,* vol. 31, no. 4-5, pp. 809-810, 1998.

[66] W. McAdams, W. Kennel and J. Addoms, "Heat Transmission," *Transactions of ASME*, vol. 72, no. 4, pp. 421-428, 1950.

[67] N. Todreas and M. Kazimi, Nuclear Systems Volume 1 Thermal Hydraulic Fundamentals, Boca Raton, FL, USA: Taylor & Francis Group, LLC, 2012.

[68] B. Petukhov and Kirillov, "About heat transfer at turbulent fluid flow in tubes, (In Russian)," *Thermal Engineering (Теплоэнергетика),* no. 4, pp. 63-68, 1958.

[69] H. Katzgraber, "Phase Transitions," Institut fur theoretische Physik ETH Zurich , Zurich , 2015.

Appendix A. Experimental Data – Inner Wall-Temperatures

Table A-1. Changes in temperature along annular channel for several heat fluxes: P = 22.6 MPa, G = 2000 kg/m^{2}s [46].

Distance from Inlet	Inner Wall Temperature				
	q = 1.543 MW/m^2 T_{in} = 205°C	q = 1.758 MW/m^2 T_{in} = 207°C	q = 2.033 MW/m^2 T_{in} = 208°C	q = 2.244 MW/m^2 T_{in} = 210°C	q = 2.547 MW/m^2 T_{in} = 214°C
0.095 m	292.1°C	307.3°C	319.5°C	332.6°C	350.9°C
0.195 m	306.8°C	319.0°C	337.0°C	354.9°C	372.2°C
0.255 m	310.7°C	325.9°C	342.9°C	359.8°C	380.9°C
0.315 m	318.6°C	334.7°C	354.6°C	371.4°C	393.5°C
0.375 m	322.5°C	339.5°C	360.4°C	375.3°C	409.0°C
0.415 m	326.4°C	343.5°C	366.2°C	384.1°C	452.0°C
0.475 m	330.3°C	351.3°C	376.0°C	393.8°C	502.0°C

Table A-2. Wall temperature along a 3-rod bundle in test (1) and control (2) rods at: P = 24.5 MPa, G = 2700 kg/m^{2}s, T_{in} = 277, q = 3.2 MW/m^2.

Distance from Inlet	Inner Wall Temperature	
	Test – Element 1	Control – Element 2
0.095 m	409.1°C	–
0.195 m	423.6°C	425.5°C
0.255 m	427.4°C	422.6°C
0.315 m	435.1°C	428.4°C
0.375 m	442.8°C	435.1°C
0.415 m	466.9°C	457.3°C
0.475 m	495.9°C	511.3°C

Table A-3. Wall temperature along a 3-rod bundle at: P = 27.5 MPa, G = 1500 kg/m^{2}s, T_{in} = 166°C/212°C, q = 3.07 MW/m^2.

Distance from Inlet	Inner Wall Temperature	
	T_{in} = 166°C	T_{in} = 212°C
0.095 m	358.3°C	402.0°C
0.255 m	415.6°C	446.7°C
0.315 m	437.9°C	516.8°C
0.375 m	436.0°C	549.0°C
0.415 m	438.9°C	516.8°C
0.475 m	462.2°C	474.9°C

Appendix B. Matlab Code for Section 3.1

```
clear all
close all
clc
tic;

%set number of iterations
L = 485E-3; %m
n = L * 1000;


% Import SS-304 properties and text files for data

%import SS-304 properties
filename = 'SS-304.txt';
delimiterIn = ' ';
headerlinesIn = 3;
DataSS = importdata(filename,delimiterIn,headerlinesIn);
%relabel SS-304 data
T_SS304 = DataSS.data(:,1); %C
rho_SS304 = DataSS.data(:,2); %ohm m
k_SS304 = DataSS.data(:,3); %W/m K

%input geometry to be analyzed
prompt = ('What Geometry would you like to analyze?: \n 1) Single-Rod \n 2) 3-Rod Bundle \n
Option: ');
Rod = input(prompt);

%Input
if Rod == 1
    prompt = ('\n what heat flux would like to use?: \n 1) 1.543 MW/m^2 \n 2) 1.758 MW/m^2
\n 3) 2.044 MW/m^2 \n 4) 2.233 MW/m^2 \n 5) 2.547 MW/m^2 \n Option: ');
elseif Rod == 2
    prompt = ('\n What is the inlet temperature?: \n 1) 166C \n 2) 212C \n 3) 277C \n
Option: ');
end
h = input(prompt);

if Rod == 1

    %call figure 1 text file
    filename = 'Figure1data.txt';
    delimiterIn = ' ';
    headerlinesIn = 1;
    A = importdata(filename,delimiterIn,headerlinesIn);
    %relabel figure data
    x = A.data(:,1).*1000; %mm
    q_ave = [1.543; 1.758; 2.033; 2.244; 2.547].*1E6; %W/m2
    T_wi_e = [A.data(:,2) A.data(:,3) A.data(:,4) A.data(:,5) A.data(:,6)]; %C
    Tb = [205 207 208 210 214]; %C
```

```
    %initial conditions
    P = 22.6E3; %kPa
    G = 2000; %kg/m2s
    u=0;

elseif Rod == 2

    if h == 3

        %call figure text file
        filename = 'Figure2data.txt';
        delimiterIn = ' ';
        headerlinesIn = 1;
        A = importdata(filename,delimiterIn,headerlinesIn);
        %relabel figure data
        x = A.data(:,1).*1000; %mm
        q_ave = 3.2E6; %W/m2
        T_wi_e(:,1) = A.data(:,2); %C
        Tb = 277; %C
        %initial conditions
        P = 24.5E3; %kPa
        G = 2700; %kg/m2s
        h=1;
        u=3;

    else

        %call figure text file
        filename = 'Figure3data.txt';
        delimiterIn = ' ';
        headerlinesIn = 1;
        A = importdata(filename,delimiterIn,headerlinesIn);
        %relabel figure data
        x = A.data(:,1).*1000; %mm
        q_ave = [3.07 3.07].*1E6; %W/m2
        T_wi_e = [A.data(:,2) A.data(:,3)]; %C
        Tb = [166 212]; %C
        %initial conditions
        P = 27.5E3; %kPa
        G = 1500; %kg/m2s
        u=2;

    end
end


% Determination of psuedocritical temperature based on pressure

i=0;
for T = 370.1:0.1:400
    i=i+1;
    cp_w(i) = refpropm('C','T',T+273.15,'P',P,'water'); %J/kg K
end
```

```
%peak cp
A = max(cp_w);
%finds the closest value to the listed energies
tmp = abs(cp_w - A);
%index of closest value
[idx idx] = min(tmp);
%psuedocritical temperature
T_pc = 370 + 0.1 * idx; %C
%pseudocritical enthalpy
h_pc = refpropm('H','T',T_pc+273.15,'P',P,'water'); %J/kg


% Channel geometry calculations

%dimensions of rod
D_sho = 5.2E-3; %m
D_shi = 4.5E-3; %m
H_rib = 0.6E-3; %m
W_rib = 1E-3; %m
dx = L / n; %m

%cross sectional area of a rod
A_cr = D_sho^2 * pi / 4 + 4 * H_rib * W_rib; %m^2

if Rod == 1

    %inner pressure tube diameter
    D_ipt = 8.4E-3; %m
    %heated perimeter
    p_h = D_sho * pi + 8 * H_rib; %m
    %coolant flow area
    A_fl = D_ipt^2 * pi / 4 - A_cr; %m^2
    %wetted perimeter
    p_w  = p_h + pi * D_ipt; %m
    %hydraulic diameter
    D_hy = 4 * A_fl / p_w; %m

elseif Rod == 2

    %heated perimeter
    p_h = 3 * (D_sho * pi + 8 * H_rib); %m
    %flow area (145E-6 obtained via nx modelling of channel)
    A_fl = 145.11E-6 - 3 * A_cr; %m^2
    %wetted perimeter (0.0605 also obtained via nx model of channel)
    p_w  = p_h + 0.0605; %m
    %hydraulic diameter
    D_hy = 4 * A_fl / p_w; %m

end

%characteristic length of rib
L_c = H_rib + W_rib / 2; %m
%surface area of rib
A_f = (2 * H_rib + W_rib) * dx; %m^2
```

```
%total surface area
A_t = p_h * dx; %m^2


% Electric Resistance Calculations

%Variable heat flux calculation
for i = 1:1:length(x)
    %finds the closest value to the listed energies
    tmp = abs(T_wi_e(i,h) - T_SS304);
    %index of closest value
    [idx idx] = min(tmp);
    %interpolation of electrical resistivity
    rho_el(i) = rho_SS304(idx) + (T_wi_e(i,h) - T_SS304(idx)) * (rho_SS304(idx+1)-
rho_SS304(idx)) / (T_SS304(idx+1) - T_SS304(idx));
    %interpolation of thermal conductivity
    k_el(i) = k_SS304(idx) + (T_wi_e(i,h) - T_SS304(idx)) * (k_SS304(idx+1)-k_SS304(idx)) /
(T_SS304(idx+1) - T_SS304(idx));
    %resistance at given points
    if Rod == 1
        R_e(i) = rho_el(i) * L / (A_cr - pi * D_shi^2 / 4); %ohm
    elseif Rod == 2
        R_e(i) = rho_el(i) * L / (A_cr - pi * D_shi^2 / 4) / 3; %ohm
    end
end
for k = 0:1:length(x)
    if (k > 0) && (k < length(x))
        for l = x(k):1:x(k+1)
            %interpolation of electrical resistance
            R_el(l) = R_e(k)+(l-x(k))*(R_e(k+1)-R_e(k))/(x(k+1)-x(k)); %ohm
        end
    elseif k == 0
        for l = x(k+1):-1:1
            %interpolation of electrical resistance
            R_el(l) = R_e(k+1)-(x(k+1)-l)*(R_e(k+2)-R_e(k+1))/(x(k+2)-x(k+1)); %ohm
        end
    elseif k == length(x)
        for l = x(k):1:n
            %interpolation of electrical resistance
            R_el(l) = R_e(k)+(l-x(k))*(R_e(k)-R_e(k-1))/(x(k)-x(k-1)); %\ohm
        end
    end
end

%Current calculation
Current = ((q_ave(h) * L * p_h) / (trapz(R_el(:)) / n))^0.5; %A


% Fluid calculations

T_b(1) = Tb(h); %C
h_b(1) = refpropm('H','T',T_b(1)+273.15,'P',P,'water'); %J/kg

for i = 1:1:n
```

```
    %axial heat flux
    q(i) = (Current^2 * R_el(i)) / (p_h * L); %W/m2
    if Rod == 1
        %volumetric heat generation in single-rod (Annular channel trials)
        q_v(i) = q(i) * p_h / (A_cr - pi * D_shi^2 / 4); %W/m^3
    else
        %volumetric heat generation in single-rod (3-rod bundle trials)
        q_v(i) = q(i)  * p_h / 3 / (A_cr - pi * D_shi^2 / 4); %W/m^3
    end

    if i < n
        %specific enthalpy
        h_b(i+1) = q(i) * dx * p_h / A_fl / G + h_b(i); %J/kg
        %temperature
        T_b(i+1,1) = refpropm('T','P',P,'H',h_b(i+1),'water')-273.15; %C
    end

    %bulk fluid properties
    rho_b(i) = refpropm('D','T',T_b(i)+273.15,'P',P,'water'); %kg/m^3
    k_b(i) = refpropm('L','T',T_b(i)+273.15,'P',P,'water'); %W/m K
    u_b(i) = refpropm('V','T',T_b(i)+273.15,'P',P,'water'); %Pa s
    cp_b(i) = refpropm('C','T',T_b(i)+273.15,'P',P,'water'); %J/kg K
    Pr_b(i) = refpropm('^','T',T_b(i)+273.15,'P',P,'water');
    Re_b(i) = G * D_hy / u_b(i);
    Xi(i) = (1.82 * log10(Re_b(i)) - 1.64)^-2;
    %Boiling Number as per Saltanov (2015)
    X(i,1) = (h_b(i) - h_pc) / (q(i)/G);

    %loop of different correlations
    for cor = 1:1:(7-u)

        if cor == 1 %Bishop et al.(1964)

            if i == 1
                Tw(i,1) = T_b(i) + 5; %C
            else
                Tw(i,1) = T_wC(i-1,cor); %C
            end
            for p = 1:1:100
                h_w(i,p) = refpropm('H','T',Tw(i,p)+273.15,'P',P,'water'); %J/kg
                rho_w(i,p) = refpropm('D','T',Tw(i,p)+273.15,'P',P,'water'); %kg/m^3
                cp_(i,p) = (h_w(i,p) - h_b(i)) / (Tw(i,p) - T_b(i)); %J/kg K
                Pr_(i,p) = cp_(i,p) * u_b(i) / k_b(i);
                Nu_bi(i,p) = 0.0069 * Re_b(i)^0.9 * Pr_(i,p)^0.66 *
(rho_w(i,p)/rho_b(i))^0.43 * (1+2.4*D_hy / i);
                HTC_bi(i,p) = Nu_bi(i,p) * k_b(i) / D_hy; %W/m^2 K
                Tw(i,p+1) = q(i) / HTC_bi(i,p) + T_b(i); %C

                %iterations stop when difference between successive values of wall
temperature is less that 0.5C
                delta = Tw(i,p+1) - Tw(i,p); %C
                if (abs(delta) < 0.5)
                    HTC(i,cor) = HTC_bi(i,p); %W/m^2 K
                    T_wC(i,cor) = Tw(i,p); %C
```

```
                    break
                end
            end

        elseif cor == 2 %Dittus and Boelter (1930)

            Nu_DB(i) = 0.023 * Re_b(i)^0.8 * Pr_b(i)^0.4;
            HTC(i,cor) = Nu_DB(i) * k_b(i) / D_hy; %W/m2 K
            T_wC(i,cor) = q(i) / HTC(i,cor) + T_b(i); %C

        elseif cor == 3 %Dyadyakin and Popov (1977)

            if i == 1
                Tw(i,1) = T_b(i) + 5; %C
            else
                Tw(i,1) = T_wC(i-1,cor); %C
            end
            for p = 1:1:100
                h_w(i,p) = refpropm('H','T',Tw(i,p)+273.15,'P',P,'water'); %J/kg
                rho_w(i,p) = refpropm('D','T',Tw(i,p)+273.15,'P',P,'water'); %kg/m3
                cp_(i,p) = (h_w(i,p) - h_b(i)) / (Tw(i,p) - T_b(i)); %J/kg K
                Pr_(i,p) = cp_(i,p) * u_b(i) / k_b(i);
                Nu_dy(i,p) = 0.021 * Re_b(i)^0.8 * Pr_(i,p)^0.7 * (rho_w(i,p)/rho_b(i))^0.45
* (u_b(i)/u_b(1))^0.2 * (rho_b(i)/rho_b(1))^0.1 * (1+2.5 *D_hy/i);
                HTC_dy(i,p) = Nu_dy(i,p) * k_b(i) / D_hy; %W/m^2 K
                Tw(i,p+1) = q(i) / HTC_dy(i,p) + T_b(i); %C

                %iterations stop when difference between successive values of wall
temperature is less that 0.5C
                delta = Tw(i,p+1) - Tw(i,p); %C
                if (abs(delta) < 0.5)
                    HTC(i,cor) = HTC_dy(i,p); %W/m^2 K
                    T_wC(i,cor) = Tw(i,p); %C
                    break
                end
            end

        elseif cor == 4 %Jackson (2002)

            if i == 1
                Tw(i,1) = T_b(i) + 5; %C
            else
                Tw(i,1) = T_wC(i-1,cor); %C
            end
            for p = 1:1:100
                if or(Tw(i,p) < T_pc, 1.2*(T_pc+273.15) < (T_b(i)+273.15))
                    m(i,p) = 0.4;
                elseif and(T_b(i) < T_pc, T_pc < Tw(i,p))
                    m(i,p) = 0.4 + 0.2 * ((Tw(i,p)+273.15) / (T_pc+273.15) - 1);
                elseif and(T_pc < T_b(i), (T_b(i)+273.15) < 1.2*(T_pc+273.15))
                    m(i,p) = 0.4+0.2*((Tw(i,p)+273.15)/(T_pc+273.15)- 1)*(1-
5*((T_b(i)+273.15)/(T_pc+273.15)-1));
                end
```

```
                h_w(i,p) = refpropm('H','T',Tw(i,p)+273.15,'P',P,'water'); %J/kg
                rho_w(i,p) = refpropm('D','T',Tw(i,p)+273.15,'P',P,'water'); %kg/m^3
                cp_(i,p) = (h_w(i,p) - h_b(i)) / (Tw(i,p) - T_b(i)); %J/kg K
                Nu_J(i,p) = 0.0183 * Re_b(i)^0.82 * Pr_b(i)^0.5 * (rho_w(i,p)/rho_b(i))^0.3
* (cp_(i,p)/cp_b(i))^m(i,p);
                HTC_J(i,p) = Nu_J(i,p) * k_b(i) / D_hy; %W/m^2 K
                Tw(i,p+1) = q(i) / HTC_J(i,p) + T_b(i); %C

                %iterations stop when difference between successive values of wall
temperature is less that 0.5C
                delta = Tw(i,p+1) - Tw(i,p); %C
                if (abs(delta) < 0.5)
                    HTC(i,cor) = HTC_J(i,p); %W/m^2 K
                    T_wC(i,cor) = Tw(i,p); %C
                    break
                end
            end

        elseif cor == 7-u; %Swenson et al. (1965)

            if i == 1
                Tw(i,1) = T_b(i) + 5; %C
            else
                Tw(i,1) = T_wC(i-1,cor); %C
            end
            for p = 1:1:100
                h_w(i,p) = refpropm('H','T',Tw(i,p)+273.15,'P',P,'water'); %J/kg
                rho_w(i,p) = refpropm('D','T',Tw(i,p)+273.15,'P',P,'water'); %kg/m^3
                u_w(i,p) = refpropm('V','T',Tw(i,p)+273.15,'P',P,'water'); %Pa s
                k_w(i,p) = refpropm('L','T',Tw(i,p)+273.15,'P',P,'water'); %W/m K
                cp_(i,p) = (h_w(i,p) - h_b(i)) / (Tw(i,p) - T_b(i)); %J/kg K
                Pr__w(i,p) = cp_(i,p) * u_w(i,p) / k_w(i,p);
                Re_w(i,p) = G * D_hy / u_w(i,p);

                Nu_S(i,p) = 0.00459 * Re_w(i,p)^0.923 * Pr__w(i,p)^0.613 *
(rho_w(i,p)/rho_b(i))^0.231;
                HTC_S(i,p) = Nu_S(i,p) * k_w(i,p) / D_hy; %W/m^2 k
                Tw(i,p+1) = q(i) / HTC_S(i,p) + T_b(i); %C

                %iterations stop when difference between successive values of wall
temperature is less that 0.5C
                delta = Tw(i,p+1) - Tw(i,p); %C
                if (abs(delta) < 0.5)
                    HTC(i,cor) = HTC_S(i,p); %W/m^2 K
                    T_wC(i,cor) = Tw(i,p); %C
                    break
                end
            end

        elseif cor == 5 %Krasnoshchekov et al. (1967)

            if i == 1
                Tw(i,1) = T_b(i) + 5; %C
            else
```

```
                Tw(i,1) = T_wC(i-1,cor); %C
            end
            for p = 1:1:100
                h_w(i,p) = refpropm('H','T',Tw(i,p)+273.15,'P',P,'water'); %J/kg
                rho_w(i,p) = refpropm('D','T',Tw(i,p)+273.15,'P',P,'water'); %kg/m^3
                cp_(i,p) = (h_w(i,p) - h_b(i)) / (Tw(i,p) - T_b(i)); %J/kg K
                Pr_(i,p) = cp_(i,p) * u_b(i) / k_b(i);
                Nu_K0(i,p)= Xi(i) / 8 * Re_b(i) * Pr_(i,p) / (12.7 * (Xi(i)/8)^0.5 *
(Pr_(i,p)^(2/3)-1) + 1.07);

                if or(Tw(i,p) <= T_pc, (T_b(i)+273.15) >= 1.2*(T_pc+273.15))
                    m(i,p) = 0.4;
                elseif and(Tw(i,p) >= T_pc, (Tw(i,p)+273.15) <= 2.5*(T_pc+273.15))
                    m(i,p) = 0.22 + 0.18 * (Tw(i,p)+273.15) / (T_pc+273.15);
                elseif and(T_b(i) >= T_pc, (T_b(i)+273.15) <= 1.2*(T_pc+273.15))
                    M(i,p) = 0.22 + 0.18 * (Tw(i,p)+273.15) / (T_pc+273.15);
                    m(i,p) = M(i,p) + (5 * M(i,p) - 2) * (1 -
((T_b(i)+273.15)/(T_pc+273.15)));
                end

                Nu_K(i,p) = Nu_K0(i,p) * (rho_w(i,p)/rho_b(i))^0.3 *
(cp_(i,p)/cp_b(i))^m(i,p);
                HTC_K(i,p) = Nu_K(i,p) * k_b(i) / D_hy; %W/m^2 k
                Tw(i,p+1) = q(i) / HTC_K(i,p) + T_b(i); %C

                %iterations stop when difference between successive values of wall
temperature is less that 0.5C
                delta = Tw(i,p+1) - Tw(i,p); %C
                if (abs(delta) < 1)
                    HTC(i,cor) = HTC_K(i,p); %W/m^2 K
                    T_wC(i,cor) = Tw(i,p); %C
                    break
                end
            end

        elseif cor == 6 %Mokry et al. (2011)

            if i == 1
                Tw(i,1) = T_b(i) + 5; %C
            else
                Tw(i,1) = T_wC(i-1,cor); %C
            end
            for p = 1:1:100
                h_w(i,p) = refpropm('H','T',Tw(i,p)+273.15,'P',P,'water'); %J/kg
                rho_w(i,p) = refpropm('D','T',Tw(i,p)+273.15,'P',P,'water'); %kg/m^3
                cp_(i,p) = (h_w(i,p) - h_b(i)) / (Tw(i,p) - T_b(i)); %J/kg K
                Pr_(i,p) = cp_(i,p) * u_b(i) / k_b(i);
                Nu_m(i,p) = 0.0061 * Re_b(i)^0.904 * Pr_(i,p)^0.684 *
(rho_w(i,p)/rho_b(i))^0.564;
                HTC_m(i,p) = Nu_m(i,p) * k_b(i) / D_hy; %W/m^2 k
                Tw(i,p+1) = q(i) / HTC_m(i,p) + T_b(i); %C

                %iterations stop when difference between successive values of wall
temperature is less that 0.5C
```

```
                delta = Tw(i,p+1) - Tw(i,p); %C
                if (abs(delta) < 0.5)
                    HTC(i,cor) = HTC_m(i,p); %W/m^2 K
                    T_wC(i,cor) = Tw(i,p); %C
                    break
                end
            end
        end

        %finds the closest value of fin thermal conductivity
        tmp = abs(T_wC(i,cor) - T_SS304);
        %index of closest value
        [idx idx] = min(tmp);
        %interpolation of thermal conductivity
        k_rib(i,cor) = k_SS304(idx) + (T_wC(i,cor)-T_SS304(idx)) * (k_SS304(idx+1)-
k_SS304(idx)) / (T_SS304(idx+1)-T_SS304(idx)); %W/m K

        %overall efficiency of fin
        m(i,cor) = (2 * HTC(i,cor) / k_rib(i,cor) / W_rib)^0.5;
        n_f(i,cor) = tanh(m(i,cor) * L_c) / m(i,cor) / L_c;
        n_o(i,cor) = 1 - 4 * A_f / A_t * (1 - n_f(i,cor));

        %outer wall temperature at fin base
        T_wo(i,cor) = q(i) / n_o(i,cor) / HTC(i,cor) + T_b(i); %C

        %perimeter not covered by fins
        base = (p_h - 8 * H_rib - 4  * W_rib) / p_h;
        ribtip = 4  * W_rib / p_h;
        %perimeter averaged outer wall temperature
        T_wo_ave(i,cor) = T_wo(i,cor)*base + T_wC(i,cor)*ribtip +
(T_wo(i,cor)+T_wC(i,cor))/2*8*H_rib/p_h; %C

        %finds the closest value of sheath thermal conductivity
        tmp = abs(T_wo(i,cor) - T_SS304);
        %index of closest value
        [idx idx] = min(tmp);
        %interpolation of electrical resistivity
        k_rod(i,cor) = k_SS304(idx) + (T_wo(i,cor)-T_SS304(idx)) * (k_SS304(idx+1)-
k_SS304(idx)) / (T_SS304(idx+1)-T_SS304(idx)); %W/m K

        %corrected volumetric heat generation for rod only
        q_vr(i) = (A_t - 4 * A_f) / A_t * q_v(i); %W/m^3
        %inner wall temperature
        T_wi(i,cor) = T_wo(i,cor) - q_vr(i) / k_rod(i,cor) * ((D_sho^2 - D_shi^2) / 16 -
D_sho^2 / 8 * log(D_sho/D_shi)); %C
    end
end

for cor = 1:1:length(T_wC(1,:))
    %error calculation
    for i = 1:1:length(x)
        %error for wall temperature
        Error_Tw(i,cor) = ((T_wi(x(i),cor) - T_wi_e(i,h)) / T_wi_e(i,h))^2;
```

```
        if cor == 1
            %surface temerature using inner wall k
            T_wo_1(i) = T_wi_e(i,h) + q_vr(x(i)) / 4 / k_el(i) * (D_sho^2 - D_shi^2) / 4 -
q_vr(i) / 2 / k_el(i) * D_sho^2 / 4 * log(D_sho/D_shi);
            T_wo_2(i) = T_wi_e(i,h) + q_v(x(i)) / 4 / k_el(i) * ((D_sho+H_rib)^2 - D_shi^2)
/ 4 - q_v(i) / 2 / k_el(i) * (D_sho+H_rib)^2 / 4 * log((D_sho+H_rib)/D_shi);
            T_wo_a(i) = (T_wo_1(i) + T_wo_2(i)) / 2;

            if Rod == 1
                T_w_out(i,1) = (T_wo_1(i) * (D_sho * pi - 4 * W_rib) + T_wo_2(i) * 4 * W_rib
+ T_wo_a(i) * 8 * H_rib) / p_h;
            elseif Rod == 2
                T_w_out(i,1) = (T_wo_1(i) * (D_sho * pi - 4 * W_rib) + T_wo_2(i) * 4 * W_rib
+ T_wo_a(i) * 8 * H_rib) / (p_h / 3);
            end

            %heat transfer coefficient
            HTC_e(i,1) = q(x(i)) / (T_w_out(i,1) - T_b(x(i)));

            %Eckert Number
            E(i,cor) = (T_pc - T_b(x(i))) / (T_w_out(i,1) - T_b(x(i)));

            %type of convection Gr/Re ratio
            j=0;
            for T = T_b(x(i)):0.1:T_w_out(i,1)
                j = j + 1;
                rho(j) = refpropm('D','T',T+273.15,'P',P,'water')*0.1;
            end
            rho_(i,1) = trapz(rho) / (T_w_out(i,1) - T_b(x(i)));
            clearvars rho

            Gr_b(i,1) = 9.81 * (rho_b(x(i)) - rho_(i)) * D_hy^3 / rho_b(x(i))^2;
            Ratio(i,1) = Gr_b(i) / Re_b(x(i))^2.7;
        end
    end
    %RMS error percentage for inner wall temperature
    RMS_Tw(cor,1) = (sum(Error_Tw(:,cor)) / length(x))^0.5 *100;

    %graph of bulk-fluid, experimental & calculated inner wall temperatures
    plot(1:1:n,T_b(:,1),1:1:n,T_wi(:,:),x,T_wi_e(:,h),'o',1:1:n,T_pc,'--');
    xlabel ('Heated Length, m');
    ylabel ('Temperature, ^oC');
    grid on;
end

toc

%publish('EM13.m','doc');
```

Appendix C. Matlab Code for Section 3.2

```
clear all
close all
clc
tic;


% Givens

%heat flux
q_ave = [1.543 1.758 2.033 2.244 2.547].*1E6; %W/m2
%inlet temperature
T_b = [205 207 208 210 214];
%pressure
P = 25E3; %MPa
%axial node
n = 485;
%radial node
s = 450;
%length
L = 0.485; %m
%mass flux
G = 2000;


% Call text file

%call text file
filename = 'SS-304.txt';
delimiterIn = ' ';
headerlinesIn = 3;
DataSS = importdata(filename,delimiterIn,headerlinesIn);
%relabel the data
T_SS304 = DataSS.data(:,1); %C
rho_SS304 = DataSS.data(:,2);
k_SS304 = DataSS.data(:,3); %W/m K

%call text file
filename = 'Figure1data.txt';
delimiterIn = ' ';
headerlinesIn = 1;
%relabel the data
F1 = importdata(filename,delimiterIn,headerlinesIn);
x = F1.data(:,1).*1000;
T_wall = F1.data(:,[2 3 4 5 6]);


% Pseudocritical point

i=0;
```

```
for T = 370.1:0.1:400
    i=i+1;
    cp_w(i) = refpropm('C','T',T+273.15,'P',P,'water'); %J/(kg*K)
end

%peak cp
A = max(cp_w);
%finds the closest value to the listed energies
tmp = abs(cp_w - A);
%index of closest value
[idx idx] = min(tmp);
%psuedocritical temperature
T_pc = 370 + 0.1 * idx;


% Channel geometry

%dimensions of rod
D_sho = 5.2E-3; %m
D_shi = 4.5E-3; %m
H_rib = 0.6E-3; %m
W_rib = 1E-3; %m
dx = L / n; %m

%cross sectional area of a rod
A_cr = D_sho^2 * pi / 4 + 4 * H_rib * W_rib; %m^2

%inner pressure tube diameter
D_ipt = 8.4E-3; %m
%heated perimeter
p_h = D_sho * pi + 8 * H_rib; %m
%coolant flow area
A_fl = D_ipt^2 * pi / 4 - A_cr; %m^2
%wetted perimeter
p_w  = p_h + pi * D_ipt; %m
%hydraulic diameter
D_hy = 4 * A_fl / p_w; %m

%characteristic length of rib
L_c = H_rib + W_rib / 2;
%surface area of rib
A_f = (2 * H_rib + W_rib) * dx; %m2
%total surface area
A_t = p_h * dx;


% Bulk-fluid Properties Electric Heating

%Input
prompt = ('What correlation would you like to use?: \n 1) None, Experimental Data \n 2)
Dittus % Boelter \n 3) Jackson \n Option: ');
cor = input(prompt);

if cor == 1
```

```
    correlation = ('Experimental Data');
elseif cor == 2
    correlation = ('Dittus & Boelter Correlation');
elseif cor == 3
    correlation = ('Jackson (2002) Correlation');
end


% Resistance and thermal conductivity calculation

for h = 1:1:length(q_ave)
    for i = 1:1:7
        %finds the closest value to the listed energies
        tmp = abs(T_wall(i,h) - T_SS304);
        %index of closest value
        [idx idx] = min(tmp);
        %interpolation of electrical resistivity
        rho_el(i,h) = rho_SS304(idx) + (T_wall(i,h) - T_SS304(idx)) * (rho_SS304(idx+1)-
rho_SS304(idx)) / (T_SS304(idx+1) - T_SS304(idx));
        %resistance at given points
        R_e(i,h) = rho_el(i,h) * L / (A_cr - pi * D_shi^2 / 4); %ohm
        %interpolation of electrical resistivity
        k_th(i,h) = k_SS304(idx) + (T_wall(i,h) - T_SS304(idx)) * (k_SS304(idx+1)-
k_SS304(idx)) / (T_SS304(idx+1) - T_SS304(idx));
    end
    for k = 0:1:7
        if (k > 0) && (k < 7)
            for l = x(k):1:x(k+1)
                %interpolation of electrical resistance
                R_el(l,h) = R_e(k,h)+(l-x(k))*(R_e(k+1,h)-R_e(k,h))/(x(k+1)-x(k)); %ohm
            end
        elseif k == 0
            for l = x(k+1):-1:1
                %interpolation of electrical resistance
                R_el(l,h) = R_e(k+1,h)-(x(k+1)-l)*(R_e(k+2,h)-R_e(k+1,h))/(x(k+2)-x(k+1));
%ohm
            end
        elseif k == 7
            for l = x(k):1:n
                %interpolation of electrical resistance
                R_el(l,h) = R_e(k,h)+(l-x(k))*(R_e(k,h)-R_e(k-1,h))/(x(k)-x(k-1)); %\ohm
            end
        end
    end

    %curent calculation accounting for heat losses
    Current = ((q_ave(h) * L * p_h) / (trapz(R_el(:,h)) / n))^0.5; %A

    %Bulk-fluid Temperature
    h_b(1,h) = refpropm('H','T',T_b(1,h)+273.15,'P',P,'water'); %J/kg

    for i = 1:1:n
        %axial heat flux
        q(i,h) = (Current^2 * R_el(i,h)) / (p_h * L); %W/m2
```

```
        %heat Generated
        qv(i,h) = 4 * q(i,h) * p_h / pi / D_shi^2; %W

        if cor == 1
            %find polynomial representing trend
            Coef = polyfit(x,T_wall(:,h),3);
            %outer fuel temperature
            T_f(i,1,h) = polyval(Coef,i); %C
        else
            %bulk fluid properties
            rho_b(i,h) = refpropm('D','T',T_b(i,h)+273.15,'P',P,'water'); %kg/m3
            k_b(i,h) = refpropm('L','T',T_b(i,h)+273.15,'P',P,'water'); %W/m K
            u_b(i,h) = refpropm('V','T',T_b(i,h)+273.15,'P',P,'water'); %Pa s
            cp_b(i,h) = refpropm('C','T',T_b(i,h)+273.15,'P',P,'water'); %J/kg K
            Pr_b(i,h) = refpropm('^','T',T_b(i,h)+273.15,'P',P,'water');
            Re_b(i,h) = G * D_hy / u_b(i,h);

            if i < n
                %specfic enthalpy
                h_b(i+1,h) = qv(i,h) * pi * D_shi^2 * dx / 4 / A_fl / G + h_b(i,h); %J/kg
                %temperature
                T_b(i+1,h) = refpropm('T','P',P,'H',h_b(i+1,h),'water')-273.15; %C
            end

            if cor == 2 %Dittus and Boelter (1930)

                Nu(i,h) = 0.023 * Re_b(i,h)^0.8 * Pr_b(i,h)^0.4;
                HTC(i,h) = Nu(i,h) * k_b(i,h) / D_hy; %W/m2 K
                T_wC(i,h) = qv(i,h) * pi * D_shi^2 / 4 / p_h / HTC(i,h) + T_b(i,h); %C

            elseif cor == 3 %Jackson (2002)

                if i == 1
                    Tw(i,1) = T_b(i,h) + 5; %C
                else
                    Tw(i,1) = T_wo(i-1,h); %C
                end
                for p = 1:1:100
                    if ((Tw(i,p) < T_pc) || (((1.2*(T_pc+273.15))) < (T_b(i,h)+273.15)))
                        m(i,p) = 0.4;
                    elseif ((T_b(i,h) < T_pc) && (T_pc < Tw(i,p)))
                        m(i,p) = 0.4 + 0.2 * ((Tw(i,p)+273.15) / (T_pc+273.15) - 1);
                    elseif ((T_pc < T_b(i,h)) && ((T_b(i,h)+273.15) < (1.2 *
(T_pc+273.15))))
                        m(i,p) = 0.4+0.2*((Tw(i,p)+273.15)/(T_pc+273.15)- 1)*(1-
5*((T_b(i,h)+273.15)/(T_pc+273.15)-1));
                    end

                    h_w(i,p) = refpropm('H','T',Tw(i,p)+273.15,'P',P,'water'); %J/kg
                    rho_w(i,p) = refpropm('D','T',Tw(i,p)+273.15,'P',P,'water'); %kg/m3
                    cp_(i,p) = (h_w(i,p) - h_b(i,h)) / (Tw(i,p) - T_b(i,h)); %J/kg K
                    Nu_J(i,p) = 0.0183 * Re_b(i,h)^0.82 * Pr_b(i,h)^0.5 *
(rho_w(i,p)/rho_b(i,h))^0.3 * (cp_(i,p)/cp_b(i,h))^m(i,p);
                    HTC_J(i,p) = Nu_J(i,p) * k_b(i,h) / D_hy; %W/m2 K
```

```
                    Tw(i,p+1) = qv(i,h) * pi * D_shi^2 / 4 / p_h / HTC_J(i,p) + T_b(i,h); %C

                    delta = Tw(i,p+1) - Tw(i,p); %C
                    if (abs(delta) < 0.5)
                        HTC(i,h) = HTC_J(i,p); %W/m2 K
                        T_wC(i,h) = Tw(i,p); %C
                        break
                    end
                end
            end

            %finds the closest value of fin thermal conductivity
            tmp = abs(T_wC(i,h) - T_SS304);
            %index of closest value
            [idx idx] = min(tmp);
            %interpolation of thermal conductivity
            k_f(i,h) = k_SS304(idx) + (T_wC(i,h)-T_SS304(idx)) * (k_SS304(idx+1)-
k_SS304(idx)) / (T_SS304(idx+1)-T_SS304(idx));

            %efficiency of fin
            m(i,h) = (2 * HTC(i,h) / k_f(i,h) / W_rib)^0.5;
            n_f(i,h) = tanh(m(i,h) * L_c) / m(i,h) / L_c;
            n_o(i,h) = 1 - 4 * A_f / A_t * (1 - n_f(i,h));

            %outer wall temperature at fin base
            T_wo(i,h) = qv(i,h) * pi * D_shi^2 / 4 / p_h / n_o(i,h) / HTC(i,h) + T_b(i,h);

            %finds the closest value to the listed energies
            tmp = abs(T_wo(i,h) - T_SS304);
            %index of closest value
            [idx idx] = min(tmp);
            %interpolation of electrical resistivity
            k_s(i,h) = k_SS304(idx) + (T_wo(i,h)-T_SS304(idx)) * (k_SS304(idx+1)-
k_SS304(idx)) / (T_SS304(idx+1)-T_SS304(idx));
            %inner sheath temperature
            T_wi(i,h) = T_wo(i,h) + qv(i,h) * pi * D_shi^2 * D_sho / 8 / p_h / k_s(i,h) *
log(D_sho/D_shi);
            %outer fuel temperature
            T_f(i,1,h) = T_wi(i,h); %C
        end

        %Outer fuel pellet radius
        r_f(1) = D_shi / 2; %m

        for j = 1:1:s
            %Concentric radius of the rings of the fuel
            r_f(j+1,1) = (s - j) / s * D_shi / 2;
            %Initial thermal conductivity of the fuel
            k_f(i,j,h) = 100 / (7.5408 + 17.692
*(T_f(i,j,h)+273.15)/1000+3.6142*((T_f(i,j,h)+273.15)/1000)^2)+
6400/((T_f(i,j,h)+273.15)/1000)^(5/2)*exp(-16350/(T_f(i,j,h)+273.15));
            %Initial fuel centerline temperature
            T_f(i,j+1,h) = T_f(i,j,h) + qv(i,h) / (4 * k_f(i,j,h)) * (r_f(j)^2 -
r_f(j+1)^2); %C
```

```
        end

        %fuel centerline temperatures
        kcl_f(i,h) = k_f(i,j,h); %W/mK
        Tcl_f(i,h) = T_f(i,j+1,h); %C
    end

    %max and min fuel temperatures for each heat flux
    a = T_f(:,:,h);
    T_max(h) = max(a(:)); %C
    T_min(h) = min(a(:)); %C

    % error calculation
    for i = 1:1:7
        %error
        Error_Tw(i,h) = ((T_f(x(i),1,h) - T_wall(i,h)) / T_wall(i,h))^2;
    end
    RMS_Tw(h,1) = (sum(Error_Tw(:,h)) / 7)^0.5 *100;
end


% Graphs

for h = 1:1:length(q_ave)
    %Cross sectional fuel temperature profile
    A = max(Tcl_f(:,h));
    %finds the closest value to the listed energies
    tmp = abs(Tcl_f(:,h) - A);
    %index of closest value
    [idx idx] = min(tmp);

    i=0;
    for theta = 1:1:360
        j=0;
        for radius = 0:5:(D_shi/2*1E6)
            i=i+1;
            j=j+1;
            c(i,1) = radius/1E6*cosd(theta)*1000; %mm
            c(i,2) = radius/1E6*sind(theta)*1000; %mm
            c(i,3) = T_f(idx,s+2-j,h);
        end
    end

    %fuel pin temperature-profiles for different heat fluxes
    [xi,yi] = meshgrid((-D_shi/2:5E-6:D_shi/2).*1000,(-D_shi/2:5E-6:D_shi/2).*1000);
    Z = scatteredInterpolant(c(:,1),c(:,2),c(:,3),'linear','none');
    zi = Z(xi,yi);

    figure(h)
    contourf(xi,yi,zi,451,'LineColor', 'none');
    Tmax = ['{\itT_m_a_x}: ',num2str(max(zi(:)),4), ' ^oC'];
    text(2.4,2,Tmax,'HorizontalAlignment','right');
    title([correlation, ' | q: ', num2str(q_ave(h)/1E6),' MW/m^2']) %
    colormap(hot)
```

```
    axis equal
    axis off
    caxis([min(floor(T_min/50)*50) max(ceil(T_max/50)*50)]);
    colorbar
end

if cor ~= 1
    figure('units','normalized','outerposition',[0 0 1 1])

    for h = 1:1:length(q_ave)
        % first row
        subplot(2,length(q_ave),h)
        plot(1:1:n,HTC(:,h)/1000);
        title(correlation)
        xlim([0 500]);
        set(gca,'XLim',[0
(ceil(L*10)/10*1000)],'XTickLabel',{'0','0.1','0.2','0.3','0.4','0.5'});
        set(gca,'YLim',[0 (ceil(max(HTC(:)/1000)/5)*5)]);
        xlabel ('Heated Length, m');
        if h == 1
            ylabel ('HTC, kW/m^2K');
        end
        grid on

        %seocnd row
        subplot(2,length(q_ave),h+length(q_ave))

plot(1:1:n,T_b(:,h),'b',1:1:n,T_wo(:,h),'g',1:1:n,T_wi(:,h),'r',1:1:n,Tcl_f(:,h),'m',1:1:n,3
75.9610,'--');
        title(['q: ' num2str(q_ave(h)/1E6) ' MW/m^2 | G: ' num2str(G) ' kg/m^2s'])
        %         legend('T_b','T_w_,_o','T_w_,_i','T_c_l')
        %         legend('boxoff')
        xlim([0 500]);
        set(gca,'XLim',[0
(ceil(L*10)*100)],'XTickLabel',{'0','0.1','0.2','0.3','0.4','0.5'});
        set(gca,'YLim',[0 (ceil(max(Tcl_f(:))/500)*500)]);
        xlabel ('Heated Length, m');
        if h == 1
            ylabel ('Temperature, ^oC');
        end
        grid on
    end
end

toc;

%publish('FuelModel.m','doc');
```

Appendix D. Text Files for Appendix B & Appendix C

Text File "Figure1data.txt" for Single-rod channels

x, m	Tw-1,C		Tw-2,C		Tw-3,C	Tw-4,C	Tw-5,C
0.095	292.1	307.3	319.5	332.6	350.9		
0.195	306.8	319.0	337.0	354.9	372.2		
0.255	310.7	325.9	342.9	359.8	380.9		
0.315	318.6	334.7	354.6	371.4	393.5		
0.375	322.5	339.5	360.4	375.3	409.0		
0.415	326.4	343.5	366.2	384.1	452.0		
0.475	330.3	351.3	376.0	393.8	502.0		

Text File "Figure2data.txt" for 3-rod bundle channels, T_{in} = 166, 212°C

x,m	Tw-1,C		Tw-2,C
0.095	358.3	402.0	
0.255	415.6	446.7	
0.315	437.9	516.8	
0.375	436.0	549.0	
0.415	438.9	516.8	
0.475	462.2	474.9	

Text File "Figure3data.txt" for 3-rod bundle channels, T_{in} = 277°C

x(mm)	Tw-1,C
0.095	409.1
0.195	423.6
0.255	427.4
0.315	435.1
0.375	442.8
0.415	466.9
0.475	495.9

Appendix E. Matlab Code for Section 3.3

```
clear all
close
clc
tic;


% Choose Figure to analyze
prompt = ('What Figure would you like to analyze?: \n 1) Fig4 \n 2) Fig7 \n Option: ');
Fig = input(prompt);

if Fig == 1

    %call text file
    filename = 'Fig4.txt';
    delimiterIn = ' ';
    headerlinesIn = 1;
    A = importdata(filename,delimiterIn,headerlinesIn);

    %relabel the data
    x = A.data(:,1).*1000;
    T_w_e = [A.data(:,2) A.data(:,3) A.data(:,4) A.data(:,5)]; %C

    %test section parameters
    P = 23E3; %kPa
    G = 900; %kg/m2s
    q = 1.2E6; %W/m2
    T_b(1) = 352;
    h_b(1) = refpropm('H','T',T_b(1)+273.15,'P',P,'water'); %J/kg
    ad = 0.0003;

elseif Fig == 2

    %call text file
    filename = 'Fig7.txt';
    delimiterIn = ' ';
    headerlinesIn = 1;
    A = importdata(filename,delimiterIn,headerlinesIn);

    %relabel the data
    x = A.data(:,1);
    T_w_e = [A.data(:,2) A.data(:,3)]; %C

    %test section parameters
    P = 23E3; %kPa
    G = 1000; %kg/m2s
    q = 0.8E6; %W/m2
    T_b(1) = 342;
    h_b(1) = refpropm('H','T',T_b(1)+273.15,'P',P,'water'); %J/kg
    ad = 0.00012;
```

```
end

% Pseudocritical point

%specific heats for temperature range
i = 0;
for T = 370.1:0.1:400
    i=i+1;
    cp_w(i) = refpropm('C','T',T+273.15,'P',P,'water'); %J/(kg*K)
end

%maximum specific heat
A = max(cp_w);
%finds the address of the maximum specific heat
tmp = abs(cp_w - A);
%index of closest value
[idx idx] = min(tmp);
%psuedocritical temperature
T_pc = 370 + 0.1 * idx;


% Bulk-fluid and Wall Calculations

%channel design
S = 20.32 / 1000; %m
D_sho = 8 / 1000; %m
D_shi = (8 - 2 * 1.5) / 1000; %m
p_h = 4 * pi * D_sho;
p_w = 4 * S + p_h;
A_fl = S^2 - 4 * pi * D_sho^2 / 4;
D_hy = 4 * A_fl / p_w;

L = 1.282-0.179; %m
n = L * 1000;
dx = L / n;

for i = 1:1:n

    if i < n
        %specfic enthalpy
        h_b(i+1,1) = (q * dx * p_h / A_fl / G + h_b(i)) * (1 - i / n * ad); %J/kg
        %bulk-fluid temperature
        T_b(i+1,1) = (refpropm('T','P',P,'H',h_b(i+1),'water')-273.15); %C
    end

    rho_b(i,1) = refpropm('D','T',T_b(i,1)+273.15,'P',P,'water'); %kg/m3
    k_b(i,1) = refpropm('L','T',T_b(i,1)+273.15,'P',P,'water'); %W/m K
    u_b(i,1) = refpropm('V','T',T_b(i,1)+273.15,'P',P,'water'); %Pa s
    cp_b(i,1) = refpropm('C','T',T_b(i,1)+273.15,'P',P,'water'); %J/kg K
    Pr_b(i,1) = refpropm('^','T',T_b(i,1)+273.15,'P',P,'water');
    Re_b(i,1) = G * D_hy / u_b(i,1);
    Xi(i,1) = (1.82 * log10(Re_b(i,1)) - 1.64)^-2;
```

```
    %loop of different heat flux
    for cor = 1:1:5

        if cor == 1 %Bishop et al.(1964)

            if i == 1
                Tw(i,1) = T_b(i) + 5; %C
            else
                Tw(i,1) = T_wC(i-1,cor); %C
            end
            for p = 1:1:100
                h_w(i,p) = refpropm('H','T',Tw(i,p)+273.15,'P',P,'water'); %J/kg
                rho_w(i,p) = refpropm('D','T',Tw(i,p)+273.15,'P',P,'water'); %kg/m3
                cp_(i,p) = (h_w(i,p) - h_b(i)) / (Tw(i,p) - T_b(i)); %J/kg K
                Pr_(i,p) = cp_(i,p) * u_b(i) / k_b(i);
                Nu_bi(i,p) = 0.0069 * Re_b(i)^0.9 * Pr_(i,p)^0.66 *
(rho_w(i,p)/rho_b(i))^0.43 * (1+2.4*D_hy / i);
                HTC_bi(i,p) = Nu_bi(i,p) * k_b(i) / D_hy; %W/m2 K
                Tw(i,p+1) = q / HTC_bi(i,p) + T_b(i); %C

                delta = Tw(i,p+1) - Tw(i,p); %C
                if (abs(delta) < 0.5)
                    HTC(i,cor) = HTC_bi(i,p); %W/m2 K
                    T_wC(i,cor) = Tw(i,p); %C
                    break
                end
            end

        elseif cor == 2 %Dittus and Boelter (1930)

            Nu_DB(i) = 0.023 * Re_b(i)^0.8 * Pr_b(i)^0.4;
            HTC(i,cor) = Nu_DB(i) * k_b(i) / D_hy; %W/m2 K
            T_wC(i,cor) = q / HTC(i,cor) + T_b(i); %C

        elseif cor == 3 %Dyadyakin and Popov (1977)

            if i == 1
                Tw(i,1) = T_b(i) + 5; %C
            else
                Tw(i,1) = T_wC(i-1,cor); %C
            end
            for p = 1:1:100
                h_w(i,p) = refpropm('H','T',Tw(i,p)+273.15,'P',P,'water'); %J/kg
                rho_w(i,p) = refpropm('D','T',Tw(i,p)+273.15,'P',P,'water'); %kg/m3
                cp_(i,p) = (h_w(i,p) - h_b(i)) / (Tw(i,p) - T_b(i)); %J/kg K
                Pr_(i,p) = cp_(i,p) * u_b(i) / k_b(i);
                Nu_dy(i,p) = 0.021 * Re_b(i)^0.8 * Pr_(i,p)^0.7 * (rho_w(i,p)/rho_b(i))^0.45
* (u_b(i)/u_b(1))^0.2 * (rho_b(i)/rho_b(1))^0.1 * (1+2.5 *D_hy/i);
                HTC_dy(i,p) = Nu_dy(i,p) * k_b(i) / D_hy; %W/m2 K
                Tw(i,p+1) = q / HTC_dy(i,p) + T_b(i); %C

                delta = Tw(i,p+1) - Tw(i,p); %C
                if (abs(delta) < 0.5)
                    HTC(i,cor) = HTC_dy(i,p); %W/m2 K
```

```
                    T_wC(i,cor) = Tw(i,p); %C
                    break
                end
            end

        elseif cor == 4 %Jackson (2002)

            if i == 1
                Tw(i,1) = T_b(i) + 5; %C
            else
                Tw(i,1) = T_wC(i-1,cor); %C
            end
            for p = 1:1:100
                if or(Tw(i,p) < T_pc, 1.2*(T_pc+273.15) < (T_b(i)+273.15))
                    m(i,p) = 0.4;
                elseif and(T_b(i) < T_pc, T_pc < Tw(i,p))
                    m(i,p) = 0.4 + 0.2 * ((Tw(i,p)+273.15) / (T_pc+273.15) - 1);
                elseif and(T_pc < T_b(i), (T_b(i)+273.15) < 1.2*(T_pc+273.15))
                    m(i,p) = 0.4+0.2*((Tw(i,p)+273.15)/(T_pc+273.15)- 1)*(1-
5*((T_b(i)+273.15)/(T_pc+273.15)-1));
                end

                h_w(i,p) = refpropm('H','T',Tw(i,p)+273.15,'P',P,'water'); %J/kg
                rho_w(i,p) = refpropm('D','T',Tw(i,p)+273.15,'P',P,'water'); %kg/m3
                cp_(i,p) = (h_w(i,p) - h_b(i)) / (Tw(i,p) - T_b(i)); %J/kg K
                Nu_J(i,p) = 0.0183 * Re_b(i)^0.82 * Pr_b(i)^0.5 * (rho_w(i,p)/rho_b(i))^0.3
* (cp_(i,p)/cp_b(i))^m(i,p);
                HTC_J(i,p) = Nu_J(i,p) * k_b(i) / D_hy; %W/m2 K
                Tw(i,p+1) = q / HTC_J(i,p) + T_b(i); %C

                delta = Tw(i,p+1) - Tw(i,p); %C
                if (abs(delta) < 0.5)
                    HTC(i,cor) = HTC_J(i,p); %W/m2 K
                    T_wC(i,cor) = Tw(i,p); %C
                    break
                end
            end

        elseif cor == 5 %Swenson et al. (1965)

            if i == 1
                Tw(i,1) = T_b(i) + 5; %C
            else
                Tw(i,1) = T_wC(i-1,cor); %C
            end
            for p = 1:1:100
                h_w(i,p) = refpropm('H','T',Tw(i,p)+273.15,'P',P,'water'); %J/kg
                rho_w(i,p) = refpropm('D','T',Tw(i,p)+273.15,'P',P,'water'); %kg/m3
                u_w(i,p) = refpropm('V','T',Tw(i,p)+273.15,'P',P,'water'); %Pa s
                k_w(i,p) = refpropm('L','T',Tw(i,p)+273.15,'P',P,'water'); %W/m K
                cp_(i,p) = (h_w(i,p) - h_b(i)) / (Tw(i,p) - T_b(i)); %J/kg K
                Pr__w(i,p) = cp_(i,p) * u_w(i,p) / k_w(i,p);
                Re_w(i,p) = G * D_hy / u_w(i,p);
```

```
                Nu_S(i,p) = 0.00459 * Re_w(i,p)^0.923 * Pr__w(i,p)^0.613 *
(rho_w(i,p)/rho_b(i))^0.231;
                HTC_S(i,p) = Nu_S(i,p) * k_w(i,p) / D_hy; %W/m2 k
                Tw(i,p+1) = q / HTC_S(i,p) + T_b(i); %C

                delta = Tw(i,p+1) - Tw(i,p); %C
                if (abs(delta) < 0.5)
                    HTC(i,cor) = HTC_S(i,p); %W/m2 K
                    T_wC(i,cor) = Tw(i,p); %C
                    break
                end
            end
        end
    end
end

%error calculation
for cor = 1:1:5
    for h = 1:1:length(T_w_e(1,:))
        for i = 1:length(x)
            if cor == 1

                %heat transfer coefficient
                HTC_e(i,h) = q / (T_w_e(i,h) - T_b(x(i)));

                %type of convection Gr/Re ratio
                j=0;
                for T = T_b(x(i)):0.1:T_w_e(i,h)
                    j = j + 1;
                    rho(j) = refpropm('D','T',T+273.15,'P',P,'water')*0.1;
                end
                rho_(i,h) = trapz(rho) / (T_w_e(i,h) - T_b(x(i)));
                clearvars rho

                %Grashof Number
                Gr_b(i,h) = 9.81 * (rho_b(x(i)) - rho_(i,h)) * D_hy^3 / rho_b(x(i))^2;
                Ratio(i,h) = Gr_b(i,h) / Re_b(x(i))^2.7;

                E(i,h) = (T_pc - T_b(x(i))) / (T_w_e(i,h) - T_b(x(i)));
            end

            %error in temperature
            Error_Tw(i) = ((T_wC(x(i),cor) - T_w_e(i,h)) / T_w_e(i,h))^2;

        end

        %RMS error of temperature
        RMS_Tw(cor,h) = (sum(Error_Tw(:)) / length(x))^0.5 *100;

    end
end

plot(1:n,T_b,1:n,T_wC,x,T_w_e,'o',1:n,377.5,'-');
grid on
```

```
toc

% publish('fourrod.m','doc');
```

Text File "Fig4.txt" for Appendix E – Fig 4

L,m	Tw-Cen		Tw-Wall		Tw-Cor	Tw-Gap
0.000	427.8	458.5	466.5	449.4		
0.050	436.9	468.7	477.8	460.7		
0.097	444.7	478.8	482.2	473.2		
0.147	418.5	427.6	431.0	423.1		
0.157	426.5	437.8	442.4	435.6		
0.166	432.1	448.1	452.6	448.1		
0.175	438.9	461.7	466.2	458.3		
0.185	446.9	463.9	473.0	461.7		
0.194	452.6	478.7	484.4	469.6		
0.248	476.3	494.5	496.8	493.4		
0.295	489.9	501.3	505.8	501.3		
0.345	497.8	512.6	517.1	511.4		
0.395	476.1	485.2	483.0	480.7		
0.448	512.4	532.9	532.9	526.1		
0.499	526.0	538.5	548.7	539.6		
0.549	538.4	554.3	557.7	549.8		
0.596	470.2	473.6	482.7	474.7		
0.646	528.1	536.0	537.1	531.5		
0.696	534.8	534.8	550.7	537.1		
0.750	541.5	552.9	556.3	552.9		
0.800	548.3	560.8	564.2	560.8		
0.850	501.6	507.3	500.5	499.4		
0.900	535.7	548.1	560.7	548.2		
0.947	544.7	552.6	573.1	552.6		
0.997	550.3	568.5	585.5	562.8		
1.048	458.2	482.0	507.0	500.2		
1.101	560.4	527.4	563.8	489.9		

Text File "Fig7.txt" Appendix E – Fig 7

L,m	Tw-C,C		Tw-Gap, C
0	380.0	385.6	

52	383.8	387.2
101	385.4	388.4
151	382.5	381.0
200	385.3	386.4
252	386.6	391.1
301	386.4	391.8
354	388.2	393.2
403	386.5	388.3
452	389.4	391.0
501	390.8	392.6
551	394.0	395.5
603	387.9	398.3
652	393.1	391.5
701	392.7	400.3
751	392.9	397.9
803	396.1	404.4
849	391.1	392.0
901	392.7	397.2
954	392.1	400.0
1003	393.9	397.3
1052	400.2	399.8
1101	403.9	405.7

Appendix F. List of Publications, Conferences Attended, and Awards Received

Journal Papers

1. V.G. Razumovskiy, Eu.N. Pis'mennyi, **Kh. Sidawi**, I.L. Pioro, and A.Eu. Koloskov, 2015. Experimental Heat Transfer in an Annular Channel and 3-Rod-Bundle Cooled with Upward Flow of Supercritical Water, ASME Journal of Nuclear Engineering and Radiation Science, Vol. 2, No. 1, 9 pages.

Papers in Refereed Conference Proceedings

1. I.L. Pioro, Kh. **Sidawi**, and R. Abdullah, 2016. Specifics of Thermophysical Properties and Heat Transfer at Supercritical Pressures, Proceedings of the 12th International Conference on Heat Transfer, Fluid Mechanics and Thermodynamics (HEFAT2016), Costa del Sol, Malaga, Spain, July 11-13, pp. 1636-1648.
2. **Kh. Sidawi** & I.L. Pioro, 2016, Modelling of Fuel Temperature Profiles for Upward Flow of SuperCritical Water in Annular Channels, Proceedings of the 36th Annual Conference of the Canadian Nuclear Society (CNS), Toronto, Canada, June 19 – 22.
3. **Kh. Sidawi**, I. Pioro, V. Razumovskiy, E. Pis'mennyi and A. Koloskov, 2015. HTC Correlation Applications to SuperCritical Water Flowing Upward in a Vertical Annular Channel and 3-rod Bundle, Proceedings of the 23rd International Conference On Nuclear Engineering (ICONE-23), Chiba, Japan, May 17 – 21.
4. **Kh. Sidawi**, 2015. Heat-Transfer Characteristics of SuperCritical Water Flowing Upward in Bare Tubes, Proceedings of the 35th Annual Conference of the Canadian Nuclear Society (CNS), Saint John, Canada, May 31 – June 3, 2015.
5. V. Razumovskiy, E. Pis'mennyi, **Kh. Sidawi**, I.L. Pioro, E. Maevskiy and A. Koloskov, 2015. Specifics of Heat Transfer to Supercritical Water Flowing Upward in Annular Channel and 3-Rod Bundle, Proceedings of the 7th International Symposium on Supercritical Water-Cooled Reactors (ISSCWR-7), Helsinki, Finland, March 15 – 18.
6. **Kh. Sidawi**, A. Vincze, R. Abdullah, M. Baldock and I. Pioro, 2014. The Viability, from a Thermalhydraulic Perspective, of the Implementation of Nuclear Steam Superheat in a Pressure-Channel Nuclear Reactor, Proceedings of the 19th Pacific

Basin Nuclear Conference (PBNC-19), Vancouver, Canada, Augeust 24 – 28.

7. **Kh. Sidawi**, R. Abdullah, M. Baldock, W. Peiman and I. Pioro, 2014. Study on the Thermalhydraulic Effects of Nuclear Steam Superheat for a generic 1200-MW_{el} Pressure Channel Reactor, Proceedings of in the 22nd International Conference On Nuclear Engineering (ICONE-22), Prague, Czech Republic, July 7 – 11.

Conferences Attended

1. 35th Annual Conference of the Canadian Nuclear Society (CNS)/39th Annual Canadian Nuclear Society (CNS)/Canadian Nuclear Association (CNA) Student Conference, Saint John, Canada, May 31 – June 03, 2015.
2. 23rd International Conference On Nuclear Engineering (ICONE-23), Chiba, Japan, May 17 – 21, 2015.
3. 19th Annual Pacific Basin Nuclear Conference (PBNC-2014)/38th Annual Canadian Nuclear Society (CNS)/Canadian Nuclear Association (CNA) Student Conference, Vancouver, Canada, August 24 – 28, 2014.
4. 22nd International Conference On Nuclear Engineering (ICONE-22), Prague, Czech Republic, July 7 – 14, 2014.

Awards and Honors

1. Recipient of a Student Best Paper Award at ICONE-23 for the paper "HTC Correlation Applications to Supercritical Water Flowing Upwards in a Vertical Annular Channel and 3-Rod Bundle."
2. Recipient of a Student Best Poster Award at ICONE-22 for the poster "Study on Thermalhydraulic Effects of Nuclear Steam Superheat for a Generic 1200-MW_{el} Pressure-Channel Reactor.